

博士論文
(Doctoral Thesis)

Comprehensive metabolomic
analysis of the fission yeast,
Schizosaccharomyces pombe

〔分裂酵母の網羅的メタボローム解析〕

Tomáš Pluskal

広島大学大学院先端物質科学研究科

〔Graduate School of Advanced Sciences of Matter
Hiroshima University〕

2014年9月
(September 2014)

Abstract

Metabolomics is a modern branch of chemical biology that aims to detect and quantify hundreds of cellular metabolites simultaneously. The fission yeast, *Schizosaccharomyces pombe*, is a unicellular model organism widely applied in many areas of cell biology research. The fission yeast genome has been sequenced and numerous high-throughput transcriptomic and proteomic analyses have been performed. However, so far this organism has not been subject to serious metabolomic study.

In this thesis we developed the methodology for metabolomic analysis of *S. pombe*, optimized mainly for extraction and detection of polar metabolites. For sample measurements we employed liquid chromatography mass spectrometry, using a high-resolution Orbitrap mass detector. Out of ~6,000 peaks detected from a single sample, we were able to assign the origin of ~1,900. Among the assigned peaks, we identified 123 distinct metabolites, 108 of which were verified using pure standards. In the initial analysis, we examined the metabolomes of *S. pombe* cells grown in a synthetic culture medium at two different cultivation temperatures, 26°C and 36°C. Further, we demonstrated the feasibility of integration of genetics and metabolomics by analyzing a deletion mutant (*sib1Δ*) that lacked a non-essential enzyme, ferrichrome synthetase, and a temperature-sensitive mutant (*hcs1-143*) defective in an essential enzyme, HMG-CoA synthase.

Our next project focused on glucose, the ubiquitous source of cellular energy for most living organisms. We investigated cell division modes of the fission yeast under a wide range of glucose concentrations (0-111 mM). Surprisingly, *S. pombe* cells proliferated normally under highly diluted glucose level, similar to that of human blood (5.6 mM). Cell division became stochastic below 4.4 mM glucose, and a transition from division to quiescence occurred between

2.2 and 1.7 mM glucose. Under starvation (1.1 mM), cells were predominantly quiescent and became greatly resistant to oxidative stress. On the contrary, cells rapidly lost viability under fasting (0 mM), unless they were pre-treated with starvation. Using metabolomic analysis, we identified specific biomarker compounds corresponding to different glucose levels. Interestingly, cells maintained high levels of nucleotide triphosphates such as ATP even under starvation. Under fasting, cells rapidly lost antioxidant and energy compounds such as glutathione and ATP. However, in cells undergoing long-term starvation, these critical metabolites remained abundant.

Among the compounds strongly up-regulated under glucose starvation was ergothioneine, a curious sulfur-containing metabolite that is synthesized only by certain species of bacteria and fungi, yet it accumulates in tissues of higher eukaryotes including humans. In the third study we identified the genes forming the ergothioneine biosynthetic pathway in fission yeast, through combined use of genetics and metabolomics. The first gene (*egt1*⁺) was identified by sequence homology to a previously published gene in *Neurospora crassa*. The second gene (*egt2*⁺) was found by metabolomic screening of four putative homologs of a corresponding bacterial gene. We confirmed the identity of the genes by metabolome analysis of deletion mutants, and constructed an *egt1*⁺ overexpression system by replacing its native promoter with an inducible *nmt1*⁺ promoter. Finally, we demonstrated that the same pathway can also synthesize a selenium-containing derivative of ergothioneine, selenoneine, if selenium is provided in the culture medium. The biosynthesis of selenoneine involved a novel intermediate metabolite, hercynylselenocysteine.

In conclusion, this thesis demonstrates the great potential of metabolomics as a modern, high-throughput, comprehensive method for studying basic cellular processes, including the effects of genetic and environmental perturbations.

Contents

Abstract	i
Contents	iii
Organization of this thesis.....	vi
Chapter 1. Introduction	1
1.1 Metabolome and its composition.....	1
1.2 Metabolomics as a research discipline.....	4
1.3 Analytical methods in metabolomics.....	7
1.3.1 Nuclear magnetic resonance spectroscopy	7
1.3.2 Mass spectrometry	8
1.4 The fission yeast, <i>Schizosaccharomyces pombe</i>	9
Chapter 2. Development of metabolomic analysis in fission yeast	11
2.1 Introduction.....	11
2.2 Scale of fission yeast metabolome.....	12
2.3 Method development	13
2.3.1 Metabolite measurement.....	13
2.3.2 Peak identification	14
2.3.3 Compound quantification	17
2.3.4 Cell cultivation.....	18
2.3.5 Quenching.....	20
2.3.6 Metabolite extraction.....	20
2.3.7 Data processing.....	22
2.4 Overview of detected metabolites.....	24
2.5 Effect of temperature stress	29
2.6 Effect of genetic perturbation	30
2.7 Summary	33
Chapter 3. Cell division patterns and metabolic profiles under limited glucose	35
3.1 Introduction.....	35
3.2 Methods	36
3.2.1 Strains and growth conditions.....	36
3.2.2 Measurement of glucose content in culture media	36

3.2.3	Perfusion system microscopy	37
3.2.4	Metabolomic analyses.....	37
3.2.5	Viability measurements	37
3.2.6	Oxidative stress staining.....	37
3.2.7	H ₂ O ₂ resistance assay.....	37
3.3	Cell division under limited glucose	38
3.3.1	Increase in cell number and cell length	38
3.3.2	Cell division timing	39
3.4	Metabolome results.....	40
3.4.1	Ten different glucose concentrations.....	40
3.4.2	Time course analysis of 0 mM glucose condition	44
3.4.3	Time course analysis of 1.1 mM glucose condition	46
3.5	Lifespan and oxidative stress resistance	47
3.6	Summary	50
Chapter 4.	Dissection of ergothioneine and selenoneine biosynthetic pathway.....	54
4.1	Introduction.....	54
4.2	Methods	56
4.2.1	Strains and growth conditions.....	56
4.2.2	Construction of mutants.....	57
4.2.3	Metabolomic analyses.....	58
4.2.4	Spot test experiments.....	58
4.3	Ergothioneine biosynthesis in <i>S. pombe</i>	59
4.3.1	Previously established biosynthetic pathways.....	59
4.3.2	Identification of <i>egt1</i> ⁺	60
4.3.3	Identification of <i>egt2</i> ⁺	61
4.3.4	Verification using deletion mutants.....	62
4.4	Overexpression of <i>egt1</i> ⁺	63
4.5	Role of <i>egt1</i> ⁺ in protection from peroxide	66
4.6	Biosynthesis of selenoneine.....	67
4.7	Summary	73
Chapter 5.	Conclusions	75
5.1	Achievements of this thesis	75
5.2	Limitations and challenges of metabolomics.....	76
5.3	Future developments.....	77

References.....	79
Acknowledgements.....	93

Organization of this thesis

Chapter 1 explains the background and terminology of metabolomics as a research discipline, reviews the available analytical methods for sample measurements and introduces the model organism used in this study, the fission yeast *Schizosaccharomyces pombe*.

Chapter 2 describes the development of metabolome analysis methods in *S. pombe*. We further test the reproducibility of the developed protocols, characterize the influence of cultivation temperature on metabolic profiles, and assess the feasibility of combined use of genetics and metabolomics. To demonstrate the effect of genetic perturbations, we analyzed one deletion strain of a non-essential gene and one temperature-sensitive mutant strain.

Chapter 3 studies the effect of glucose starvation on *S. pombe* cells, focusing mainly on cell division phenotypes and metabolic profiles. As glucose is the most essential nutrient that provides both energy and carbon source, we characterize in detail the effect of various glucose concentrations on cell proliferation. In addition, chronological lifespan, resistance to oxidative stress, and accumulation of specific ‘biomarker’ metabolites are discussed.

Chapter 4 examines in detail the biosynthetic pathway of a proposed antioxidant compound, ergothioneine, in *S. pombe*. As ergothioneine was found to be accumulated in multiple conditions including glucose starvation, we employed genetic and metabolomic analyses to dissect the biosynthetic pathway of this compound in *S. pombe*. In addition, we describe biosynthesis of a selenium-containing ergothioneine derivative, selenoneine.

Finally, **Chapter 5** concludes this thesis, summarizes the achieved progress and discusses the limitations and pitfalls of the introduced technique, as well as potential future developments in this exciting research field.

"If I were doing a PhD, I'd be doing it in metabolomics".

James D. Watson (2013)

Chapter 1. Introduction

1.1 Metabolome and its composition

Metabolites are commonly defined as small molecules that participate in the metabolism of living organisms, either as intermediates or as end products. The exact definition of ‘small molecule’ varies depending on publication, usually referring to molecules having molecular weight (MW) of less than 1,000 Da [1-3]. Some authors set the MW threshold to 1,500 Da [4,5]. Nevertheless, such definitions are not exhaustive, as even some common metabolites can be heavier than the proposed limits. For example, a disulfide form of coenzyme A has a molecular weight of 1,533 Da [6]. Among the largest and most complex natural molecules that are neither polypeptides nor polysaccharides (and can thus be considered metabolites), we can find maitotoxin produced by *Gambierdiscus toxicus*, with molecular weight of 3,424 Da [7]. Furthermore, some metabolites can form polymeric chains, and no clear border exists in terms of number of chain units to distinguish between metabolites and large molecules. Empirically, short peptides (up to ~14 amino acids) and small oligonucleotides (up to ~5 bases) are still regarded as metabolites. The practical definition of metabolite thus depends on the subject being studied.

Metabolites can be hydrophobic or hydrophilic, and can vary greatly in their chemical structures and properties. Majority of metabolites, however, can be classified by their chemical structures into several categories: amino acids, nucleotides, carbohydrates (sugars), organic acids, fatty acids, lipids, alcohols and aldehydes. Larger metabolites can be composed of several units that belong to different chemical categories (Fig. 1.1).

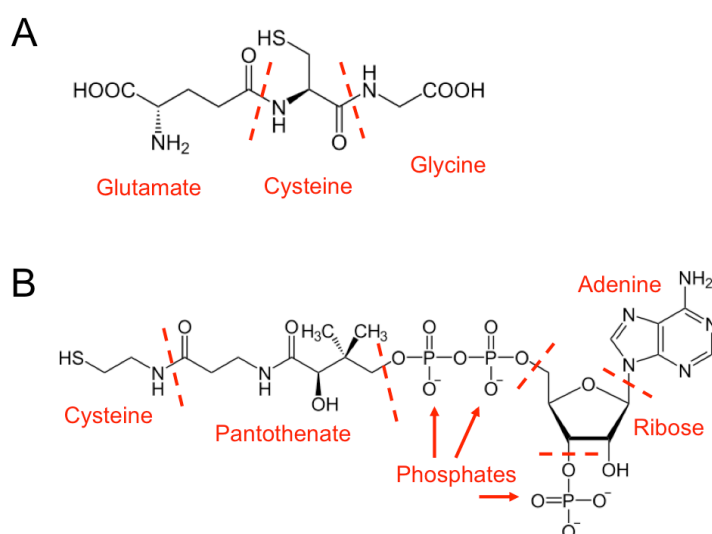


Fig. 1.1. Some metabolites are composed of building blocks that may belong to same or different chemical categories. Common antioxidant glutathione (panel A) is composed of three different amino acids (glutamate, cysteine, and glycine), while coenzyme A (panel B) is composed of a nucleotide base (adenine), a carbohydrate (ribose), an organic acid (pantothenate), an amino acid (cysteine) and three functional groups (phosphates).

From functional perspective, metabolites are divided into two groups: primary metabolites are those directly involved in normal growth, development, and reproduction, while secondary metabolites are compounds nonessential for survival, usually performing ecological function [8]. Examples of secondary metabolites include antibiotics or pigments [9]. Secondary metabolites are often specific to particular taxonomic groups, and outnumber primary metabolites by many orders of magnitude. The variety of secondary metabolites is especially apparent in the plant kingdom, where over 200,000 different structures are known [10]. This can be explained by specific needs of plants, which, unable to move, must rely on chemical warfare to defend themselves from predators. Apart from primary and secondary metabolites, chemical compounds introduced into the organism from outer environment, or xenobiotics, can also participate in cellular metabolism [11].

Metabolites, in conjunction with enzymes, are linked into metabolic pathways, which

together form a broader cell-wide metabolic network (Fig. 1.2). The collection of all metabolites found in a particular biological system is called a ‘metabolome’, in analogy to genome, transcriptome, or proteome, representing collections of all genes, messenger RNAs, or proteins, respectively. The term metabolome was first coined by Oliver et al. [12]. Metabolome can be further divided into endometabolome (metabolites present within cells) and exometabolome (metabolites excreted or produced outside of cells).

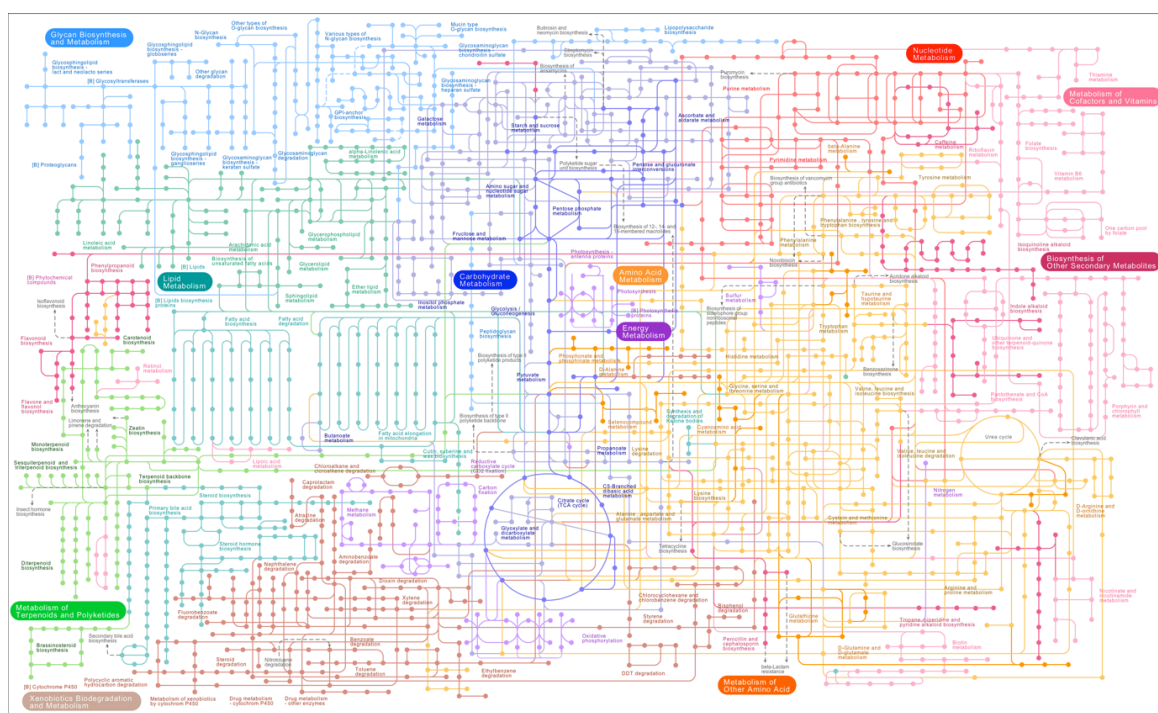


Fig. 1.2. The global metabolic network. Dots denote individual metabolites, while lines indicate enzymatic reactions among them. Colors represent particular areas of metabolism. Image reprinted from the KEGG database [13] with permission.

The knowledge on chemical structures of metabolites and relationships among them in the global metabolic network is essential for successful interpretation of metabolome research data. Various databases are available that collect and curate such information (Table 1.1).

Table 1.1. List of major databases of metabolites and metabolic pathways. For each database, a number of metabolites in it (at the time of writing) and latest reference are indicated. The HMDB, BMDB, YMDB, ECMDB, and StreptomeDB databases are restricted to particular species (human, cow, budding yeast, *E. coli*, and *Streptomyces*, respectively), while other databases are multi-species.

Database	Metabolites	Reference
Kyoto Encyclopedia of Genes and Genomes (KEGG)	17,254	[13]
MetaCyc	11,227	[14]
METLIN Metabolite Database	242,766	[15]
Human Metabolome Database (HMDB)	41,815	[16]
Bovine Metabolome Database (BMDB) ¹	7,859	
Yeast Metabolome Database (YMDB)	2,027	[17]
<i>E. coli</i> Metabolome Database (ECMDB)	2,717	[18]
StreptomeDB	2,444	[19]
The Small Molecule Pathway Database (SMPDB)	1,569	[20]
KNAPSAcK	50,897	[21]
Manchester Metabolomics Database (MMD)	42,687	[22]
Lipid Maps	37,566	[23]

1.2 Metabolomics as a research discipline

‘Metabolomics’ is an experimental approach that aims to qualitatively and quantitatively analyze the metabolome [24]. Although it is a relatively new discipline, it has been rapidly gaining recognition in recent years (Fig. 1.3). The international Metabolomics Society was founded in 2004 with the goal to support research in metabolomics by development of standards, databases, and software tools, and by providing a common platform for communication among researchers in this field. The publication of the Society’s official research journal, *Metabolomics*, commenced in 2005 [25].

¹ Unpublished, accessible on-line at <http://www.cowmetdb.ca>

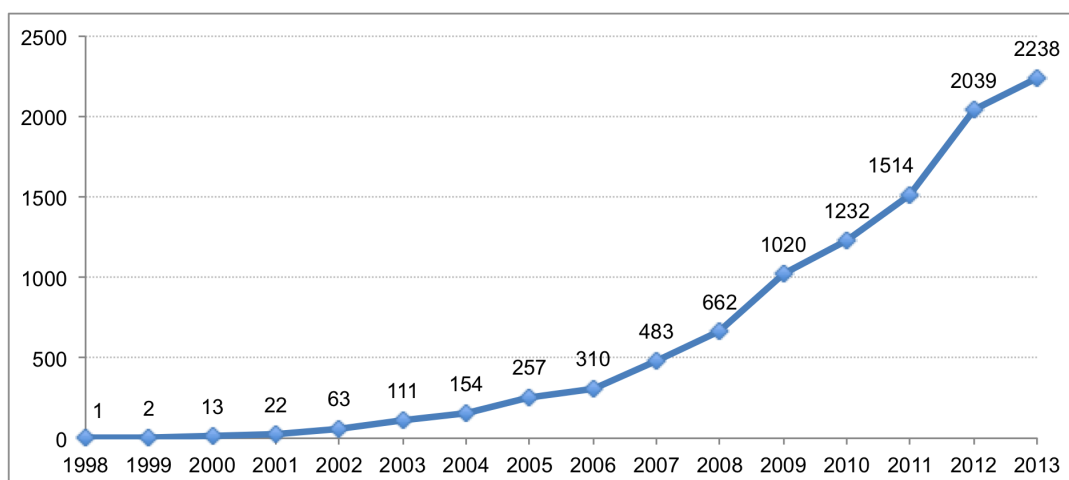


Fig. 1.3. Number of publications per year in the PubMed database² that include any of the terms *metabolome*, *metabolomic*, *metabolomics*, *metabonomic*, or *metabonomics*, in their title or abstract.

The ‘*omics*’ suffix in metabolomics indicates a high-throughput, global analytical approach. Among other *omics* methods, we find genomics (study of genomes), epigenomics (study of epigenetic regulations), transcriptomics (study of messenger RNAs, or transcripts), proteomics (study of proteins), lipidomics (study of lipids), fluxomics (study of molecular fluxes), interactomics (study of molecular interactions), and others. Combined together, these disciplines constitute a research field known as ‘systems biology’, sometimes referred to as ‘systemics’. Systems biology aims to understand biological systems in a global, comprehensive manner. Its approach is closely related to the central dogma of molecular biology, which initially described the information transfer in living systems from DNA to RNA to protein [26]. This original hierarchy can be extended to incorporate modern systems biology view (Fig. 1.4). Notably, in this hierarchy, metabolome comes closest to the cellular phenotype. Metabolomic analysis thus allows detection of otherwise unnoticeable changes in phenotypes, analysis of gene functions, and determination of biomarkers for various cellular conditions [27].

² Accessible on-line at <http://www.pubmed.gov>

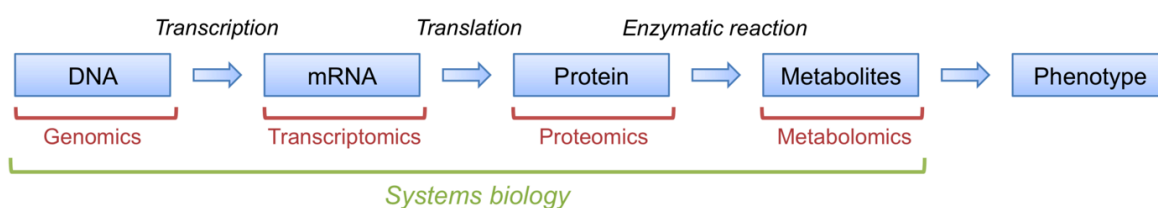


Fig. 1.4. The central dogma of molecular biology, expanded from its original definition [26] to encompass the perspective of systems biology. Arrows indicate normal transfer of information. Figure is inspired by the work of Patti et al. [28].

Some research groups restrict the use of the term ‘metabolomics’ to untargeted studies that aim to characterize all metabolites found in a particular biological system (including unknowns), and prefer to use other terms for specific types of metabolome analyses [27,29-32]:

- **Metabonomics.** Study of metabolic responses to external stimuli, such as genetic or environmental perturbations, disease, or drug treatment.
- **Metabolite target analysis.** Targeted, quantitative measurement of a small set of selected metabolites. Sample preparation methods are optimized for the target compounds.
- **Metabolite profiling.** Measurement of a specific subset of the metabolome. In clinical environment, this often means tracing the metabolic fate of a drug or a target molecule.
- **Metabolic fingerprinting.** Measurement of the overall signature of the metabolome, often for diagnostic purposes. Recognition of patterns is more important than identification of specific metabolites.
- **Metabolic footprinting.** Measurement of the exometabolome, or compounds excreted from a cell or an organism, typically for the purpose of taxonomic classification.

However, as the terminology is not perfectly established in the research community, I shall continue using the term ‘metabolomics’ in its broader meaning throughout this thesis.

1.3 Analytical methods in metabolomics

Although biologists have studied individual metabolic reactions and pathways for centuries, comprehensive metabolomic analyses have become possible only in recent years owing to advancements in measurement technology. The two methods most commonly applied to analyze and quantify metabolites are nuclear magnetic resonance spectroscopy (NMR) and mass spectrometry (MS) [33,34].

1.3.1 Nuclear magnetic resonance spectroscopy

NMR is an analytical technique that exploits magnetic properties of certain atomic nuclei (^1H and ^{13}C being most commonly used for measurements of organic molecules). It detects transitions between the spin states of the nuclei as they absorb and re-emit electromagnetic radiation, while polarized by a strong magnetic field (1-20 T magnets are used in modern NMR instruments). The spectra produced by NMR are diagnostic of the chemical structures of analyzed molecules. The main advantages of NMR are simple sample preparation, non-destructive analysis that typically does not require any chromatographic separation (samples can thus be completely recovered), and high analytical reproducibility, making NMR an optimal technique for quick pattern recognition (metabolic fingerprinting). On the other hand, the sensitivity of NMR is relatively poor compared to MS, and identification of individual metabolite signals in complex NMR spectra is rather difficult.

NMR is a well established technique in metabolomics, and has been successfully applied in toxicology [35], drug discovery [36], or targeted quantitative metabolomics [37]. Another advantage of NMR is the ability to provide structural information on unknown molecules, if these can be purified in sufficient amounts. In most cases, an amount in the order

of 1 mg of pure substance is required to successfully establish its chemical structure using NMR [38].

1.3.2 Mass spectrometry

Mass spectrometry is a powerful and versatile analytical technique with a wide range of applications in biology and chemistry. In principle, it measures mass-to-charge ratios (m/z) of ionized molecules. A mass spectrometer is composed of an ion source, a mass analyzer and a mass detector [39]. The ion source is responsible for converting sample molecules into ions, the mass analyzer separates the ions by their m/z ratio, and the mass detector measures the actual m/z values, providing also quantitative data on the abundance of ions at each m/z . Modern mass analyzers such as time-of-flight (TOF) or Orbitrap provide very accurate m/z measurements, with errors in the order of several ppm [40].

As the capacity of ions that can be measured simultaneously in the mass analyzer is limited, chromatographic separation is often employed to improve the coverage of complex mixtures, giving rise to hyphenated techniques: gas chromatography-mass spectrometry (GC-MS), liquid chromatography-mass spectrometry (LC-MS), or capillary electrophoresis-mass spectrometry (CE-MS) [41]. Chromatographic separation adds another dimension (retention time) to the MS-based separation by m/z . The characteristics of the three most common hyphenated techniques are summarized below:

- GC-MS is based on passing molecules in gas phase through a long capillary column (typically 15 m or longer) under a temperature gradient. It has the longest history among the hyphenated methods, provides very high chromatographic resolution, but requires chemical derivatization for non-volatile compounds. Furthermore, as only fragments of the original molecules are detected, identification of unknown compounds is difficult.

Recent developments of this technique include GC×GC-MS (two dimensional separation) or GC-HRMS (high resolution mass spectrometry).

- LC-MS separates molecules by flowing a liquid solvent (mobile phase) through a separation column (stationary phase). The enormous variability of mobile and stationary phase choices allows for development of separation methods for virtually any kind of molecules. On the other hand, no single method is suitable for all types of compounds. LC-MS offers the best sensitivity among these methods, however reproducibility of separation can be affected by complicated chemical interactions among the mobile phase, stationary phase, and sample matrix.
- CE-MS is based on migrating analytes through an electrolyte solution in the presence of an electric field. This technique is therefore only applicable to charged molecules. However, due to polar nature of many cellular metabolites, CE-MS is a convenient technique for common metabolomic applications. Its advantages are very good chromatographic resolution, and low consumption of sample.

In addition to hyphenated MS methods, recent developments of ambient ionization techniques such as direct analysis in real time [DART; 42] or desorption electrospray ionization [DESI; 43] allow for rapid, non-destructive surface analyses of any kind of materials such as tissues, thus competing with NMR for quick metabolic fingerprinting. Overall, the versatility and sensitivity of mass spectrometry makes it the analytical technique of choice for many research groups in metabolomics [44].

1.4 The fission yeast, *Schizosaccharomyces pombe*

The fission yeast *Schizosaccharomyces pombe* (Fig. 1.5) is an excellent unicellular

eukaryotic model organism. Its relatively small genome consists of three chromosomes and ~13 Mbp DNA [45], encoding about five thousand protein-coding genes that are thoroughly annotated in a convenient on-line database [PomBase; 46]. Fission yeast is thus one of the simplest known organisms in the Eukaryota domain, in terms of genome complexity. Detailed methods for its cultivation and genetic manipulation have been developed [47,48]. In addition, a genome-wide library of gene deletion strains is commercially available [49].

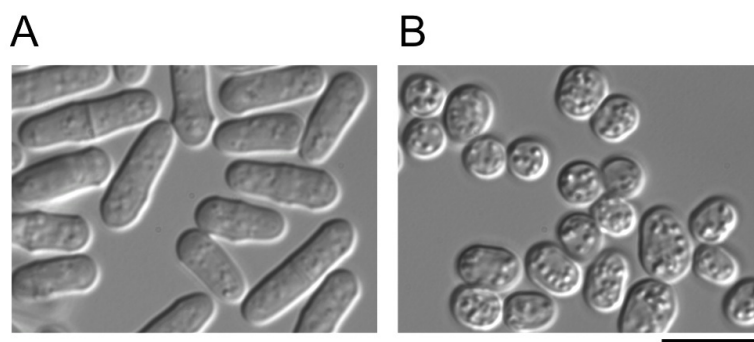


Fig. 1.5. Micrographs of fission yeast *Schizosaccharomyces pombe* cells in vegetative (A) and quiescent (B) phases. The quiescent phase was induced by nitrogen starvation [50]. Bar = 10 μ m.

Fission yeast has been successfully employed in the studies of numerous basic cellular processes, such as cell division cycle [51], chromosome segregation [52], meiosis [53], cytoskeletal organization [54], DNA damage repair [55], DNA replication [56], gene silencing [57], or RNA interference [58]. Furthermore, genome-wide transcriptomic [59-61] and proteomic [62-64] analyses have been performed using this organism.

Our laboratory employs fission yeast as a model organism to study cellular quiescence and its regulation by nutrition [65,66]. As nutrients are also metabolites, we consider metabolomic analysis an essential tool to address these biological problems. Prior to this work, however, the techniques of metabolomic analysis were not seriously explored in *S. pombe*. We thus proceeded to develop the basic protocols and methods for metabolite extraction and measurement.

Chapter 2. Development of metabolomic analysis in fission yeast

Note: This study was published in *Molecular BioSystems* [67]. Majority of figures and tables in this Chapter were adapted from the published article with slight modifications (reproduced by permission of The Royal Society of Chemistry).

2.1 Introduction

The fission yeast truly earned its respect as a model organism by the discovery of a conserved genetic control of the cell division cycle [51]. It is worth noting, however, that basic cellular processes – including, but not limited to, cell division – are also regulated by extracellular environment and nutrition. Understanding the cellular conditions at metabolic level is thus important for studying certain cellular phenomena such as quiescence, senescence, or aging, or for modeling metabolic diseases (e.g. diabetes). Arguably, these aspects of biomedical research might become central in the 21st century, and metabolomics is thus turning into an essential tool to obtain a whole, system-level picture of the cellular conditions.

The budding yeast *Saccharomyces cerevisiae* was among the first microorganisms to be thoroughly analyzed using the metabolomic approach [68]. Since then, a number of studies were reported on various aspects of cell metabolism, growth-rate control, and metabolic engineering [69-72]. In case of fission yeast, however, the exploration of its metabolome has begun much more recently. The first reference to metabolomics in relation to *S. pombe* occurred in the study of a MAP-kinase deletion mutant $\Delta sty1$ under oxidative stress by a combination of proteomic

analysis and a small-scale (29 metabolites) metabolomic analysis using $^1\text{H-NMR}$ [73]. Later, Bolten and Wittmann [74] validated two common microbial metabolome sampling protocols for the analysis of intracellular amino acids in five different yeasts, including *S. pombe*. To our knowledge, however, the present study is the first attempt to characterize the fission yeast metabolome in a comprehensive manner.

2.2 Scale of fission yeast metabolome

Unlike the genome, the composition of metabolome is not encoded in a single readable entity such as DNA. New chemical structures can be produced from existing compounds by enzymes or by spontaneous interactions with reactive molecules such as free radicals. The total number of distinct metabolites present in a cell can thus only be estimated. This is further complicated by the fact that the constitution of the metabolome greatly depends on the outer environment, especially on chemical composition of available nutrients and their abundance.

To estimate the approximate scale of the whole fission yeast metabolome, we can first examine the results published about its sister model organism, the budding yeast. The Yeast Metabolome Database (YMDB), an on-line curated resource that annotates all metabolites reported so far in budding yeast [17], contains 2,027 unique metabolite structures in total (see Table 1.1). Another estimate can be obtained from reconstructed genome-wide metabolic models published using the Systems Biology Markup Language [SBML; 75]. For budding yeast, several models were constructed in the past [76], finally culminating into a consensus community-driven metabolic network model [77]. The latest version of this model (v. 7.11)³ contains 2,386 metabolites annotated with chemical formulas. In case of fission yeast, the first genome-scale SBML-based metabolic model SpMBEL1693 was recently introduced,

³ Accessible on-line at <http://yeast.sf.net>

containing 1744 metabolites and 1693 metabolic reactions [78]. It should be noted, however, that due to the nature of these systems biology models, identical chemical compounds present in different cellular compartments (e.g. ATP in cytoplasm vs. ATP in mitochondria) are counted as different metabolites. On the other hand, some entities in the models are described using ‘Markush’ structures containing R-groups and represent thus heterogeneous chemical compounds. In conclusion, we can roughly estimate that the total number of distinct metabolites present in a fission yeast cell might lie somewhere in the order of several thousand.

2.3 Method development

2.3.1 Metabolite measurement

For analysis of metabolite extracts, we decided to employ high resolution MS, because this technology is particularly suited for microbial metabolomics [79] and allows unambiguous isolation of individual molecular signals, even for yet unidentified metabolites. We considered such capability essential, as little was known about the overall composition of fission yeast metabolome. For chromatographic separation, we selected LC for its superior sensitivity and versatility. A mixture of pure metabolite standards was prepared for initial LC-MS method development. After testing several types of separation columns (C18, Hypersil GOLD, Hypercarb, and others), as well as different compositions of mobile phase, we settled on a method using a hydrophilic interaction liquid chromatography (HILIC) column. HILIC is particularly suitable for separation and detection of polar compounds in combination with MS [80]. Due to the polar nature of many cellular metabolites, HILIC presents a very convenient separation technique. The complete specification of the developed chromatographic method is as follows: 100% acetonitrile was used as mobile phase A; 10 mM ammonium carbonate

(pH 9.3) was used as mobile phase B; gradient elution from 80% A to 20% A was performed in 30 min; flow rate was set to 100 $\mu\text{L}/\text{min}$. The MS instrument was equipped with electrospray ionization (ESI) interface and mass spectra were acquired in full scan mode (100 – 1,000 m/z). The raw LC-MS data of a mixture of pure metabolite standards analyzed using this method are shown in Fig. 2.1.

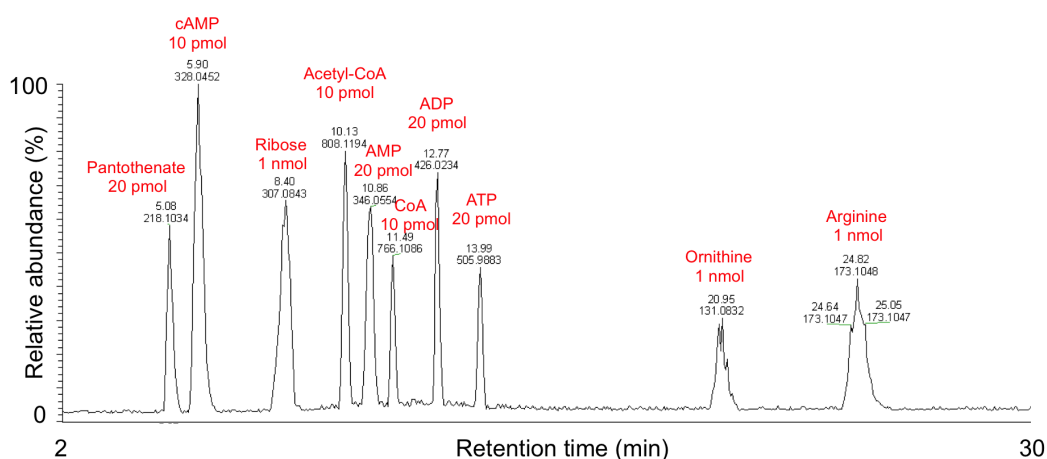


Fig. 2.1. Raw LC-MS data (total ion chromatogram) of a mixture of pure metabolites analyzed by MS in negative ionization mode. A total amount (mol) of each injected metabolite is indicated above each peak.

2.3.2 Peak identification

We employed the Orbitrap MS detector, which offers very high mass accuracy (less than 5 ppm m/z error), and also allows automatic collection of fragmentation spectra through tandem MS, or MS/MS [81]. We found that in positive ionization mode using ESI, most metabolite ions were singly charged, protonated type (usually designated $[\text{M}+\text{H}]^+$). Conversely, in negative ionization mode, majority of metabolite ions were produced by deprotonation (designated $[\text{M}-\text{H}]^-$). To identify compounds, we first calculated the neutral molecular mass by removing or adding the mass of a proton ($\text{neutral mass} = m/z \pm 1.0078 \text{ Da}$), depending on the ionization mode. The molecular mass was then searched in metabolite databases (see Table 1.1) within 5-ppm tolerance window, to obtain metabolite candidates. For reasonable candidates,

pure standards were purchased and analyzed to verify their retention times. For mass signals that are not found in any metabolite database, a generic chemical structure databases can be searched, such as the PubChem Compound Database⁴ maintained by the National Center for Biotechnology Information (contains over 50 million chemical structures to date) or the ChemSpider Database⁵ maintained by the Royal Society of Chemistry (contains over 30 million structures).

The structural information that can be obtained by MS is limited, however the option to acquire fragmentation spectra was found very useful for identification of certain isomeric compounds (Fig. 2.2). Isomers, by definition, have the same molecular mass, and their retention times can, in some cases, be very similar. MS/MS analysis can thus provide an additional degree of confidence for correct compound identification. Furthermore, MS/MS spectra can be searched in spectral databases such as MassBank [82] or MetiTree [83], or compared to predicted fragmentation spectra [84,85]. Recently, Gerlich and Neumann [86] introduced an integrated identification strategy called MetFusion that combines a spectral database search with *in silico* fragmentation prediction.

⁴ Available on-line at <http://pubchem.ncbi.nlm.nih.gov/>

⁵ Available on-line at <http://www.chemspider.com/>

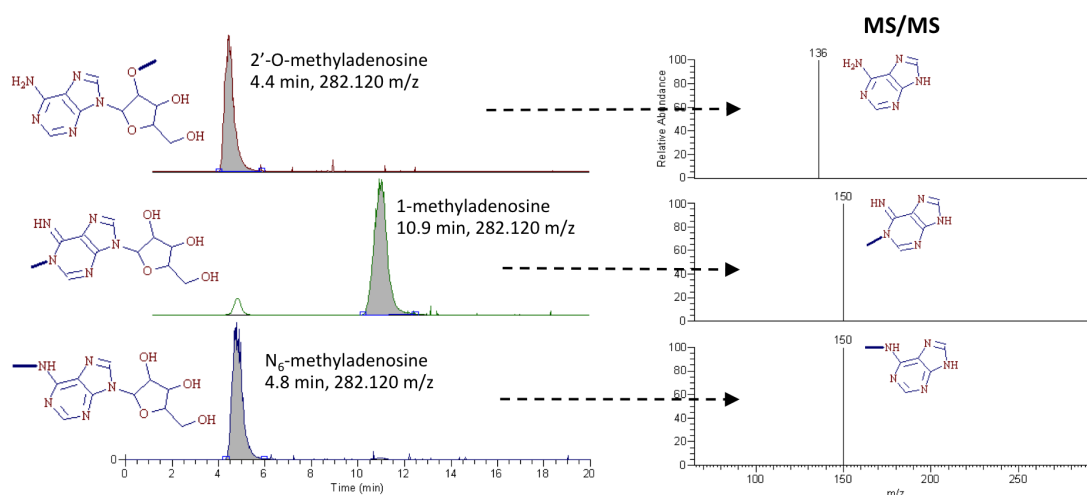


Fig. 2.2. The LC-MS data of three isomers of methyladenosine were compared. While 2'-*O*-methyladenosine and *N*₆-methyladenosine could not be distinguished solely using their *m/z* values and retention times, they could be clearly distinguished by their MS/MS fragmentation patterns.

Another technique, which was found very useful for identification of certain types of molecules, is isotopic pattern analysis. Isotopes of chemical elements are distributed in nature in constant, well-described abundances [87]. The chemical formula of each compound thus determines the pattern of isotopes that are detected in its mass spectrum. Typically, besides the main (monoisotopic) peak, signals of naturally occurring ¹³C, ¹⁵N, or ³⁴S are detected from organic molecules. However, the unique isotopic distributions of certain elements (e.g. Fe, Cu, Cl, Br, B, and some others) produce characteristic patterns that can reveal the presence of such elements, and thus greatly support the identification of compounds (Fig. 2.3). We later developed an automated software tool for prediction of chemical formulas from mass spectra, taking advantage of the isotopic distributions [88].

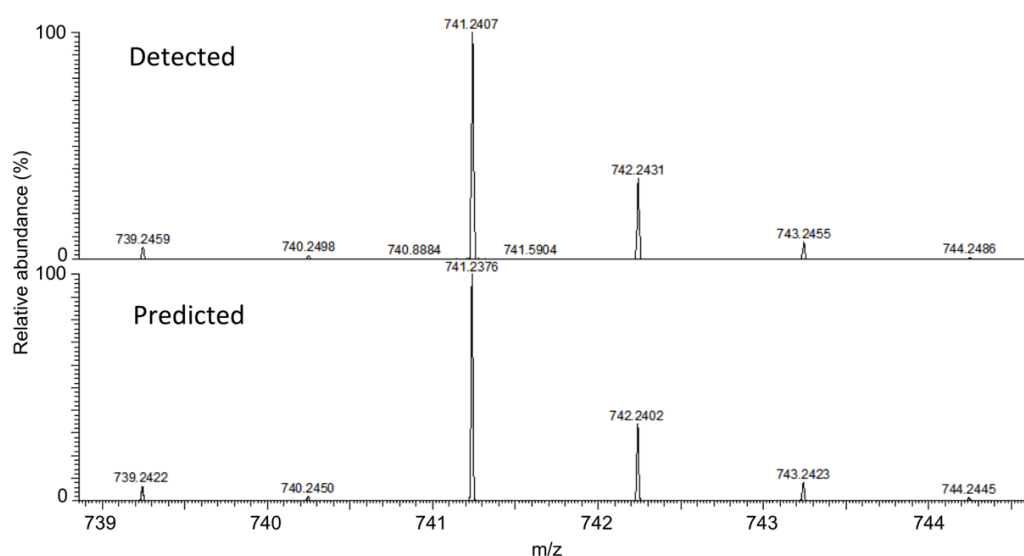


Fig. 2.3. Comparison of narrow sections of mass spectra (approx. 739 – 744 m/z) showing the isotopes of a cellular siderophore compound, ferrichrome [89]. The detected spectrum (upper panel) was acquired from a sample containing ferrichrome. The predicted spectrum (bottom panel) was calculated from the chemical formula of the ferrichrome $[M+H]^+$ ion ($C_{27}H_{43}FeN_9O_{12}^+$), assuming naturally distributed isotopes.

2.3.3 Compound quantification

The quantitative potential of the developed LC-MS method was assessed by injecting pure standards of several metabolites in 10-fold dilutions, and integrating the areas of the peaks corresponding to each metabolite ion (Fig 2.4.). For each individual compound, we found a good correlation between the injected amount and the resulting peak area. However there were significant differences among the compounds. For example, the peak area produced by 1 pmol injection of arginine was almost 1,000-fold smaller than that of 1 pmol injection of UDP-glucose. This implies that such LC-MS measurements should be considered strictly semi-quantitative, and comparisons among samples should be restricted to the peak areas of the same compound.

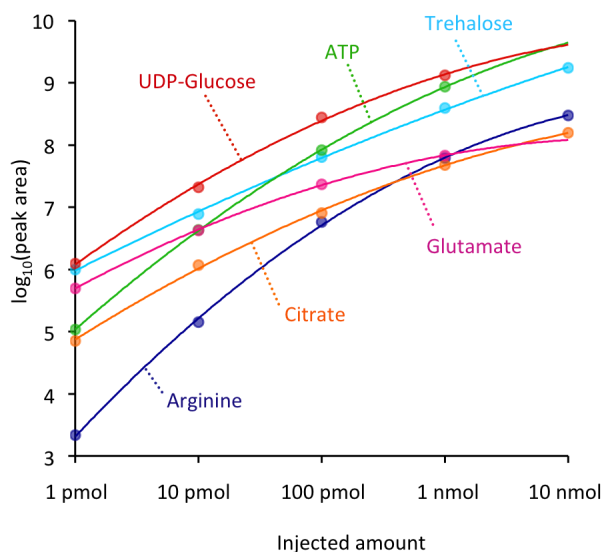


Fig. 2.4. The amount of injected pure compounds (mol, X-axis) and resulting size of peak area (arbitrary units, Y-axis) obtained by LC-MS were plotted for six compounds. Trend lines were constructed by applying quadratic regression on the \log_{10} -scale data.

2.3.4 Cell cultivation

Various culture media are used for the cultivation of fission yeast [47], as summarized in Table 2.1. For metabolomic analysis, we decided to cultivate the cells in a synthetic culture medium EMM2, which is based mostly on glucose and ammonium chloride, with supplements of vitamins and minerals. We assume that rich media with unknown chemical composition, such as YE (based on yeast extract) or YPD (based on yeast extract and polypeptone), cannot guarantee reproducible metabolic conditions, particularly among different laboratories.

For the preparation of metabolite extracts, liquid cell cultures were incubated in water-bath shakers. Temperature of the shakers was maintained at 26°C or 36°C, depending on experiment.

Table 2.1. Composition of the synthetic (EMM2), rich (YE and YPD), and sporulation-inducing (MEA) culture media for cultivation of fission yeast, as used in our laboratory. Media are sterilized by autoclaving. Solid media (plates) are prepared by the addition of 17 g/L agar.

Medium	Component	Amount	Concentration
EMM2	Potassium hydrogen phthalate	3 g/L	14.7 mM
	Disodium hydrogen phosphate	2.2 g/L	15.5 mM
	Ammonium chloride	5 g/L	93.5 mM
	Glucose	20 g/L	111 mM
	Magnesium chloride hexahydrate	1.05 g/L	5.2 mM
	Calcium chloride dihydrate	14.7 mg/L	0.1 mM
	Potassium chloride	1 g/L	13.4 mM
	Sodium sulfate	40 mg/L	0.3 mM
	Calcium pantothenate	1 mg/L	2.1 μ M
	Nicotinic acid	10 mg/L	81.2 μ M
	myo-Inositol	10 mg/L	55.5 μ M
	Biotin	0.01 mg/L	0.04 μ M
	Boric acid	0.5 mg/L	8.1 μ M
	Manganese(II) sulfate pentahydrate	0.63 mg/L	2.6 μ M
	Zinc sulfate heptahydrate	0.4 mg/L	1.4 μ M
	Iron(III) chloride hexahydrate	0.2 mg/L	0.7 μ M
	Molybdcic acid	0.04 mg/L	0.3 μ M
	Potassium iodide	0.1 mg/L	0.6 μ M
	Copper(II) sulfate pentahydrate	0.04 mg/L	0.2 μ M
Citric acid monohydrate	1 mg/L	4.8 μ M	
YE	Yeast extract	5 g/L	
	Glucose	30 g/L	167 mM
YPD	Yeast extract	10 g/L	
	Polypeptone	20 g/L	
	Glucose	20 g/L	111 mM
MEA	Malt extract	30 g/L	

2.3.5 Quenching

Prior to metabolome sample preparation, cells must be rapidly quenched to cease further chemical reactions and provide a snapshot of the immediate state of the metabolism. In budding yeast, the most commonly used method for rapid quenching is based on submerging the cells into a cold (-40°C) methanol solution (50%, 60% or 100%, depending on publication), as originally introduced by de Koning and van Dam [90]. Later, it was demonstrated that using 100% methanol for quenching prevents leakage of metabolites [91]. We thus applied pure -40°C methanol as a quenching solution for *S. pombe*.

2.3.6 Metabolite extraction

For the extraction of intracellular metabolites from budding yeast, a number of protocols have been developed [92]. Unfortunately, due to a huge variation in physical and chemical properties, as well as intracellular concentrations, no single method can guarantee an efficient extraction of all classes of metabolites. Villas-Bôas et al. [93] compared six different protocols for extraction of intracellular metabolites from budding yeast, concluding that freeze-thawing in liquid nitrogen followed by centrifugation in pure cold methanol (-40°C) provided the best recovery of a wide range of compounds. However, Canelas et al. [94] argued that the freeze-thawing method did not ensure proper inactivation of enzymatic activity. They recommended the use of boiling ethanol or chloroform-methanol extractions. Sporty et al. developed a protocol for the measurement of NAD⁺ and NADH, applying bead beating in ice-cold ammonium acetate for cell lysis [95]. Recently, Kim et al. [96] proposed the use of acetonitrile/water mixture (1:1 v/v) at -20°C as an efficient extraction solvent.

As there is no single protocol to extract and measure all metabolites, we decided to

focus our analysis on polar metabolites such as amino acids, organic acids, nucleotides, sugars, or sugar-phosphates. These compounds perform a variety of functions in the cells and collectively thus provide a good description of the overall cellular condition. The development of our metabolite extraction protocol for *S. pombe* was based on the goal that it should be easily applicable to a wide range of cell culture volumes (a few mL for quick screening experiments, up to a several L for the purpose of purification of unknown metabolites). We thus adopted a combination of fast filtration and cold methanol quenching. First, the cell cultures were vacuum-filtered on a methanol-resistant membrane filter, and the filter including the cell biomass was immediately submerged into 25 mL pure -40°C methanol. This method allows rapid collection and quenching of even large volumes of cell cultures. After quenching, we added 10 nmol of 4-(2-hydroxyethyl)-1-piperazineethanesulfonic acid (HEPES) and 10 nmol of piperazine-*N,N'*-bis(2-ethanesulfonic acid) (PIPES) into each sample, as internal standards.

We found that metabolites from vegetatively growing *S. pombe* cells could be efficiently extracted by repeated centrifugation in 50% cold methanol, as demonstrated by propidium iodide (PI) staining (Fig. 2.5). However, in case of nitrogen-starved quiescent cells, the staining by PI was considerably less intense, indicating inefficient disruption of cellular membranes. We thus decided to employ a Multi-Beads Shocker system (Yasui Kikai, Osaka, Japan) for cell disruption. This system can efficiently and completely disrupt even highly resistant nitrogen-starved cells, as also shown in Fig. 2.5.

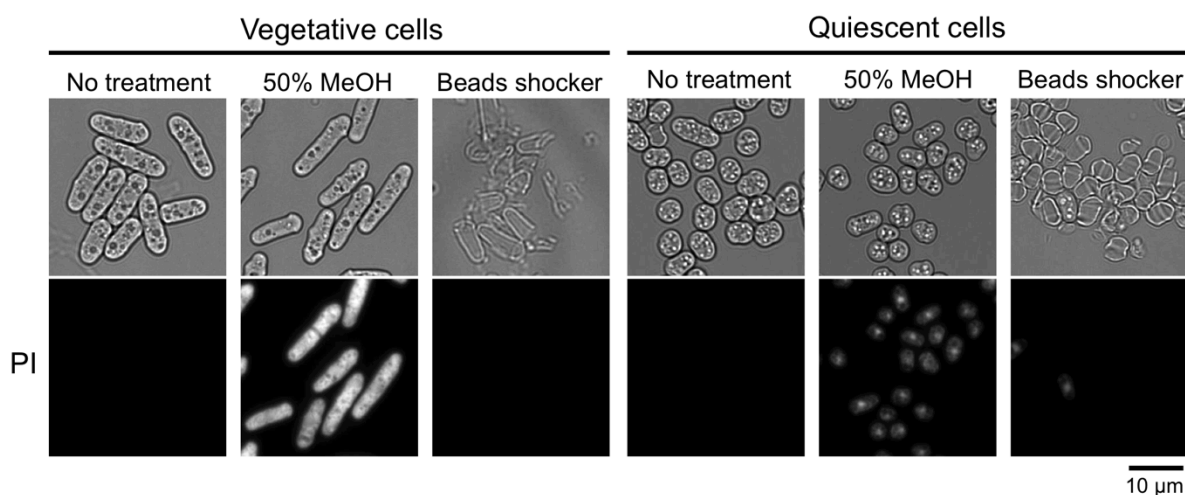


Fig. 2.5. Propidium iodide (PI) staining of nucleic acids. Bright staining indicates successful disruption of cellular membranes. Vegetative cells were cultivated in EMM2 medium. Quiescent cells were produced by nitrogen starvation (24 h in EMM2-N medium).

Following the extraction of metabolites, we applied 10-kDa cut-off filtration to remove proteins and other crude cellular components from the samples. As a final step of sample preparation, we concentrated the samples on a vacuum evaporator. After evaporation, the samples were re-suspended in 40 μL of 50% acetonitrile for LC-MS analysis. The complete workflow is summarized in Fig. 2.6.

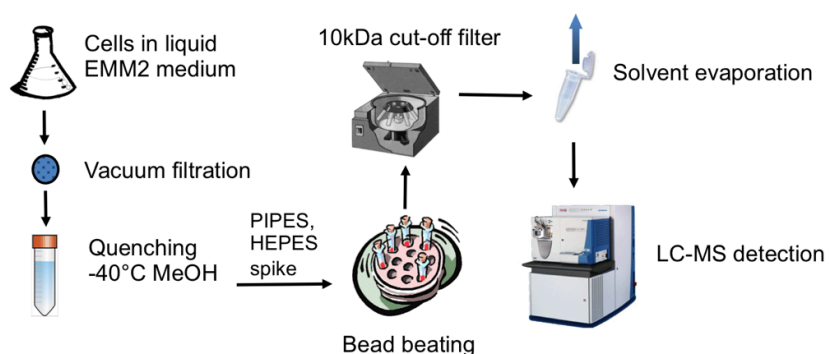


Fig. 2.6. A schema of the metabolome sample preparation workflow.

2.3.7 Data processing

Raw LC-MS data produced by the instrument has three dimensions: retention time

(measured by LC), m/z (measured by MS), and signal intensity (also measured by MS). An example of such three-dimensional data set is shown in Fig. 2.7.

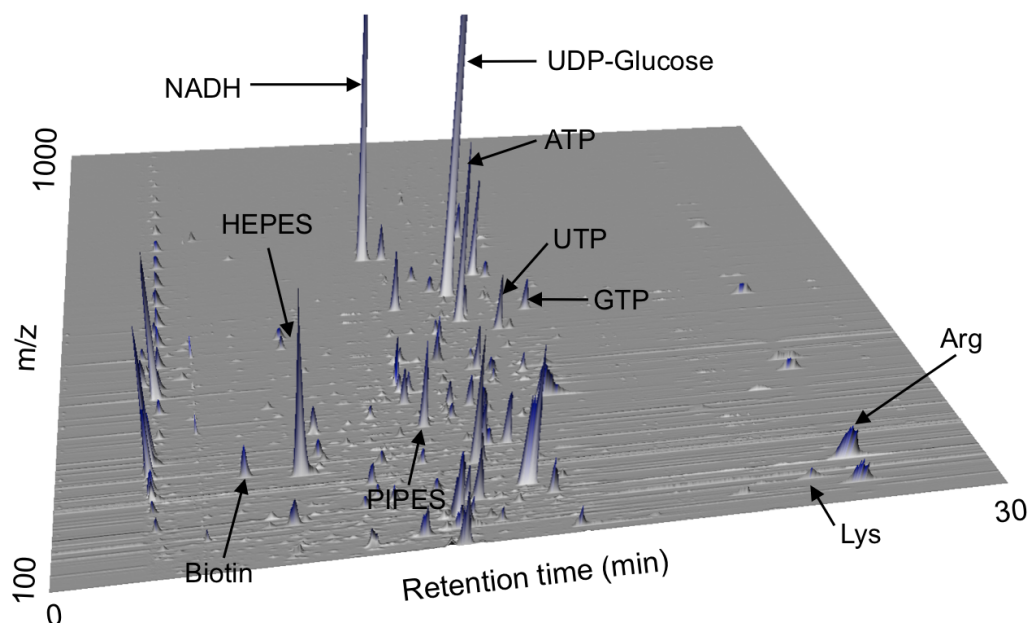


Fig. 2.7. A three-dimensional plot of raw LC-MS data of a single sample injection, acquired in negative ionization mode. Z-axis represents signal intensity. Several identified metabolites are annotated by labels. PIPES and HEPES peaks correspond to the spiked internal standards.

In order to extract biologically relevant information from such raw LC-MS data, the data must first be processed, that is translated into lists of detected peaks. A number of software tools for processing of raw LC-MS data have been introduced [97,98]. We have applied a data processing protocol using the free MZmine 2 framework for MS data visualization and analysis, which was co-developed by the author [99; see Thesis Supplements]. The minimal steps required for processing of the raw MS data include:

1. **Raw data preprocessing.** Depending on the quality of the LC-MS instrumentation, raw data might benefit from application of filtering or smoothing algorithms to produce better results in peak detection.

2. **Peak detection (also called feature detection).** Each detected peak is characterized by its retention time (from LC), m/z value (from MS) and area (obtained by integrating the peak shape over retention time, for quantification).
3. **Deisotoping.** Isotopic signals, produced by naturally occurring heavy isotopes of common elements (such as ^{13}C , ^{15}N , ^{34}S etc.) are removed from the produced peak lists.
4. **Alignment.** Peak lists generated from each raw data file are aligned to match corresponding signals with the same m/z and retention time. In the aligned data sets, gaps (misaligned or undetected peaks) may be filled by secondary peak detection
5. **Normalization.** Signal intensities and peak areas are normalized using the spiked internal standards (PIPES and HEPES, in our case). This step is optional, but it helps to reduce the effects of daily instrument variation.

The detailed description of the data processing steps and parameters we applied is included in the published article [67].

2.4 Overview of detected metabolites

Table 2.2 summarizes the number of peaks detected from a single metabolite extract prepared from a vegetative *S. pombe* culture. In total, over 6,000 peaks were detected in both ionization modes. We employed the detection modules of the MZmine 2 software to identify ionization artifacts, such as adducts or fragments (781 peaks in the negative ESI mode and 946 peaks in the positive ESI mode), leaving a total of 4,476 (1,942 + 2,534) potential metabolite peaks. Among these, 335 were detected in both ionization modes (these were recognized by showing the same retention time and a mass difference of 2.016 m/z = two protons). Among the potential metabolite peaks, we successfully identified 123 distinct metabolites, and 108 of these were verified by pure standards (Table 2.3).

Table 2.2. Summary of detected peaks and their classification.

	Negative ESI mode	Positive ESI mode
Total detected peaks	2723	3480
Non-metabolite peaks	781	946
Na adducts	172	207
K adducts	12	55
Mg adducts	4	6
NH ₃ adducts	4	54
H ₃ PO ₄ adducts	16	4
H ₂ SO ₄ adducts	17	4
H ₂ CO ₃ adducts	39	57
Peak complexes	255	214
In-source fragments	262	345
Potential metabolite peaks	1942	2534
	(335 in both modes)	
Identified metabolites	98	102
	(77 in both modes)	

Table 2.3. List of all identified metabolites, sorted alphabetically. Compounds in *italics* could not be verified using a pure standard, therefore representing only putative identification. Ionization modes (neg, pos) indicate in which ionization modes the metabolite was detected. The ionization mode indicated in **bold** provided better signal intensity. RT = retention time.

Metabolite	Chemical formula	Ionization modes	m/z	RT (min)
1-Methyladenosine	C ₁₁ H ₁₅ N ₅ O ₄	pos	282.121	10.8
1-Methylguanosine	C ₁₁ H ₁₅ N ₅ O ₅	pos	298.116	6.4
2-Aminoadipate	C ₆ H ₁₁ NO ₄	pos	162.076	11.9
2-Keto-3-deoxyoctonate	C ₈ H ₁₄ O ₈	neg	237.061	10.7
2-Oxoglutarate	C ₅ H ₆ O ₅	neg	145.014	12.1
3'-5'-cAMP	C ₁₀ H ₁₂ N ₅ O ₆ P	neg pos	328.044	5.8
4-Guanidinobutyrate	C ₅ H ₁₁ N ₃ O ₂	pos	146.093	12.0
5-Aminovalerate	C ₅ H ₁₁ NO ₂	neg	116.072	11.8
5-Phosphoribose-1-diphosphate	C ₅ H ₁₃ O ₁₄ P ₃	neg pos	388.943	16.3
6-Phospho-gluconate	C ₆ H ₁₃ O ₁₀ P	neg pos	275.017	14.8
Acetyl-CoA	C ₂₃ H ₃₈ N ₇ O ₁₇ P ₃ S	neg pos	810.137	10.1
<i>Acetyl-glutamine</i>	C ₇ H ₁₂ O ₄ N ₂	neg pos	189.088	7.0

Table 2.3 (continued)

Metabolite	Chemical formula	Ionization modes	m/z	RT (min)
Adenine	C ₅ H ₅ N ₅	pos	136.062	6.2
Adenosine	C ₁₀ H ₁₃ N ₅ O ₄	pos	268.105	5.9
ADP	C ₁₀ H ₁₅ N ₅ O ₁₀ P ₂	neg pos	426.021	12.3
AMP	C ₁₀ H ₁₄ N ₅ O ₇ P	neg pos	346.055	10.7
Arabitol	C ₅ H ₁₂ O ₅	neg	151.061	9.4
Arginine	C ₆ H ₁₄ N ₄ O ₂	neg pos	175.119	22.8
Asparagine	C ₄ H ₈ N ₂ O ₃	neg	131.046	11.7
Aspartate	C ₄ H ₇ NO ₄	neg pos	134.045	11.9
ATP	C ₁₀ H ₁₆ N ₅ O ₁₃ P ₃	neg pos	505.988	13.5
Betaine (trimethyl-glycine)	C ₅ H ₁₁ NO ₂	pos	118.087	8.0
Biotin	C ₁₀ H ₁₆ N ₂ O ₃ S	neg pos	245.096	5.2
CDP	C ₉ H ₁₅ N ₃ O ₁₁ P ₂	neg pos	402.010	14.2
Citramalate	C ₅ H ₈ O ₅	neg	147.030	12.0
Citrate	C ₆ H ₈ O ₇	neg pos	191.019	15.0
Citrulline	C ₆ H ₁₃ N ₃ O ₃	neg pos	176.104	12.8
CMP	C ₉ H ₁₄ N ₃ O ₈ P	neg pos	322.044	12.8
Coenzyme A	C ₂₁ H ₃₆ N ₇ O ₁₆ P ₃ S	neg pos	768.128	11.4
<i>Coenzyme B</i>	C ₁₁ H ₂₂ NO ₇ PS	neg pos	344.092	9.6
CTP	C ₉ H ₁₆ N ₃ O ₁₄ P ₃	neg pos	481.976	15.3
Cytidine	C ₉ H ₁₃ N ₃ O ₅	pos	244.094	8.6
Deferriferrichrome	C ₂₇ H ₄₅ N ₉ O ₁₂	neg	686.312	5.5
Dimethyl-arginine	C ₈ H ₁₈ N ₄ O ₂	pos	203.151	18.9
<i>Dimethyl-glutamate</i>	C ₇ H ₁₃ NO ₄	pos	176.092	8.0
Dimethyl-guanosine	C ₁₂ H ₁₇ N ₅ O ₅	pos	312.132	5.6
Dimethyl-lysine	C ₈ H ₁₈ N ₂ O ₂	pos	175.145	18.4
<i>Disaccharide-phosphate</i>	C ₁₂ H ₂₃ O ₁₄ P	neg	421.074	14.4
Ectoine	C ₆ H ₁₀ N ₂ O ₂	neg	141.067	10.4
Ergothioneine	C ₉ H ₁₆ N ₃ O ₂ S	pos	230.097	11.5
FAD	C ₂₇ H ₃₃ N ₉ O ₁₅ P ₂	neg pos	786.168	8.5
Ferrichrome	C ₂₇ H ₄₂ FeN ₉ O ₁₂	neg pos	739.222	4.4
<i>FGAR</i>	C ₈ H ₁₅ N ₂ O ₉ P	neg pos	313.044	12.2
Fructose-1-6-diphosphate	C ₆ H ₁₄ O ₁₂ P ₂	neg pos	338.988	15.5
Fructose-6-phosphate	C ₆ H ₁₃ O ₉ P	neg	259.022	13.0
Fumarate	C ₄ H ₄ O ₄	neg	115.004	12.7
GDP	C ₁₀ H ₁₅ N ₅ O ₁₁ P ₂	neg pos	442.016	14.9
GDP-glucose	C ₁₆ H ₂₅ N ₅ O ₁₆ P ₂	neg pos	604.070	15.1

Table 2.3 (continued)

Metabolite	Chemical formula	Ionization modes	m/z	RT (min)
<i>Gluconate</i>	C ₆ H ₁₁ O ₇	neg	195.051	10.5
Glucose-6-phosphate	C ₆ H ₁₃ O ₉ P	neg pos	259.022	13.8
Glutamate	C ₅ H ₉ NO ₄	neg pos	148.061	11.4
Glutamate methyl ester	C ₆ H ₁₁ NO ₄	pos	162.077	7.7
Glutamine	C ₅ H ₁₀ N ₂ O ₃	neg pos	147.077	11.9
Glutaric acid	C ₅ H ₈ O ₄	neg	131.035	11.0
Glutathione	C ₁₀ H ₁₇ N ₃ O ₆ S	neg pos	308.092	11.2
Glutathione (oxid.)	C ₂₀ H ₃₂ N ₆ O ₁₂ S ₂	neg pos	613.161	14.6
Glycerol-phosphate	C ₃ H ₉ O ₆ P	neg pos	171.006	11.9
<i>Glycerophosphocholine</i>	C ₈ H ₂₀ NO ₆ P	neg pos	258.111	11.7
<i>Glycerophosphoethanolamine</i>	C ₅ H ₁₄ NO ₆ P	neg pos	214.048	12.6
GMP	C ₁₀ H ₁₄ N ₅ O ₈ P	neg pos	362.050	13.6
GTP	C ₁₀ H ₁₆ N ₅ O ₁₄ P ₃	neg pos	521.983	16.1
Guanosine	C ₁₀ H ₁₃ N ₅ O ₅	neg pos	282.084	9.2
<i>Heptose-diphosphate</i>	C ₇ H ₁₆ O ₁₃ P ₂	neg pos	368.998	15.7
<i>Heptose-phosphate</i>	C ₇ H ₁₅ O ₁₀ P	neg pos	289.032	13.2
Histidine	C ₆ H ₉ N ₃ O ₂	neg pos	156.077	11.3
IMP	C ₁₀ H ₁₃ N ₄ O ₈ P	neg pos	347.039	12.5
Inosine	C ₁₀ H ₁₂ N ₄ O ₅	neg pos	267.073	7.5
Isoleucine	C ₆ H ₁₃ NO ₂	neg pos	130.088	8.0
Leucine	C ₆ H ₁₃ NO ₂	neg pos	130.087	7.5
Leucine methyl ester	C ₇ H ₁₅ NO ₂	pos	146.118	3.3
Lysine	C ₆ H ₁₄ N ₂ O ₂	neg pos	145.098	21.7
Malate	C ₄ H ₆ O ₅	neg	133.014	12.8
Methionine	C ₅ H ₁₁ NO ₂ S	neg pos	150.059	8.1
<i>N</i> -acetyl-arginine	C ₈ H ₁₆ O ₃ N ₄	neg pos	217.130	11.9
<i>N</i> -acetyl-glutamate	C ₇ H ₁₁ NO ₅	neg pos	190.072	11.0
<i>N</i> -acetyl-histidine	C ₈ H ₁₁ N ₃ O ₃	neg pos	198.088	6.6
<i>N</i> -acetyl-ornithine	C ₇ H ₁₄ N ₂ O ₃	neg pos	175.108	12.4
<i>N</i> ₂ -acetyl-lysine	C ₈ H ₁₆ O ₃ N ₂	pos	189.124	12.2
<i>N</i> ₆ -acetyl-lysine	C ₈ H ₁₆ O ₃ N ₂	neg pos	189.124	9.8
NAD ⁺	C ₂₁ H ₂₇ N ₇ O ₁₄ P ₂	neg pos	664.118	11.4
NADH	C ₂₁ H ₂₉ N ₇ O ₁₄ P ₂	neg pos	666.135	10.5
NADP ⁺	C ₂₁ H ₂₉ N ₇ O ₁₇ P ₃	neg pos	744.086	14.1
NADPH	C ₂₁ H ₃₀ N ₇ O ₁₇ P ₃	neg pos	746.102	14.7
Nicotinamide	C ₆ H ₆ N ₂ O	pos	123.056	4.7

Table 2.3 (continued)

Metabolite	Chemical formula	Ionization modes	m/z	RT (min)
<i>Nicotinate D-ribonucleoside</i>	C ₁₁ H ₁₄ NO ₆	pos	256.083	10.1
<i>Nicotinate D-ribonucleotide</i>	C ₁₁ H ₁₄ NO ₉ P	pos	336.050	12.4
<i>Octose-diphosphate</i>	C ₈ H ₁₈ O ₁₄ P ₂	neg pos	399.009	15.9
<i>Octose-phosphate</i>	C ₈ H ₁₇ O ₁₁ P	neg pos	319.043	13.5
Ophthalmic acid	C ₁₁ H ₁₉ N ₃ O ₆	neg pos	290.136	10.3
Ornithine	C ₅ H ₁₂ N ₂ O ₂	neg pos	131.083	19.5
Pantothenate	C ₉ H ₁₇ NO ₅	neg pos	220.119	5.1
Phenylalanine	C ₉ H ₁₁ NO ₂	neg pos	166.087	6.8
Phospho-glyceric acid	C ₃ H ₇ O ₇ P	neg pos	184.985	14.0
Phosphoenolpyruvate	C ₃ H ₅ O ₆ P	neg pos	166.975	14.6
<i>Phosphopantothenate</i>	C ₉ H ₁₈ NO ₈ P	neg	298.069	12.4
Phthalic acid	C ₈ H ₆ O ₄	neg pos	165.019	10.1
Proline	C ₅ H ₉ NO ₂	neg pos	116.071	9.5
Propylmalate	C ₇ H ₁₂ O ₅	neg	175.061	8.5
Pyridoxine	C ₈ H ₁₁ NO ₃	pos	170.082	5.2
Pyroglutamic acid	C ₅ H ₇ NO ₃	neg	128.035	6.5
Quinic acid	C ₇ H ₁₂ O ₆	neg	191.056	9.0
Riboflavin	C ₁₇ H ₂₀ N ₄ O ₆	pos	377.147	5.5
Ribose-5-phosphate	C ₅ H ₁₁ O ₈ P	neg pos	229.011	12.5
Ribulose (in complex with boron) ⁶	C ₁₀ H ₁₆ O ₁₀ B	neg	307.083	7.5
<i>S</i> -adenosyl-homocysteine	C ₁₄ H ₂₀ N ₆ O ₅ S	pos	385.130	10.6
<i>S</i> -adenosyl-methionine	C ₁₅ H ₂₂ N ₆ O ₅ S	neg pos	399.146	13.8
Saccharopine	C ₁₁ H ₂₀ N ₂ O ₆	neg pos	277.140	12.7
Serine	C ₃ H ₇ NO ₃	pos	106.050	12.4
Threonine	C ₄ H ₉ NO ₃	neg pos	120.066	11.0
Trehalose	C ₁₂ H ₂₂ O ₁₁	neg pos	341.108	13.0
<i>Trimethyl histidine</i>	C ₉ H ₁₆ N ₃ O ₂	pos	198.124	9.3
Trimethyl lysine	C ₉ H ₂₀ N ₂ O ₂	pos	189.160	19.8
Tryptophan	C ₁₁ H ₁₂ N ₂ O ₂	neg pos	205.098	8.2
Tyrosine	C ₉ H ₁₁ NO ₃	neg pos	182.082	9.5
UDP	C ₉ H ₁₄ N ₂ O ₁₂ P ₂	neg pos	402.994	13.6
UDP-acetyl-glucosamine	C ₁₇ H ₂₇ N ₃ O ₁₇ P ₂	neg pos	606.074	12.2
UDP-glucose	C ₁₅ H ₂₄ N ₂ O ₁₇ P ₂	neg pos	565.048	13.3
UMP	C ₉ H ₁₃ N ₂ O ₉ P	neg pos	323.028	12.1

⁶ We observed that pentose sugars often formed complexes with boron atoms during the sample analysis process. This occurred even when analyzing pure pentose standards. The source of the boron was unknown.

Table 2.3 (continued)

Metabolite	Chemical formula	Ionization modes	m/z	RT (min)
Uracil	C ₄ H ₄ N ₂ O ₂	neg	111.020	5.3
UTP	C ₉ H ₁₅ N ₂ O ₁₅ P ₃	neg pos	482.960	14.8
Valine	C ₅ H ₁₁ NO ₂	neg pos	118.087	9.2
Xanthine	C ₅ H ₄ N ₄ O ₂	neg	151.026	7.6
Xanthosine	C ₁₀ H ₁₂ N ₄ O ₆	neg pos	283.068	8.3

2.5 Effect of temperature stress

Focusing on the 123 identified metabolites, we compared metabolic profiles of WT *S. pombe* cells exponentially grown in a synthetic culture medium (EMM2) at two different temperatures, 26°C and 36°C. Fig. 2.8A shows the comparison of peak areas detected in negative ESI mode from two extracts from independent cultures cultivated at 26°C. Each dot indicates a single identified metabolite. As 96% of the signals remained within a 2-fold change of the peak area, we consider the 2-fold variation a good threshold for common sample-to-sample variation. When two cultures cultivated at 26°C and 36°C for 6 h were compared, however, a number of compounds showed dramatic changes (Fig. 2.8B).

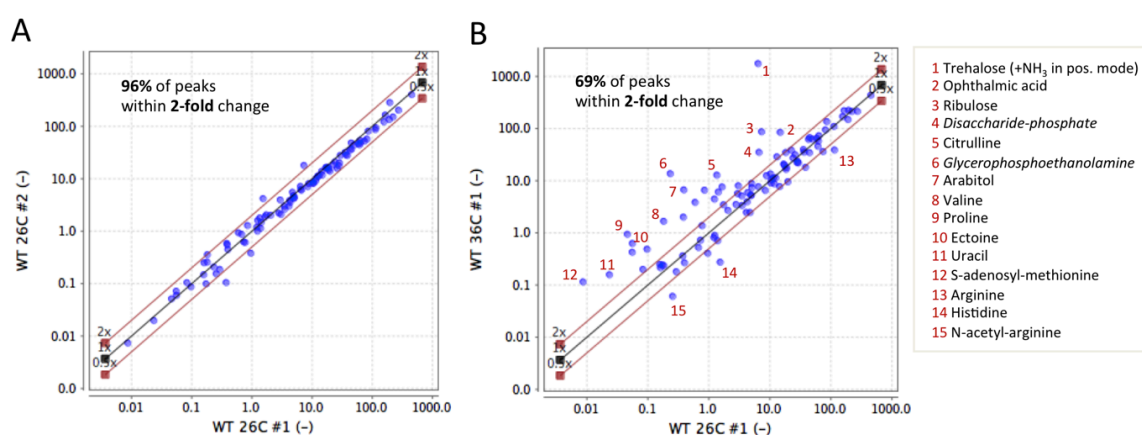


Fig. 2.8. Peak areas of metabolites detected in negative ESI mode. Each dot represents a single metabolite. **A.** Two independent cultures cultivated at 26°C. **B.** Comparison of two cultures cultivated at 26°C and 36°C. Significantly altered metabolites are annotated in the inset table.

The most prominent change between the two cultivation temperatures was the rise of trehalose (a disaccharide formed from two glucose units) at 36°C, showing over 200-fold increase in peak area. Other changes included increase in ophthalmic acid, ribulose, and glycerophosphoethanolamine, and a small decrease in arginine, histidine, and *N*-acetyl-histidine. The observation that majority of the changes was in the ‘up’ direction (increase in metabolite amount) might reflect the fact that WT *S. pombe* cells grow and divide faster at 36°C compared to 26°C. A larger amount of cellular metabolites might be produced to support the faster rate of basic cellular processes, such as protein synthesis.

2.6 Effect of genetic perturbation

To test the effect of gene disruption on cellular metabolome, we employed a deletion mutant of a non-essential enzyme, ferrichrome synthetase *Sib1*. Ferrichrome (Fig. 2.9A), first isolated in 1952 from *Ustilago sphaerogena* [100], is a high-affinity iron chelating compound (siderophore) produced mainly by fungi of the genera *Aspergillus*, *Ustilago*, and *Penicillium*; it is also produced by *S. pombe* [89]. The Δ *sib1* deletion strain was obtained from the Bioneer haploid deletion strain collection [49]. Ferrichrome is dispensable for normal growth and proliferation of *S. pombe*, and the deletion mutant Δ *sib1* showed no obvious phenotype.

Fig. 2.9B shows a scatter plot-based comparison of metabolic profiles of WT and Δ *sib1* strains. Interestingly, among the identified metabolites (denoted by yellow dots in the figure), only two compounds showed a significant (over 2-fold) change in peak area. One was ferrichrome, the signal of which was reduced to noise level. Another one was a dipeptide of ornithine and glycine, which increased 45-fold. As ferrichrome is a cyclic hexapeptide composed of three ornithine and three glycine residues, this result strongly suggests that the orn-gly dipeptide might be a direct precursor for *Sib1*-mediated ferrichrome synthesis.

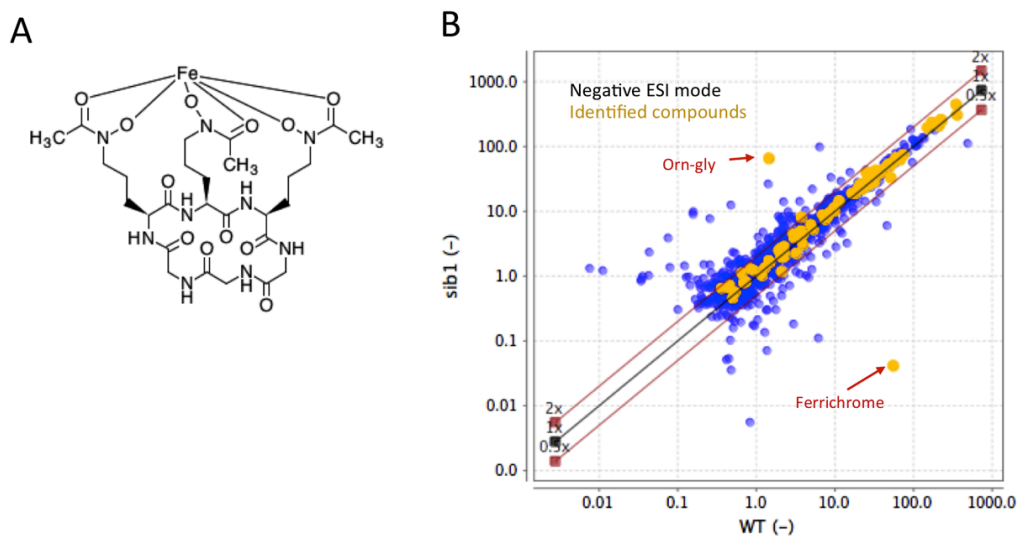


Fig. 2.9. **A.** Chemical structure of ferrichrome. Image reprinted from KEGG database [13] with permission. **B.** Comparison of the metabolic profiles of WT and Δ *sib1* cells in negative ESI mode. Yellow dots indicate identified metabolites, while blue dots indicate remaining unidentified peaks.

In the next step, we analyzed the metabolome of a temperature-sensitive mutant defective in HMG-CoA synthase. HMG-CoA (3-hydroxy-3-methylglutaryl coenzyme A; Fig. 2.10) is an important intermediate in highly conserved mevalonate and ketogenesis pathways, which are required for a number of diverse cellular processes. In *S. pombe*, HMG-CoA is synthesized by the HMG-CoA synthase *hcs1*⁺ [101]. As this gene is essential and cannot thus be completely disrupted, we employed a temperature-sensitive (*ts*) mutant strain *hcs1-143*, obtained from a *ts* strain collection previously generated by random mutagenesis [102]. This strain can grow at permissive temperature (26°C), but becomes defective in the Hcs1 enzyme at restrictive temperature (36°C).

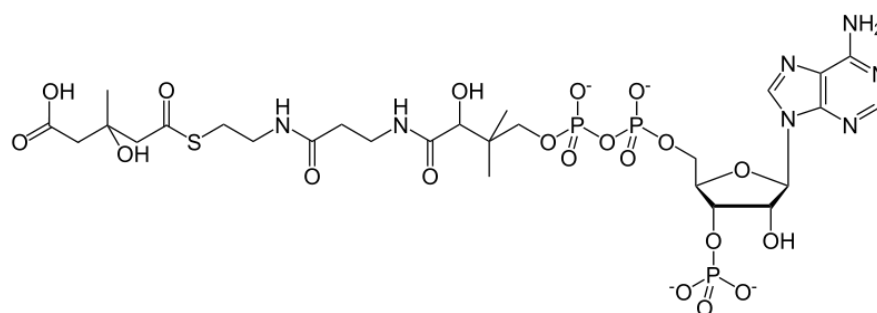


Fig. 2.10. Chemical structure of HMG-CoA

As HMG-CoA was not detected in previous experiments, we restricted the MS scan range to 900 – 950 m/z , targeting the molecular mass of HMG-CoA (911 Da). Using this strategy, we could successfully detect a peak of HMG-CoA in WT cells, but not in the *hcs1-143* mutant (Fig. 2.11A). In addition, we observed extensive secondary effects (Fig. 2.11B). Among the 90 identified metabolites shown as yellow dots in this figure, 39 compounds changed over 2-fold and 17 compounds over 4-fold. Interestingly, urea cycle intermediates, arginine, citrulline, and arginino-succinate, decreased over 4-fold. On the other hand, a number of acetylated compounds (acetyl-ornithine, acetyl-lysine, acetyl-glutamine, acetyl-glutamate, and acetyl-CoA) increased in the mutant. Ergothioneine, a protective compound with antioxidative properties, and its precursor trimethyl-histidine, also increased in mutant cells. Unexpectedly, ferrichrome peak also increased over 3-fold (including the deferri- form that lacks the iron atom). These results suggest that the disruption of the essential HMG-CoA synthase function had a complex, far-reaching effect on the stability of the whole metabolome, affecting also distant and directly unrelated mechanisms of acetylation, urea cycle, oxidative stress response and non-ribosomal peptide synthesis.

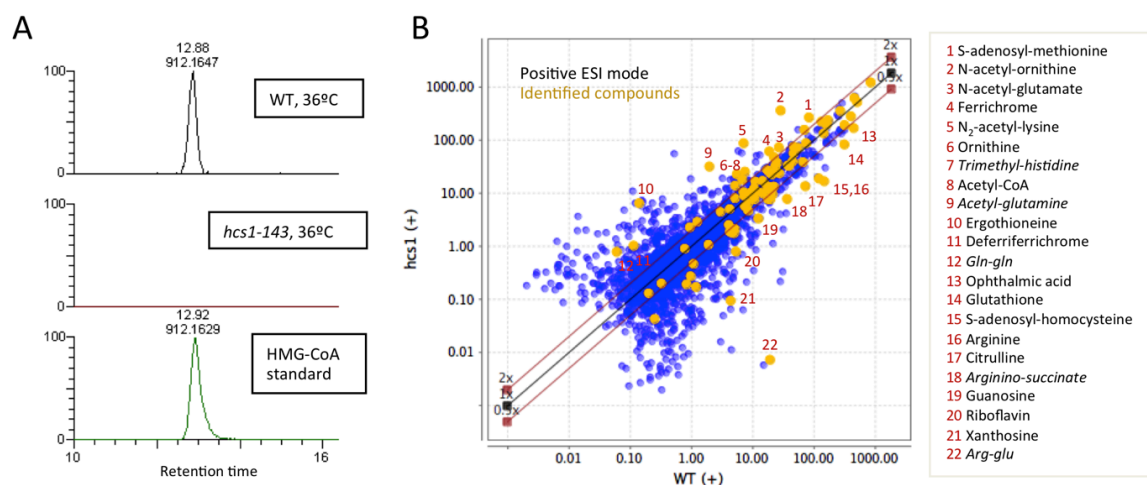


Fig. 2.11. A. The extracted ion chromatograms 912.1647 m/z (± 5 ppm), corresponding to the protonated $[M+H]^+$ ion of HMG-CoA. Scan range was narrowed to 900-950 m/z for this experiment. Data from WT and *hcs1-143* mutant cells cultivated at 36°C for 6 h are shown, together with the data of HMG-CoA standard. **B.** Scatter plot comparison of WT and *hcs1-143* mutant metabolomes. Cells were cultivated at 36°C for 6 h. Yellow dots indicate identified metabolites, while blue dots indicate remaining unidentified peaks.

2.7 Summary

In this study we introduced the methodology for global metabolomic analysis of the fission yeast *S. pombe*, thus enabling the use of a full spectrum of systems biology methods for this organism. We developed and evaluated protocols for extraction and semi-quantitative measurement of 123 cellular metabolites, which were identified among ~6,000 detected peaks. Among these peaks, 1,727 were recognized as chemical noise (781 in negative ionization mode + 946 in positive ionization mode). Interestingly, 63% (77/123) of the identified metabolites were detected in both ionization modes, whereas only 7.5% (335/4,476) of the remaining potential metabolite peaks could be detected in both modes. Assuming that the 63% ratio is empirically valid for all cellular metabolites, we can estimate that ~530 (335/63%) total metabolites could be found among the ~4,000 remaining peaks. To further increase the coverage

of *S. pombe* metabolome (expected to contain several thousand metabolites), a combination of different extraction and detection methods should probably be employed.

Reproducibility of the measurements was demonstrated by comparing two independent extracts from cells cultivated at the same conditions. In that case, 96% of the measured compounds remained within the boundary of 2-fold change. The comparison of metabolomes of cells cultivated at 26°C and 36°C revealed that majority of the metabolites (69%) still remained within 2-fold change, however certain compounds showed a dramatic increase. The most prominent among them was trehalose, which showed a striking 200-fold increase in peak area. The interpretation of this change is not difficult, however, as trehalose is a well known stabilizer of proteins and membranes, produced in response to heat, cold, and dehydration [103,104]. The accumulation of trehalose can thus be considered a generic stress response mechanism.

Since genetics represents the most powerful tool in yeast research, we examined the feasibility of a combined use of genetics and metabolomics. We demonstrated that the deletion of a non-essential gene had very little effect on the overall metabolic profile, as the deletion mutant of ferrichrome synthetase, *sib1*Δ, showed no significant changes except the disappearance of ferrichrome and appearance of a putative precursor, ornithine-glycine. On the other hand, we showed that a *ts* mutant strain *hcs1-143*, defective in the function of an essential enzyme, HMG-CoA synthase, exhibited complex and broad perturbations in its metabolome at restrictive temperature. The combination of genetics and metabolomics seems to be most promising for future applications of the methods developed in this chapter. We further pursue this direction in Chapter 4 of this thesis, which describes the application of genetics and metabolomics to dissect the biosynthetic pathway of two metabolites, ergothioneine and selenoneine.

Chapter 3. Cell division patterns and metabolic profiles under limited glucose

Note: This study was published in *FEBS Journal* [105]. Majority of figures and tables in this Chapter were adapted from the published article with slight modifications.

3.1 Introduction

Glucose is a principal source of cellular energy in most living organisms. Common laboratory media for cultivation of *S. pombe* cells contain 111 – 167 mM glucose [47]. Human cells obtain glucose from blood, and its level in blood is tightly regulated. Normal concentration of blood glucose in the morning before breakfast is between 3.9 and 6.1 mM [106]. Elevated blood glucose levels to 7 mM or higher indicate a diabetic condition [107]. This stark contrast in the level of glucose that is available to human and *S. pombe* cells under laboratory conditions might implicate that biological processes related to metabolism cannot always be correlated between the two organisms. In order to employ *S. pombe* as a model for studying human metabolic diseases such as diabetes, it might be necessary to use similar glucose concentration for cell cultivations. Furthermore, glucose availability might regulate the function of glycolysis and mitochondrial respiration, mechanisms that are also involved in human cancer due to phenomenon known as “Warburg effect” [108]. Abundance of glucose is known to promote aging in many organisms, including *S. pombe* [109], therefore its concentration has to be taken into account in aging research [110]. For genetic studies, it is important to consider that some non-essential genes might become essential if glucose concentration in the culture medium is

reduced to a blood-like level [111]. It is thus advisable to study the biology of *S. pombe* under reduced glucose levels. However, prior to this work the true glucose requirements of this organism for growth and proliferation were mostly unknown.

In this study we applied perfusion system microscopy and metabolomic analysis (introduced in Chapter 2) to study the cell division phenotypes and metabolic responses of *S. pombe* to reduced glucose levels. We investigated a wide range of glucose concentrations (0 – 111 mM) in the synthetic culture medium EMM2 and designated a new terminology for specific levels of glucose, corresponding to observed phenotypes. In addition, we identified several metabolites as biomarkers of the designated phenotypes.

3.2 Methods

3.2.1 Strains and growth conditions

All experiments in this chapter were performed using the WT *S. pombe* strain h⁻972 [112]. Cells were cultivated in synthetic EMM2 medium (Table 2.1) with modified glucose concentrations. The media were prepared by mixing the regular EMM2 (20 g/L glucose) medium with EMM2-G (no glucose) medium in an appropriate ratio. Cultivation temperature was 26°C unless stated otherwise.

3.2.2 Measurement of glucose content in culture media

Glucose content in the culture media was measured using Glucose (HK) Assay Kit (Sigma-Aldrich) according to manufacturer's instructions.

3.2.3 Perfusion system microscopy

Cells were fixed in a microscopic specimen chamber Onix Microfluidic Perfusion System (CellASIC) connected to DeltaVision microscope system (Applied Precision). The perfusion chamber was continuously supplied with fresh culture medium at a 3 $\mu\text{L/h}$ flow rate. Temperature was maintained at 26°C. Photos of cells were taken every 3 min. Cell length was measured from the micrographs using the Adobe Photoshop software.

3.2.4 Metabolomic analyses

Metabolomic experiments were performed using the protocol introduced in Chapter 2.

3.2.5 Viability measurements

Cell viability was measured by plating approximately 300 cells on a YPD agar plate (see Table 2.1). Plates were incubated at 26°C for several days, and colonies were counted. Viability was calculated as follows: $viability (\%) = \text{number of formed colonies} / 300$.

3.2.6 Oxidative stress staining

Cells were incubated in the dark with H₂DCFDA dye (Invitrogen) in 10 $\mu\text{g/mL}$ final concentration, according to a previously published protocol [113]. Incubation time was 80 min, followed by two rounds of washing with 50 mM sodium citrate (pH 7.0). Micrographs were taken using an AxioPlan 2 microscope (Zeiss).

3.2.7 H₂O₂ resistance assay

Cells were incubated in described conditions H₂O₂ was added to each culture to the

final concentration of 40 mM, according to a previously published protocol [114]. Viability was measured in 20 min intervals (see Viability measurements).

3.3 Cell division under limited glucose

3.3.1 Increase in cell number and cell length

In the first experiment, we tested whether *S. pombe* cells can grow and divide in EMM2 medium with 25-fold diluted glucose to a human blood-like concentration (4.4 mM). We measured the remaining glucose in the culture medium to estimate the time span of glucose consumption. As shown in Fig. 3.1, *S. pombe* cells proliferated quite normally in 4.4 mM glucose, albeit slightly slower than in 111 mM glucose. At 26°C, glucose was nearly exhausted (below 1 mM) after ~14 h, while at 30°C, it was nearly exhausted after ~8 h, reflecting the increased speed of cell division at 30°C. We thus concluded that *S. pombe* cells can be cultivated and observed in reduced glucose medium (4.4 mM) at least for several hours.

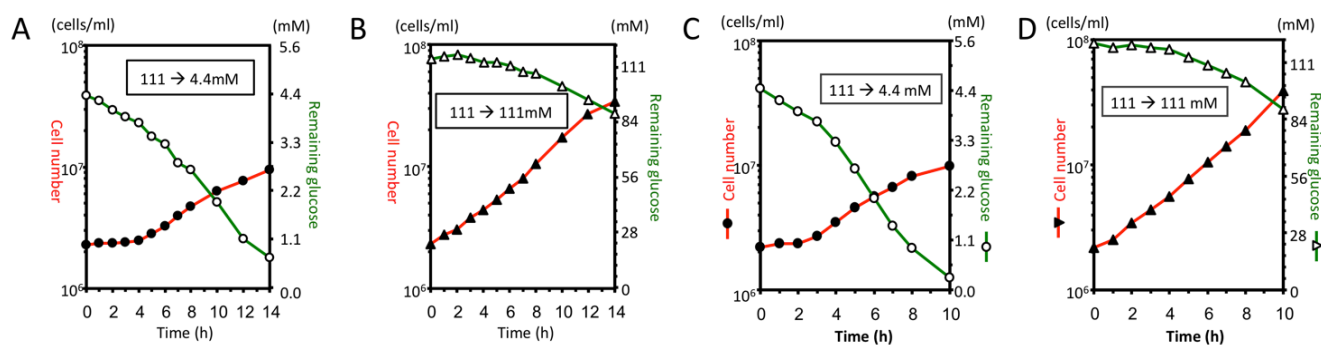


Fig. 3.1. Glucose concentration in the culture medium (green lines) and cell numbers (red lines) were measured in time course. Initial cultures were cultivated in standard EMM2 medium at 26°C to mid-log phase and then transferred into a new medium at a starting concentration of 2×10^6 cells/mL. **A.** Cells transferred to 4.4 mM glucose at 26°C. **B.** Cells transferred to 111 mM glucose at 26°C. **C.** Cells transferred to 4.4 mM glucose at 30°C. **D.** Cells transferred to 111 mM glucose at 30°C.

Next, we measured the cell length increase over time for two individual cells and their progeny. Cells cultivated in EMM2 medium to mid-log phase (2×10^6 cells/mL) were transferred into 111 (control), 4.4, 2.2, and 1.7 mM glucose media (Fig 3.2). Cell length at the time of division was reduced from a $\sim 15 \mu\text{m}$ in 111 mM glucose to $\sim 13 \mu\text{m}$ in 4.4 mM and $\sim 10 \mu\text{m}$ in 2.2 mM glucose. Cell division was regular in 4.4 mM glucose, with only slightly longer division timing compared to 111 mM glucose. In 2.2 and 1.7 mM glucose, however, cell division became stochastic.

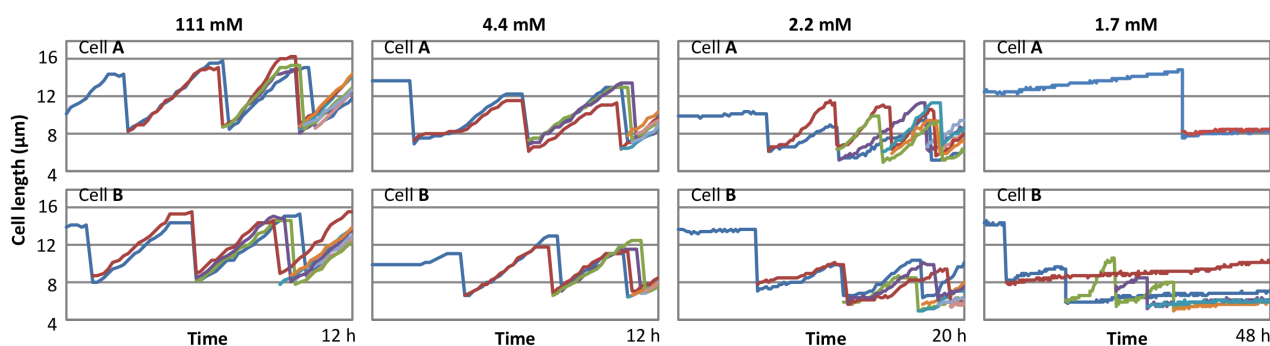


Fig. 3.2. Cell length (μm) increase over time (h) of 2 individual cells (cell A and cell B) fixed in a perfusion system. Cell length was measured from micrographs taken every 3 min.

3.3.2 Cell division timing

We used the time course micrographs of cells in 111 (control), 4.4, 2.2, 1.7, and 1.1 mM glucose media to measure the division timing (h) of individual cells for 1st, 2nd and 3rd division after the media change (Fig. 3.3). Similar to previous results, only mild change in division timing distribution was observed in 4.4 mM glucose. In 2.2 mM glucose, however, distribution became wider and some cells failed to perform 2nd or 3rd division. In 1.7 and 1.1 mM glucose, majority of cells became quiescent after 1st or 2nd division. We thus concluded that the threshold for transition from vegetative proliferation to quiescence lies between 1.7 and 1.1 mM glucose.

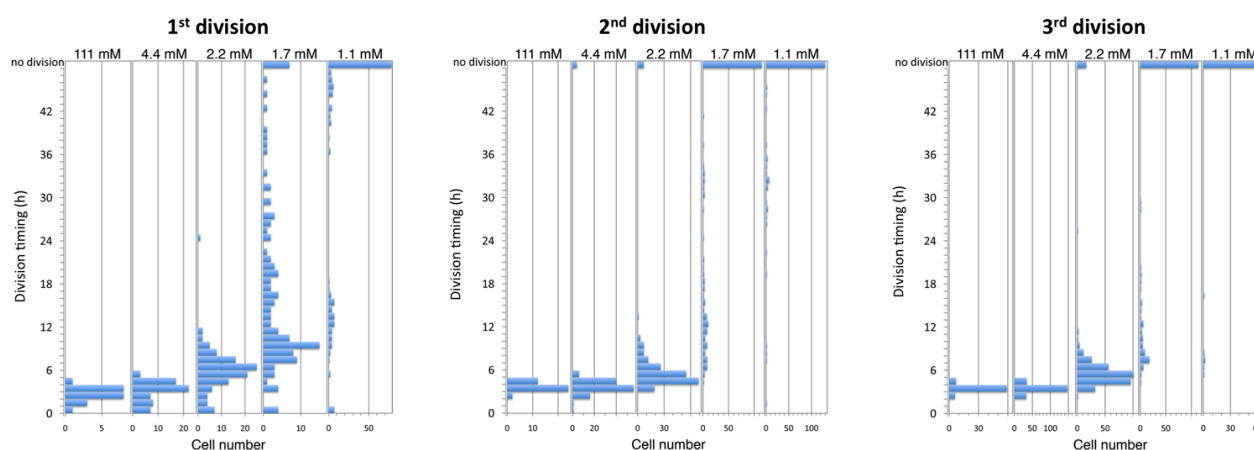


Fig. 3.3. Division timing (h) distribution for the first 3 divisions after media switch to 111 (control), 4.4, 2.2, 1.7, and 1.1 glucose. Division timings of individual cells were measured from time course micrographs.

Table 3.1 shows the calculated mean and standard deviations of the division timings for 2nd and 3rd division after the media change to six different glucose concentrations. Cells that failed to divide were ignored for this calculation.

Table 3.1. Mean \pm standard deviations of division timings in different glucose concentrations.

Glucose (mM)	2 nd division	3 rd division
111	3.8 \pm 0.4	3.5 \pm 0.4
11.1	3.6 \pm 0.5	3.6 \pm 0.4
4.4	3.8 \pm 0.7	3.5 \pm 0.5
2.2	5.6 \pm 1.6	5.6 \pm 1.8
1.7	15.1 \pm 8.8	10.7 \pm 4.9
1.1	29.7 \pm 9.9	8.7 \pm 3.8

3.4 Metabolome results

3.4.1 Ten different glucose concentrations

We applied the metabolomic analysis technique described in Chapter 2 to study the

metabolic profiles of *S. pombe* cells cultivated in different concentrations of glucose. First, we analyzed the profiles of cells cultivated for 6 h in liquid EMM2 medium with ten different glucose concentrations (Fig. 3.4). Note that the indicated glucose concentrations are initial ones, immediately after the transfer of cells from the original stock culture. The actual glucose concentrations at the time of metabolite extraction (6 h later) were likely much lower, although for initial concentrations of 4.4 mM or higher we assume glucose was not exhausted in 6 h (see Fig. 3.1). Over 100 metabolites were identified in our LC-MS data, however the levels of majority of them remained stable despite the changes in glucose levels. We thus focused on metabolites that showed differential regulation.

Interestingly, levels of adenosine nucleotides including ATP remained very high at glucose concentrations from 111 mM down to 1.1 mM (Fig 3.4A). Even at glucose concentrations below 2.2 mM, which could not support cell division, *S. pombe* cells maintained the ability to produce energy in the form of ATP, albeit its level was slightly lower than in dividing cells (4.4 mM glucose or more). Only at 0 mM glucose we observed complete absence of ATP, accompanied by the rise of AMP and adenosine. CDP-choline and CDP-ethanolamine also sharply increased at 0 mM glucose (Fig. 3.4B). The only known function of these two compounds is as precursors for phosphatidyl choline and phosphatidyl ethanolamine, respectively. Their increase might thus indicate an attempt of cells to build cellular lipid membranes.

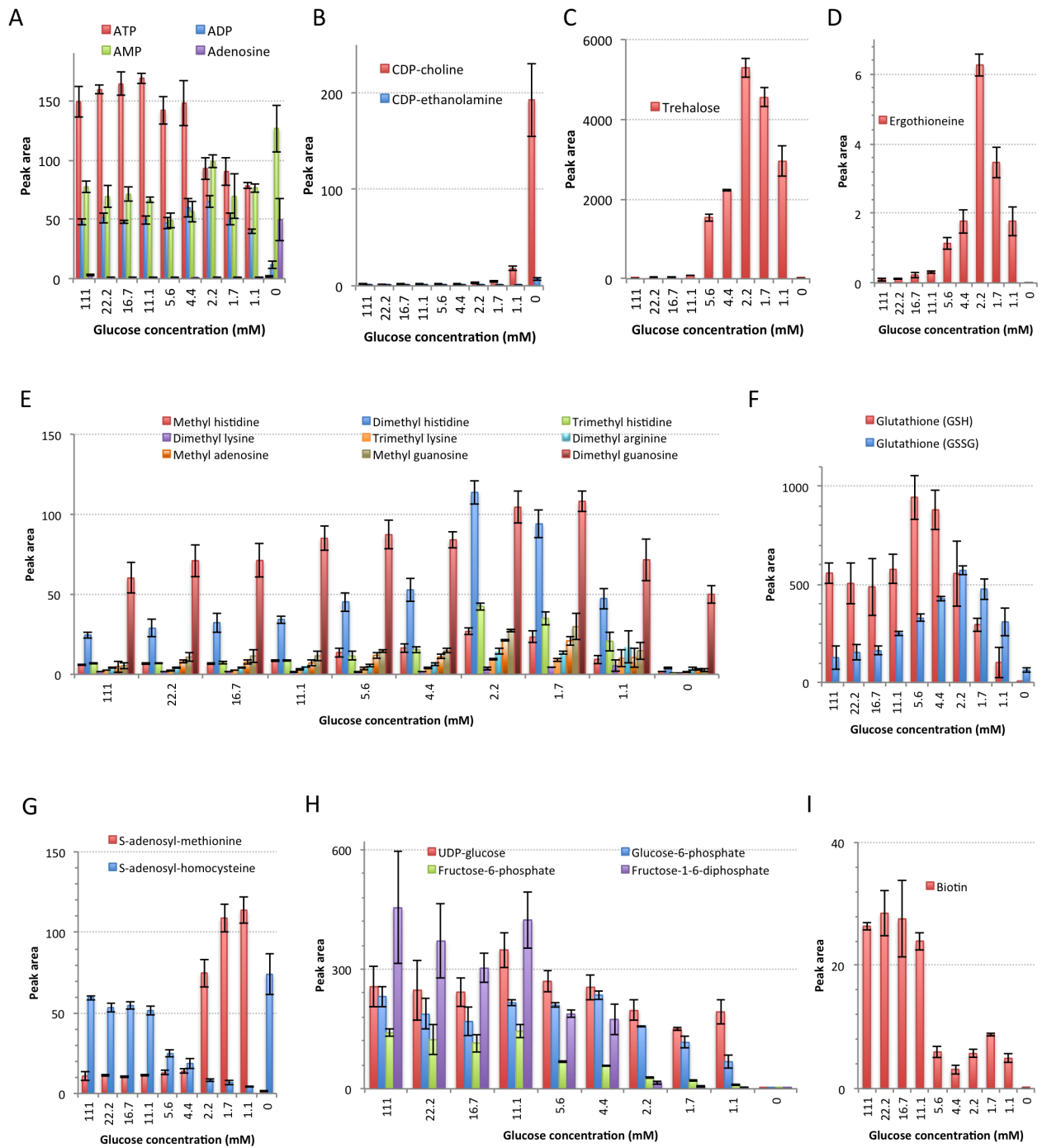


Fig. 3.4. Normalized peak areas of selected metabolites obtained by metabolome analysis of cells cultivated for 6 h in ten different glucose concentrations, as indicated. Plots show means and standard deviations of 3 independent experiments. **A.** Adenosine nucleotides; **B.** CDP-choline, CDP-ethanolamine; **C.** trehalose; **D.** ergothioneine; **E.** methylated amino acids and nucleosides; **F.** reduced (GSH) and oxidized (GSSG) glutathione; **G.** *S*-adenosyl-methionine, *S*-adenosyl-homocysteine; **H.** UDP-glucose, and sugar phosphates; **I.** biotin.

Trehalose, a disaccharide with stabilizing properties [103], and ergothioneine, a proposed antioxidant compound [115], appeared with similar profiles, although with very different scales of peak area (trehalose peak was almost 1,000-fold larger than that of ergothioneine; Fig. 3.4C and D). Both increased at glucose levels below 5.6 mM, suggesting that ~5 mM glucose might represent the critical threshold for activation of stress response mechanisms. Several methylated compounds also increased in low glucose (Fig. 3.4E). Among them were methyl-, dimethyl-, and trimethyl-histidine, intermediates in the biosynthetic pathway of ergothioneine [116,117], but also other, apparently unrelated, methylated amino acids and nucleosides. The increase in methylated compounds could be the result of a change in osmotic pressure under low glucose, as methylated compounds often act as natural osmolytes in biological systems [118].

Glutathione, a principal antioxidant found in most living organisms, remained abundant at all glucose concentrations except 0 mM (Fig. 3.4F). The ratio between reduced (GSH) and oxidized (GSSG) forms of glutathione, however, decreased at lower glucose concentrations. This might reflect the increased activity of mitochondria at low glucose, as mitochondria represent the major producer of reactive oxygen species (ROS) in cells. The absence of glutathione at 0 mM glucose suggests that cells in this condition might be sensitive to oxidative stress.

The ratio between *S*-adenosyl-methionine and *S*-adenosyl-homocysteine became inverted under low glucose (Fig. 3.4G). This might reflect the change in methylated compounds, as *S*-adenosyl-methionine is the principal methyl group donor, while *S*-adenosyl-homocysteine is the demethylated form of *S*-adenosyl-methionine. Interestingly, under 0 mM glucose, this inversion did not occur, and *S*-adenosyl-homocysteine was abundant. Possibly, a lack of cellular energy (ATP) prevented the recycling of *S*-adenosyl-homocysteine back to

S-adenosyl-methionine. Another possible explanation could be that a broader failure to adapt to low glucose conditions occurred when cells were abruptly switched to 0 mM glucose.

UDP-glucose, the activated form of glucose for glucosyltransferases [119], maintained its high level at all glucose concentrations except 0 mM (Fig. 3.4H), suggesting that despite its reduced level in the medium, glucose was actually still available for certain chemical reactions within the cells. On the other hand, glycolysis intermediates (sugar-phosphates) gradually decreased with decreasing concentration of glucose in the medium. Particularly, fructose-1-6-diphosphate, an intermediate in glycolysis prior to the breakdown of the hexose ring, greatly decreased in glucose concentrations below 11.1 mM. These results might reflect reduced reliance on glycolysis pathway and activation of mitochondrial respiration at reduced levels of glucose. The vitamin biotin appeared as an interesting marker of cell proliferation (Fig. 3.4H), as its initially high levels at 111 – 11 mM glucose were reduced at glucose concentrations below 5.6 mM, showing thus opposite trend than that of trehalose or ergothioneine. At 0 mM glucose, biotin was completely absent, as well as trehalose, ergothioneine, *S*-adenosyl-methionine, ATP, UDP-glucose and sugar-phosphates.

To improve our understanding of the two extreme conditions, 0 mM and 1.1 mM glucose, we performed time-course metabolomic analyses. Large volume cell cultures were cultivated to mid-log phase (5×10^6 cells/mL) in the standard EMM2 medium and transferred into media with 0 mM or 1.1 mM glucose, respectively. Aliquots of the cell cultures were taken at indicated times for preparation of metabolome samples.

3.4.2 Time course analysis of 0 mM glucose condition

Results of 0 mM glucose cultures are shown in Fig. 3.5. UDP-glucose and sugar-phosphate compounds became completely undetectable after 5 min (Fig. 3.5A). This

suggests that cells, which were abruptly shifted to 0 mM glucose, quickly consumed remaining free glucose metabolites, presumably by ongoing glycolysis. Lack of these metabolites also explains why no accumulation of trehalose was observed in this condition, as trehalose is synthesized from UDP-glucose and glucose-6-phosphate by trehalose-phosphate synthase/phosphatase pathway [120,121].

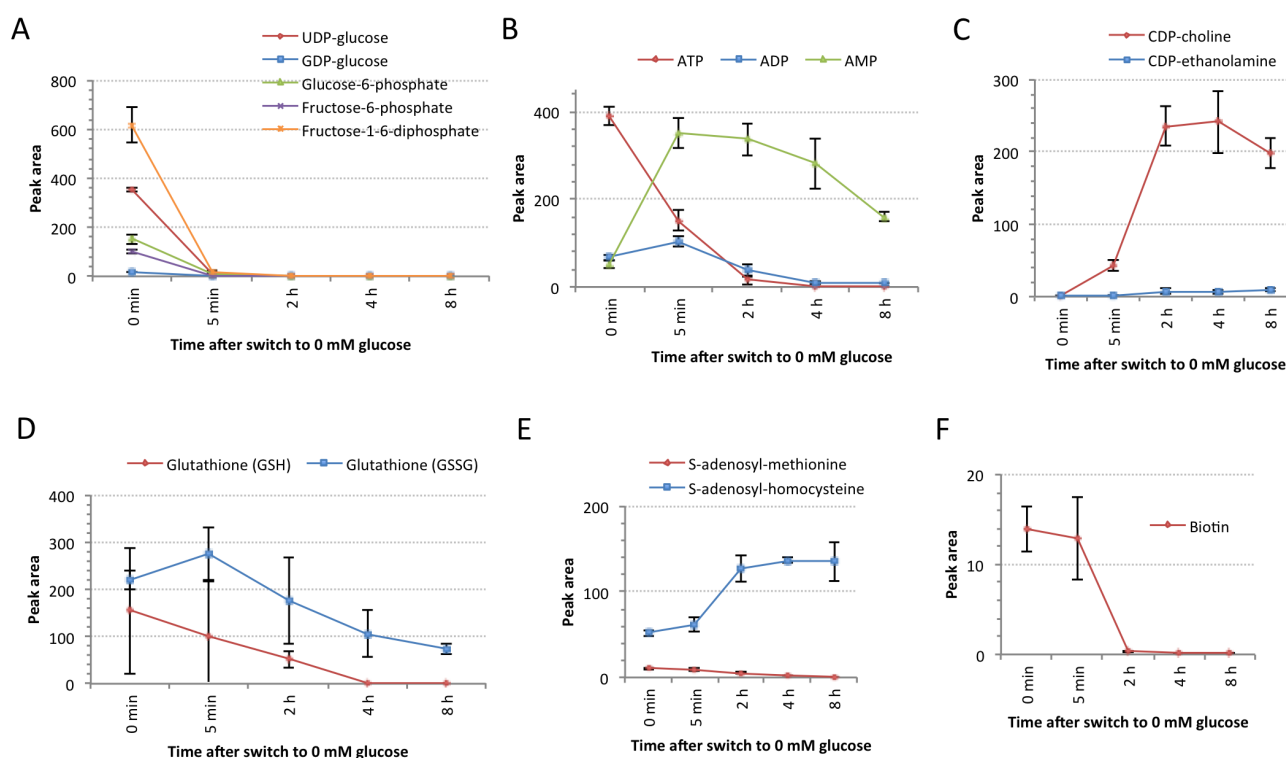


Fig. 3.5. Normalized peak areas of selected metabolites in 0 mM glucose medium. Metabolome samples were prepared at indicated time points (0 min = prior to transfer). Mean peak areas with standard deviations of three samples are shown. **A.** UDP-glucose, GDP-glucose, sugar-phosphates; **B.** Adenosine nucleotides; **C.** CDP-choline, CDP-ethanolamine; **D.** reduced (GSH) and oxidized (GSSG) glutathione; **E.** *S*-adenosyl-methionine, *S*-adenosyl-homocysteine; **F.** biotin.

Intracellular ATP decreased 3-fold in 5 min, and was completely diminished (~3% of the original level) in 4 h after the media shift (Fig. 3.5B). The increase of CDP-choline and CDP-ethanolamine, compounds that were characteristic markers of 0 mM glucose condition (see previous section), occurred steadily, culminating after 4 h (Fig. 3.5C). Glutathione, *S*-adenosyl

methionine, and biotin (Fig. 3.5 D, E, and F) steadily decreased to undetectable levels after 4-8 h. The changes could be direct consequences of the lack of intracellular ATP, as ATP is required for many enzymatic reactions, including the production of glutathione and *S*-adenosyl methionine. Biosynthesis of biotin requires both ATP and *S*-adenosyl methionine. In summary, the cells' response to 0 mM glucose was rapid, with major changes in metabolome occurring within 5 mM from the media shift.

3.4.3 Time course analysis of 1.1 mM glucose condition

While many important metabolites were exhausted after only several hours in 0 mM glucose condition, the situation was dramatically different in 1.1 mM glucose. It is reasonable to assume that after transferring the cells to 1.1 mM glucose medium, remaining glucose would be consumed within less than one day (based on the results shown in Fig. 3.1A, where remaining glucose in the 4.4 mM glucose medium was virtually exhausted after 14 h). Nevertheless, the cells maintained full viability for 7 days (Fig. 3.6A) and no absence of energy metabolites was observed like in 0 mM glucose condition. The level of ATP decreased steadily (Fig. 3.6A), but even after 7 days some ATP signal was still detectable. The decrease of ATP was accompanied by a gradual increase of AMP. Anti-stress compounds ergothioneine and trehalose showed similar profiles, peaking after 1-2 days of starvation (Fig. 3.6B and C). The ratio between *S*-adenosyl methionine and *S*-adenosyl-homocysteine became inverted already after 1 h of starvation in 1.1 mM glucose (Fig. 3.6D). *S*-adenosyl methionine further increased, suggesting this compound might be important to maintain quiescence. We thus designated *S*-adenosyl-methionine a marker of starvation. Level of CDP-choline increased greatly after 1 day (Fig. 3.6E), and this compound thus appears to be a good marker for complete glucose exhaustion, consistently with our results in 0 mM glucose (Fig. 3.5C). Interestingly, siderophore

compound ferrichrome (see Fig. 2.9A) also greatly increased after 1 day (Fig. 3.6F). Possibly, iron metabolism might be affected in glucose starvation-induced quiescent cells, due to changes in mitochondrial activity [122].

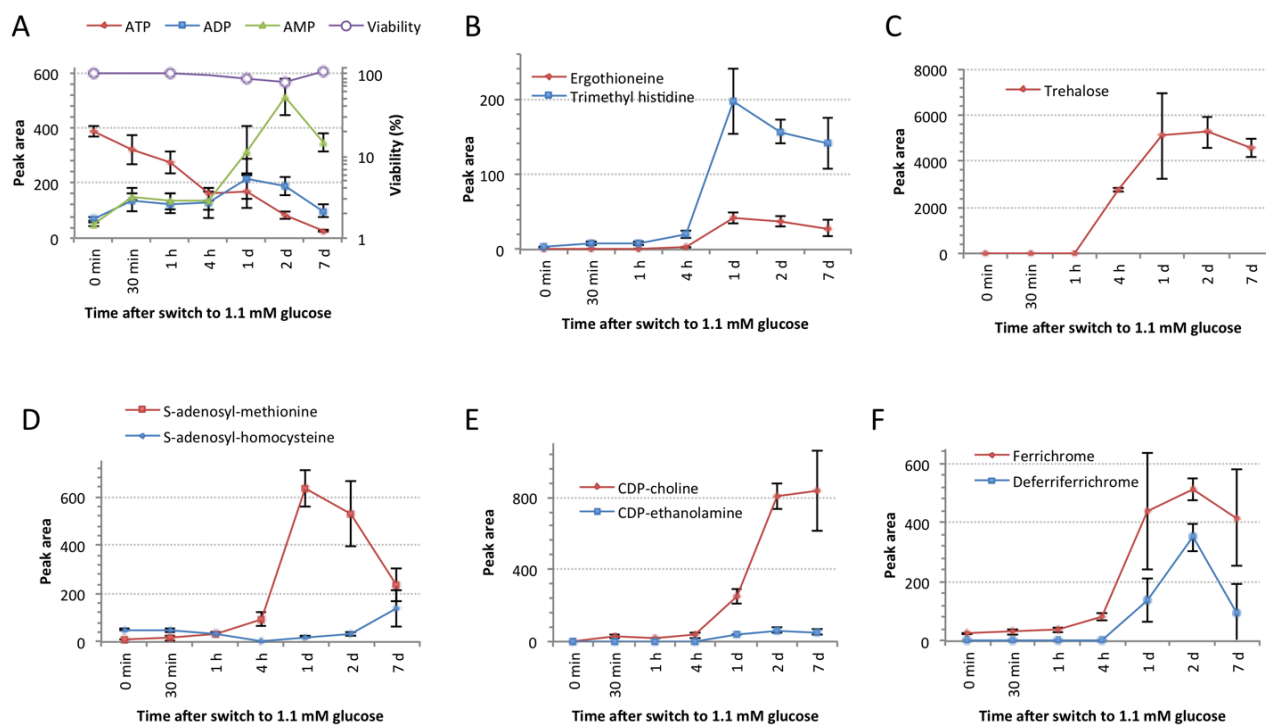


Fig. 3.6. Normalized peak areas of selected metabolites in 1.1 mM glucose medium. Metabolome samples were prepared at indicated time points (0 min = prior to transfer). Mean peak areas with standard deviations of three samples are shown. **A.** Adenosine nucleotides. Cell viability is also shown in this plot.; **B.** ergothioneine and its precursor, trimethyl-histidine; **C.** trehalose; **D.** *S*-adenosyl-methionine, *S*-adenosyl-homocysteine ; **E.** CDP-choline, CDP-ethanolamine; **F.** ferrichrome, deferriferrichrome.

3.5 Lifespan and oxidative stress resistance

To check how long *S. pombe* cells could survive in the complete absence of glucose, we performed time course viability experiments. When cells were transferred directly from the standard EMM2 medium (111 mM glucose) to 0 mM glucose, decrease in viability was observed after 8 h (Fig. 3.7), with complete loss of viability occurring after about 32 h. However,

when cells were first cultivated in reduced glucose medium for 16 h, their survival in 0 mM glucose was prolonged. In case of pre-treatment with 4.4 mM glucose, loss of viability occurred after about 4 days. Interestingly, after pre-cultivation in 1.1 mM glucose medium, viability remained high for over 2 weeks. This suggests that cultivation in glucose starvation condition can trigger adaptation to 0 mM glucose and prolong the lifespan of cells in such condition.

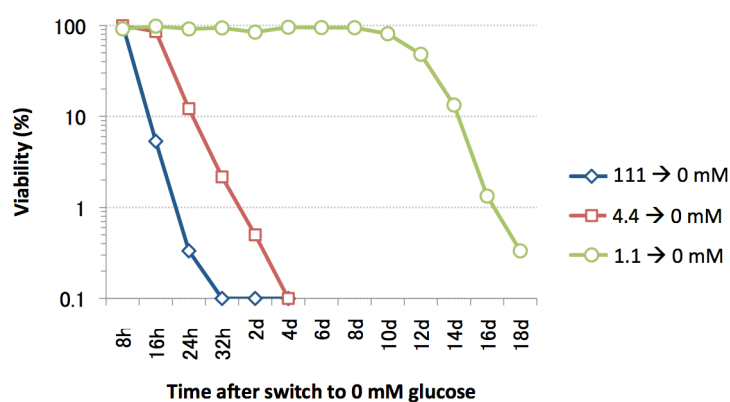


Fig. 3.7. Time-course viability measurement in 0 mM glucose medium (also named EMM2-G). First, WT *S. pombe* cells were cultivated for 16 h in EMM2 medium with 111 mM (blue line), 4.4 mM (red line) or 1.1 mM (green line) glucose. After transferring the cells to EMM2 with 0 mM glucose, viability (%) was measured at indicated times.

Considering the absence of antioxidants glutathione and ergothioneine in 0 mM glucose, we employed a fluorescent dye H₂DCFDA to visualize reactive oxygen species (Fig. 3.8). Strong fluorescence was observed in cells cultivated in 0 mM glucose for 6 h after abrupt shift from 111 mM. However, no fluorescence appeared in any other condition, including cells in 0 mM glucose previously pre-treated with 1.1 mM glucose (rightmost panel in the figure). These results confirmed that cells transferred from 111 mM to 0 mM glucose suffered from severe oxidative stress, possibly due to the absence of antioxidant metabolites. Note that the loss of viability occurred only after 8 h (Fig. 3.7), cells were thus still fully viable at the time of H₂DCFDA observation. The observed oxidative stress might represent the major factor

contributing to the loss of viability in 0 mM glucose. Resistance to oxidative stress after treatment with 1.1 mM glucose might be linked to the observed accumulations of trehalose and ergothioneine.

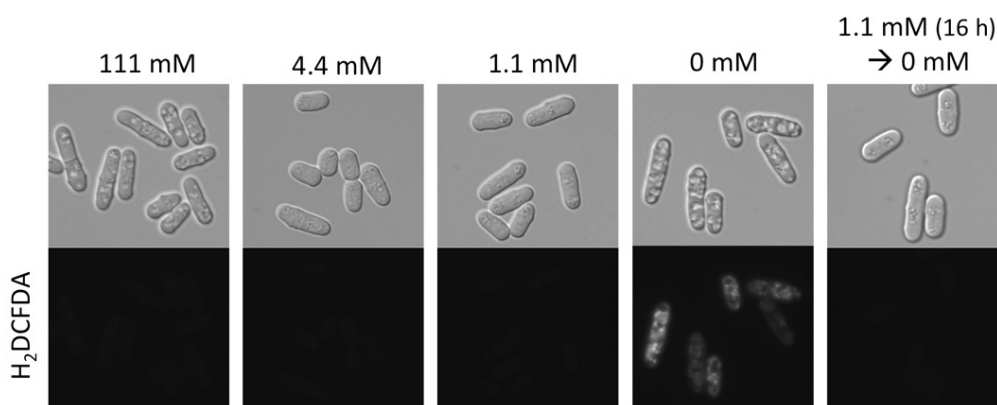


Fig. 3.8. Staining with H_2DCFDA dye, which produces fluorescence in the presence of reactive oxygen species. Cells were cultivated for 6 h in EMM2 medium with indicated concentrations of glucose. In the rightmost panel, cells were first treated with 1.1 mM glucose medium for 16 h, and then transferred to 0 mM glucose medium for 6 h.

To check whether *S. pombe* cells in 1.1 mM gain additional resistance to oxidative stress, we challenged the cells with 40 mM hydrogen peroxide (H_2O_2 ; Fig. 3.9). The concentration of 40 mM should reportedly kill WT *S. pombe* cells within one hour [114]. As expected, cells incubated in 0 mM glucose for 6 h (blue rectangles) were highly sensitive to H_2O_2 (in comparison to 111 mM glucose, red rectangles), while cells cultivated in 1.1 mM glucose (green rectangles) became completely resistant and retained full viability even after one hour. According to Zuin et al. [123], glucose starvation in *S. pombe* activates the Sty1-dependent MAP kinase stress response pathway, which results in antioxidant production and increased resistance to oxidative stress. Our results are thus consistent with this model.

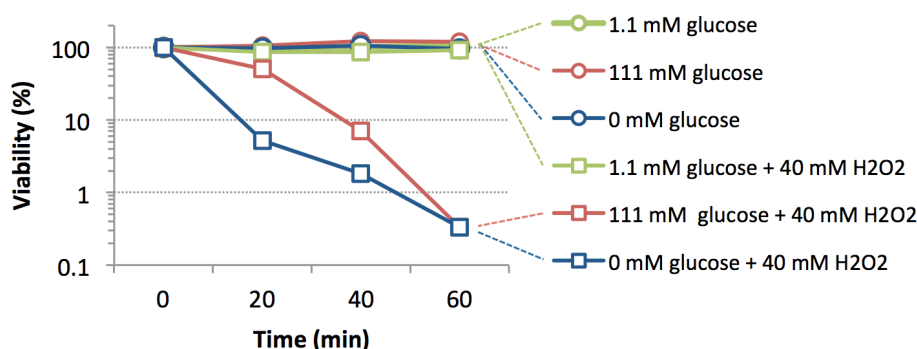


Fig. 3.9. Time course viability measurement in the presence (squares) and absence (circles) of 40 mM H₂O₂. Cells were incubated in 111 mM, 1.1 mM and 0 mM glucose conditions for 6 h, followed by the addition of H₂O₂ to the final concentration of 40 mM at time 0. Viability (%) was measured in 20 min intervals.

3.6 Summary

S. pombe is widely distributed in nature [124,125], but little is known about its minimal and optimal nutritional requirements. Its response to nitrogen starvation has been well characterized in laboratory conditions [50,59], and nitrogen starvation is now being applied as a model system for the study of cellular quiescence [65,66]. On the other hand, the effects of glucose starvation in this organism, and the thresholds of glucose levels for regular proliferation or long-term quiescence, were mostly unknown. This study represents the first systematic attempt to answer these questions.

We employed microfluidic perfusion system microscopy and metabolomic analysis to study the cell division modes and metabolic profiles under glucose concentrations from 0 to 111 mM. Based on the observed phenotypic and metabolic profiles, we designated a new terminology and metabolic biomarkers for certain glucose concentrations thresholds (Table 3.2). Although the terminology is inspired by terms from human life, we do not intend to imply any direct relationship between the glucose levels for *S. pombe* and in human blood. In humans,

blood levels below 2.7 mM cause hypoglycemia. If glucose drops to 1.7 mM, seizures occur. Glucose level below 0.5 mM cannot anymore support the function of neurons, thus resulting in coma. It is so far unknown if any of the metabolic markers that we established can be also observed in human body cells.

Table 3.2. Summary of the glucose concentrations described in this study (mM, w/v and mg/dL, for clarity). Terminology designated for each threshold concentration, characteristic metabolites (biomarkers), and observed cell division phenotypes are shown.

Glucose content			Designated terminology	Biomarker metabolites	Cell division
mM	w/v(%)	mg/dL			
111	2	2,000	<i>Excess</i> ⁷	Biotin ↑	Regular
11.1	0.2	200	<i>Regular</i>	Biotin ↑	Regular
4.4	0.08	80	<i>Diet</i>	Trehalose ↑, ergothioneine ↑	Regular, cell length is reduced
2.2	0.04	40	<i>Severe diet</i>	Fructose-1,6-diphosphate ↓	Stochastic
1.7	0.03	30	<i>Sub-starvation</i>		Stochastic
1.1	0.02	20	<i>Starvation</i>	S-adenosyl-methionine ↑	Only occasional division
0	0	0	<i>Fasting</i>	CDP-choline ↑, ATP ↓, S-adenosyl-homocysteine ↑	No division

This study was initiated by the remarkable finding that *S. pombe* could proliferate in 4.4 mM glucose with almost identical doubling times as in standard EMM2 medium (111 mM glucose). Such concentration of glucose is roughly equivalent to the human blood glucose level before breakfast (usually denoted as fasting blood sugar, FBS, or fasting plasma glucose, FPG). We thus assume *S. pombe* can be applied as a model to study various metabolic mechanisms of mammalian body cells that obtain glucose from blood. The observed reduction in cell size at 4.4 mM glucose (designated ‘diet’ condition) might at least partially explain the similar doubling

⁷ Note: 111 mM is the glucose content of standard EMM2 medium, but we designated this concentration “excess” based on the observation that *S. pombe* cells could divide with a similar division timing even in 25-fold diluted glucose (4.4 mM).

time: under reduced glucose, cells may economize their growth to maintain the speed of the cell division cycle. Identification of metabolic biomarkers for different glucose concentrations by metabolomic analysis may indicate the key pathways that are implicated in the adaptation to reduced glucose conditions. Furthermore, the levels of certain key metabolites such as ATP or glutathione provide us with important information about the homeostasis of the cells. In the future, the same biomarkers may be observed in other metabolomic datasets, thus providing more clues about the underlying mechanisms.

Under glucose levels below 4.4 mM, the regularity of cell division was disrupted. The transition from division to quiescence occurred between the ‘severe diet’ (2.2 mM) and ‘sub-starvation’ (1.7 mM) levels. Under ‘starvation’ (1.1 mM), cell division was mostly arrested, but viability was maintained for at least one week. The level of ATP was also maintained under starvation, suggesting cells prioritize ATP production over growth and cell division. Cells treated with starvation accumulated large amounts of protective compounds like trehalose and ergothioneine, and appeared highly resilient, as demonstrated by their resistance to 40 mM H₂O₂.

Under ‘fasting’ (0 mM) condition, glycolysis intermediates disappeared within 5 min. After 8 hours, following the exhaustion of remaining ATP, cells started to quickly lose viability. Interestingly, cells pre-treated with starvation maintained long viability even under fasting. Sugar phosphate compounds might represent the metabolic markers of healthy cells, as their levels were maintained in all conditions that supported cell viability, but quickly decayed under abrupt fasting leading to cell death. The rise of lipid precursors CDP-choline and -ethanolamine under fasting condition points to the involvement of lipid metabolism. The exact function of these compounds can be further studied by applying genetic methods, as their biosynthetic genes are already known. Importantly, CDP-choline and –ethanolamine do not seem to be markers of

cell death, as they also appeared in cells under long-term starvation, where viability was fully maintained.

Chapter 4. Dissection of ergothioneine and selenoneine biosynthetic pathway

Note: This study was published in *PLOS ONE* [117]. Majority of figures and tables in this Chapter were adapted from the published article with slight modifications.

4.1 Introduction

Ergothioneine (Fig. 4.1) is a small metabolite (229 Da) derived from histidine and cysteine. It was first isolated from rye ergot (*Claviceps purpurea*) in 1909 by a French pharmacist and chemist Charles J. Tanret [126]. Later, it was discovered that its biosynthesis occurs only in a limited number of microorganisms (notably, actinobacteria, cyanobacteria, and some fungi). However, higher organisms including humans obtain ergothioneine through diet [127] and accumulate it in certain tissues or cells up to millimolar levels [128,129]. In mammals, ergothioneine is mostly concentrated in erythrocytes, bone marrow, liver, kidney, eye lens and seminal fluid [128,130,131]. This tissue specific distribution is achieved by expressing a specific transporter for ergothioneine (ETT/OCTN1/SLC22A4 in humans) [132]. Interestingly, ergothioneine does not seem to be metabolized in mammalian body [133] and its uptake is non-essential [134]. This metabolite thus appears to be neither a nutrient nor a vitamin. The present knowledge on ergothioneine was extensively reviewed by Cheah and Halliwell [115].

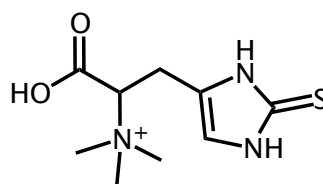


Fig. 4.1. Chemical structure of ergothioneine

Ergothioneine is widely regarded as an antioxidant compound, due to its free radical-scavenging and metal cation-chelating properties reported *in vitro* [129,135-139]. However, its true role *in vivo* is still debated, due to a lack of convincing evidence. It is unclear whether ergothioneine supplementation would have any favorable effects on human health, although several ergothioneine-containing products (nutraceuticals) are already on the market. Nevertheless, the ubiquitous presence of ergothioneine in almost all living organisms suggests a beneficial role for life. There is thus a strong motivation to study the mechanisms of ergothioneine metabolism at molecular level. The discovery of biosynthetic genes of ergothioneine has recently been reported in *Mycobacterium smegmatis* [140] and *Neurospora crassa* [116], opening thus the possibility to apply genetic methods.

Ergothioneine is apparently produced by *S. pombe*, as it was among the compounds detected in our initial metabolomic analysis (see Chapter 2). As described in Chapter 3, ergothioneine was accumulated in *S. pombe* cells under glucose starvation. In addition, we previously reported increased levels of ergothioneine in WT cells at the onset of nitrogen starvation [141], in proteasome regulatory subunit mutant *mts3-1*, which suffers from severe oxidative stress caused by mitochondrial dysfunctions under quiescence [142], and in the Krüppel-like C₂H₂ zinc-finger transcription factor mutant $\Delta klf1$, which exhibits defects in long-term quiescence [143] (see Thesis Supplements). Based on these observations, we decided to examine ergothioneine biosynthesis and function deeper. In this study we characterize the complete biosynthetic pathway of ergothioneine in *S. pombe* through combined use of genetics

and metabolomics. In addition, we demonstrate that the same pathway can also synthesize selenoneine, a selenium-containing derivative of ergothioneine, if selenium is provided in the culture medium.

4.2 Methods

4.2.1 Strains and growth conditions

The fission yeast strains used in this study are listed in Table 4.1.

Table 4.1. *S. pombe* strains used in this study. × = crossing; → = marker switch.

Name	Genotype	Source
972	<i>h</i> ⁻ (WT)	Leupold [144]
975	<i>h</i> ⁺ (WT)	
KS1366	<i>h</i> ⁻ Δ <i>styl1::ura4</i> ⁺ <i>ura4-D18</i>	Shiozaki and Russell [145]
TP1701	<i>h</i> ⁻ Δ <i>nfs1::kanMX4</i>	Bioneer haploid deletion mutant collection ⁸ [49]
TP1704	<i>h</i> ⁻ Δ <i>SPBC660.12c::kanMX4</i>	
TP1705	<i>h</i> ⁻ Δ <i>SPAC11D3.10::kanMX4</i>	
TP1706	<i>h</i> ⁺ Δ <i>SPCC777.03c::kanMX4</i>	
TP1770	<i>h</i> ⁻ Δ <i>egt1::kanMX6</i>	Constructed for this study.
TP1771	<i>h</i> ⁻ Δ <i>egt2::kanMX6</i>	
TP1857	<i>h</i> ⁻ <i>egt1::P81nmt1-egt1</i> ⁺	
TP1855	<i>h</i> ⁻ <i>egt1::P41nmt1-egt1</i> ⁺	
TP1803	<i>h</i> ⁻ <i>egt1::P3nmt1-egt1</i> ⁺	
TP1813	<i>h</i> ⁻ Δ <i>egt2::hphMX6</i>	TP1771 → <i>hphMX6</i>
TP1814	<i>h</i> ⁺ Δ <i>egt2::hphMX6</i>	TP1813 × WT 975
TP1879	<i>h</i> ⁻ <i>egt1::P3nmt1-egt1</i> ⁺ Δ <i>egt2::hphMX6</i>	TP1803 × TP1814

Standard EMM2, YE, and MEA media were used for cell cultivations (see Table 2.1).

⁸ The strains were backcrossed once with WT 972 to remove the auxotrophic markers *ade6 ura4 leu1* that were present in the genotype of the original Bioneer strains.

Modified formulations of the EMM2 medium were used as follows: EMM2+Se denotes EMM2 with the addition of 10 μ M Na₂SeO₄; EMM2-N denotes EMM2 without NH₄Cl; EMM2-LG denotes EMM2 with low glucose (1.1 mM, equal to 1/100 of the standard EMM2 glucose content). Cultivation temperature was 26°C in all experiments.

4.2.2 Construction of mutants

The marker switch from kanamycin-resistant (kanMX) to hygromycin-resistant (hphMX) strain (TP1813) was performed as described previously [146,147]. Crosses were performed by inducing meiosis on an MEA plate followed by tetrad dissection and selection on YE plates containing geneticin (G418), hygromycin, or both (depending on strain).

DNA recombinant strains were constructed by PCR method in two steps. First, two 500-bp regions were amplified using the WT genomic DNA as a template, corresponding to forward and reverse ends of the recombination cassette. Second, both modules were combined with the appropriate plasmid containing the kanamycin resistance marker (kanMX). Transformants were selected by resistance to geneticin (G418) and correct integrations were verified by colony PCR. The primer sequences used for all PCR amplifications are included in Table 4.2.

The gene disruption strains (TP1770 and TP1771) were constructed using the *pFA6a-kanMX6* plasmid [148]. The overexpression strains (TP1857, TP1855, and TP1803) were constructed using the *pFA6a-kanMX6-P81nmt1*, *pFA6a-kanMX6-P41nmt1*, and *pFA6a-kanMX6-P3nmt1* plasmids, respectively [148].

Table 4.2. Sequences of DNA primers used for PCR amplifications in this study.

Strain	Primer set	Sequence (5'-3')
TP1770	Forward module	CAGAATCCCTGTTACCCGGCTAGGTTGTAG
		TTAATTAACCCGGGGATCCGACAGCGTCTCAATGCTTATGCTTGCTTTTT
	Reverse module	CATTACTACGACGTTTGGCTGCTACTTTGT
		GTTTAAACGAGCTCGAATTCTTTAGCATACATACTACAATAGCATCGTCA
TP1771	Forward module	ACCTTCAGTAAACCTTGACAACGAGAGAT
		TTAATTAACCCGGGGATCCGACAGTGAATTTCCGGAATCCCAATTTGTAG
	Reverse module	TAAATATGATTTGTGATTATTCCTGGCT
		GTTTAAACGAGCTCGAATTCTAACTATGCTTCACAATGCATCCTCTGACT
TP1857	Forward module	TAATGTTTCTTTTCAAGTGTATGCGATGTA
		CCGCCATCCAGTTTAAACGAGCTCGAATTCATGGATAGTAGTATGTGTTAGAGAGTTA
	Reverse module	GACACCTTAACATGCTGATAATTGGTAGTT
		TCTGACTTATAGTCGCTTTGTAAATCATGACAGAAATAGAAAACATTGGCGCATTAGAA
TP1855	Forward module	TAATGTTTCTTTTCAAGTGTATGCGATGTA
		CCGCCATCCAGTTTAAACGAGCTCGAATTCATGGATAGTAGTATGTGTTAGAGAGTTA
	Reverse module	GACACCTTAACATGCTGATAATTGGTAGTT
		TCTGACTTATAGTCGCTTTGTAAATCATGACAGAAATAGAAAACATTGGCGCATTAGAA
TP1803	Forward module	TAATGTTTCTTTTCAAGTGTATGCGATGTA
		CCGCCATCCAGTTTAAACGAGCTCGAATTCATGGATAGTAGTATGTGTTAGAGAGTTA
	Reverse module	GACACCTTAACATGCTGATAATTGGTAGTT
		TCTGACTTATAGTCGCTTTGTAAATCATGACAGAAATAGAAAACATTGGCGCATTAGAA

4.2.3 Metabolomic analyses

Metabolomic experiments were performed using the protocol introduced in Chapter 2.

4.2.4 Spot test experiments

Plates for spot tests were prepared using EMM2 recipe with 17 g/L agar. Additional reagents (H_2O_2 , t -BOOH, and Na_2SeO_4) were added to the media after autoclaving to the indicated final concentrations. Cell cultures were prepared in liquid EMM2 (5×10^6 cells/mL) and diluted in 6 steps (5-fold dilution in each step). 5 μ L of culture was plated in each spot. Plates were incubated at 26°C for 6 days before taking photos.

4.3 Ergothioneine biosynthesis in *S. pombe*

4.3.1 Previously established biosynthetic pathways

The previously published biosynthetic pathways of ergothioneine in *M. smegmatis* [140] and *N. crassa* [116] are shown in Fig. 4.2. In the first step, histidine is methylated to *N,N,N*-trimethyl histidine (hercynine). In *M. smegmatis*, γ -glutamyl cysteine is then conjugated with hercynine by EgtB, followed by the removal of the glutamyl residue by EgtC to form hercynylcysteine sulfoxide. In *N. crassa*, however, cysteine is directly bound to hercynine by *Egt-1*, the same enzyme that performs the methylation of histidine in the first step. *NcEgt-1* is thus a fusion enzyme, homologous to both EgtD and EgtB. Such fusion enzymes performing both functions of EgtD and EgtB can be found in most eukaryotes that produce ergothioneine [140]. In the final step, catalyzed by EgtE in mycobacteria, hercynylcysteine sulfoxide is cleaved at the cysteine residue to produce ergothioneine. EgtE homolog in *N. crassa* is unknown.

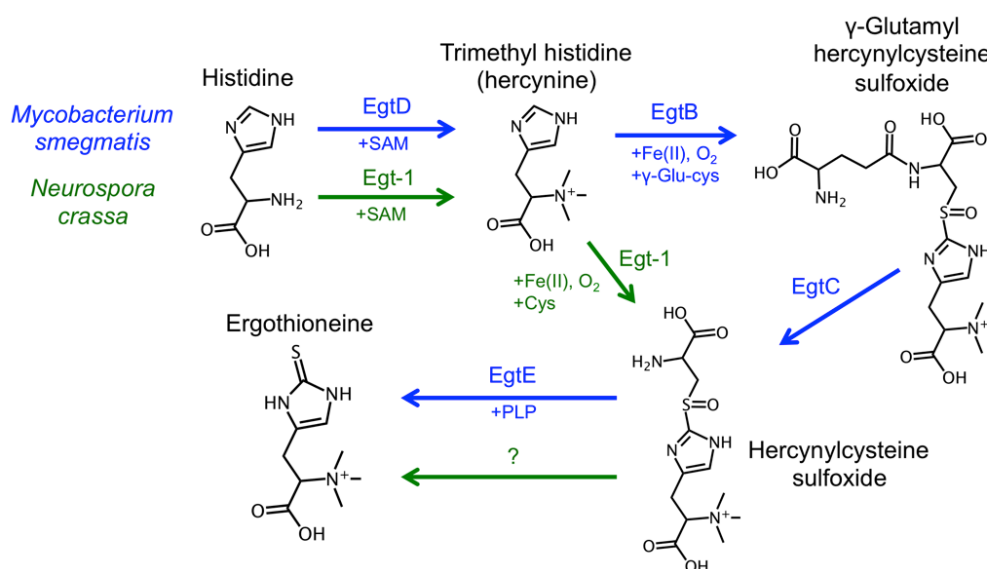


Fig. 4.2. Ergothioneine biosynthetic pathways in *M. smegmatis* (blue) and *N. crassa* (green). Note that

the *NcEgt-1* enzyme catalyzes two different reactions. SAM = *S*-adenosyl methionine; PLP = pyridoxal phosphate.

4.3.2 Identification of *egt1*⁺

The *S. pombe* locus SPBC1604.01 (previously named *mug158*⁺, denoting meiotically up-regulated gene 158 [60]) is the closest homolog of *N. crassa Egt-1*, with 38% amino acid sequence identity. Using data from the Conserved Domain Database [149], we compared the conserved domain structure of this enzyme with its homologs in *Schizosaccharomyces japonicus* (one of the closest relatives of *S. pombe*), *N. crassa*, and *M. smegmatis* (Fig. 4.3). All proteins contain an *S*-adenosyl methionone (SAM)-dependent methyltransferase domain (including a domain of unknown function, DUF2260), an uncharacterized DinB_2 domain (including an iron-binding motif HX₃HXE), and a formylglycine generating enzyme (FGE)-sulfatase domain. In *N. crassa*, the FGE-sulfatase domain contains a split, the function of which is unknown. Such splits, however, can be found in *NcEgt-1* homologs in many organisms, mostly in FGE-sulfatase and in SAM-dependent methyltransferase domains [116]. Based on the sequence homology and conserved domain analysis, we designated the SPBC1604.01 locus *egt1*⁺, standing for ergothioneine biosynthesis protein 1.

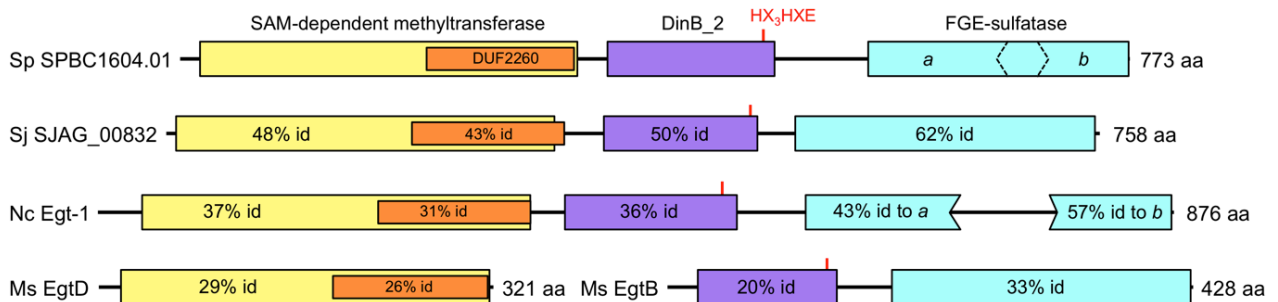


Fig. 4.3. Conserved domain structure of *S. pombe* SPBC1604.01 protein compared with *S. japonicus* SJAG_00832, *N. crassa* Egt-1, and *M. smegmatis* EgtD/EgtB. Percentage identity (% id) of amino acid sequences is calculated by comparison to corresponding sequences in *S. pombe*

4.3.3 Identification of *egt2*⁺

The mycobacterial EgtE enzyme is a pyridoxal-phosphate (PLP)-binding cysteine desulfurase. As no homolog of EgtE has to date been characterized in eukaryotes, we searched for candidate homologs in *S. pombe* genome based on the amino acid sequence of *M. smegmatis* EgtE. Using the Basic Local Alignment Search Tool [BLAST; 150] algorithm for protein sequences, we identified four putative homologs of EgtE that contain a single cysteine desulfurase domain: Nfs1 (SPBC21D10.11c), SPBC660.12c, SPAC11D3.10, and SPCC777.03c (Fig. 4.4).

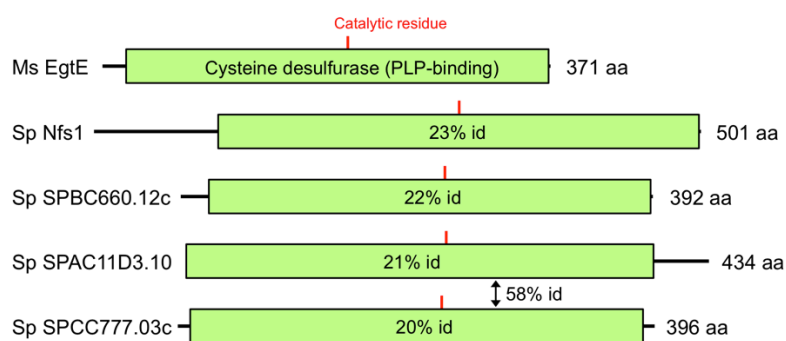


Fig. 4.4. Conserved domain structure of *M. smegmatis* EgtE in comparison with its four putative *S. pombe* homologs. The conserved catalytic residue is indicated by a red line. Percentage identity (% id) of the amino acid sequences is calculated by comparison to the corresponding sequence in *M. smegmatis*.

SPAC11D3.10 and SPCC777.03c have highly similar sequences.

We then obtained deletion mutant strains of these genes from the Bioneer deletion strain collection [49]. The strains were cultivated in EMM2-N medium for 24 hours to stimulate the production of ergothioneine, and performed metabolomic analysis (Fig. 4.5). Among the four deletion mutants tested, only Δ SPBC660.12c was showed a significant decrease in ergothioneine and an increase in its direct precursor, hercynylcysteine sulfoxide. We thus designated the SPBC660.12c locus *egt2*⁺, standing for ergothioneine biosynthesis protein 2.

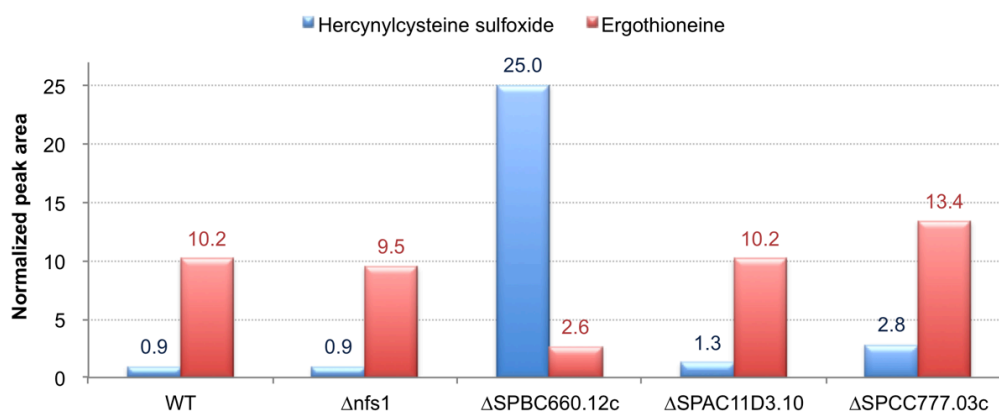


Fig. 4.5. Normalized peak areas of ergothioneine and hercynylcysteine sulfoxide (direct ergothioneine precursor), obtained by metabolomic analysis. Cells were cultivated in EMM2-N medium for 24 h.

4.3.4 Verification using deletion mutants

To verify the correct assignment of the *egt1*⁺ and *egt2*⁺ genes, we constructed deletion mutants of these genes (strains TP1770 and TP1771, see Methods). The strains were constructed by replacing the whole open reading frame with a kanamycin resistance marker (kanMX). No growth defects or phenotypes were observed in these strains. Since vegetatively growing *S. pombe* cells contain only trace amounts of ergothioneine, we analyzed the metabolome of these mutants under nitrogen starvation (24 h cultivation in EMM2-N medium). As shown in Fig. 4.6, all intermediates of the ergothioneine pathway were completely absent in the $\Delta egt1$ strain. In $\Delta egt2$ strain, hercynylcysteine sulfoxide accumulated, as expected. Ergothioneine was not completely diminished in the $\Delta egt2$ strain, but that is not a surprising result, as Seebeck [140] previously reported that hercynylcysteine sulfoxide can spontaneously convert into ergothioneine in the presence of PLP, and this reaction can even be catalyzed by an unrelated β -lyase. We thus assume the ergothioneine found in the $\Delta egt2$ strain is a product of such spontaneous conversion, possibly catalyzed by unrelated PLP-binding enzymes. *S. pombe* has at least 26 PLP-binding enzymes in its genome, according to the genome annotation database

[PomBase; 46].

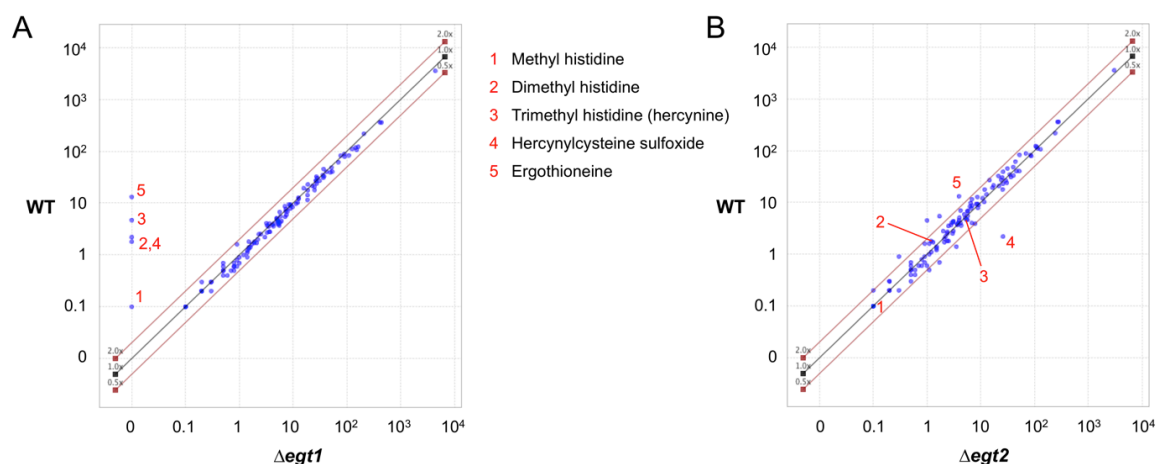


Fig. 4.6. A scatter plot comparing results of metabolomic analysis of WT vs. $\Delta egt1$ (A) or $\Delta egt2$ (B) strains under nitrogen starvation (24 h in EMM2-N medium). Blue dots denote identified metabolites. Intermediates in the ergothioneine pathway are annotated by red digits. Values on both axes indicate normalized peak areas. Red diagonal lines indicate a 2-fold difference.

Importantly, except the ergothioneine pathway intermediates, all other metabolites remained within a 2-fold difference compared to WT, in both $\Delta egt1$ and $\Delta egt2$ strains. We thus conclude that the absence of ergothioneine did not cause any significant perturbations to the metabolomes of these strains. This is a similar observation as with the $\Delta sib1$ (ferrichrome synthetase) deletion strain, the metabolome of which we analyzed in Chapter 2.

4.4 Overexpression of $egt1^+$

To study the effects of excess ergothioneine production, we constructed overexpression strains of $egt1^+$, by introducing the native $nmt1^+$ promoter that triggers gene expression in the absence of thiamine [151]. We employed three versions of the $nmt1^+$ promoter with increasing strength of expression, using previously described plasmids $pFA6a-kanMX6-P81nmt1$,

pFA6a-kanMX6-P41nmt1, and *pFA6a-kanMX6-P3nmt1* [148]. Using this method we constructed strains *P81nmt1-egt1⁺* (lowest level of expression), *P41nmt1-egt1⁺* (middle level of expression), and *P3nmt1-egt1⁺* (highest level of expression).

Fig. 4.7 shows the results of metabolomic analysis of these strains in the regular EMM2 medium, which does not contain thiamine. Ergothioneine and its precursors were clearly accumulated in the overexpression strains, as expected. Their accumulation was suppressed by addition of 5 $\mu\text{g}/\text{mL}$ thiamine. This experiment thus provided an additional confirmation of the correct assignment of *egt1⁺*. The highest detected signal was that of hercynylcysteine sulfoxide in the *P3nmt1-egt1⁺* strain, suggesting that the intense activity of Egt1 in this strain might have produced such amounts of hercynylcysteine sulfoxide that could not be efficiently converted into ergothioneine by the natively present Egt2.

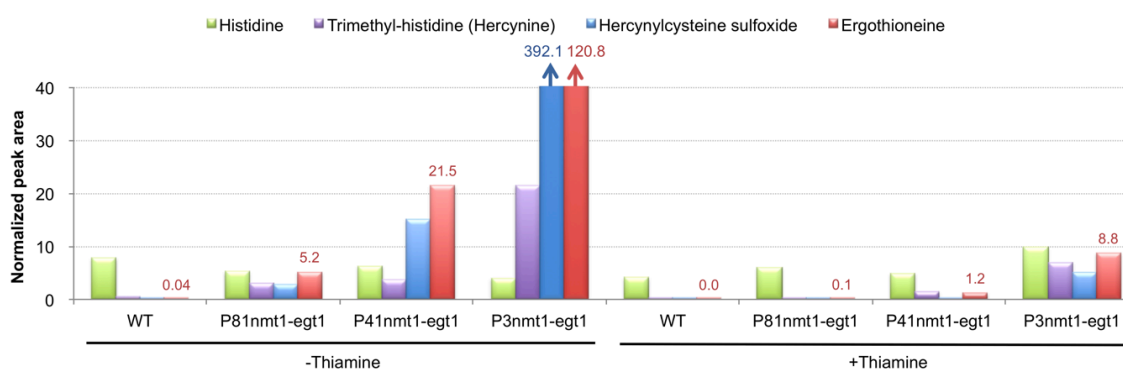


Fig. 4.7. Metabolome analysis results of *egt1⁺* overexpression strains in EMM2 medium.

+Thiamine = addition of 5 $\mu\text{g}/\text{mL}$ thiamine for 24 h.

To obtain the absolute concentrations of ergothioneine in *S. pombe* cells in vegetative, quiescent, as well as *egt1⁺*-overexpressing conditions, we performed LC-MS injections of a pure ergothioneine standard in 10-fold dilutions, in a broad range of amounts ranging from 1 fmol to 10 nmol (Fig. 4.8).

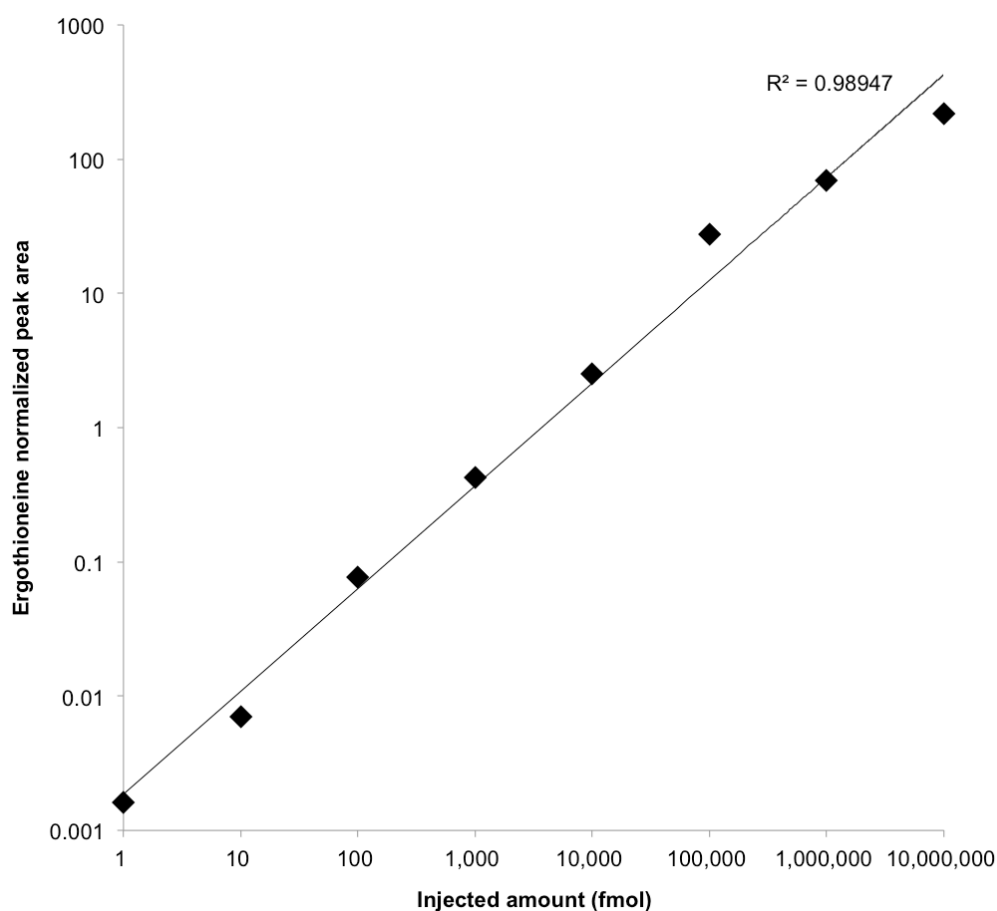


Fig. 4.8. Calibration curve of ergothioneine, showing the relationship between injected amount (fmol) and normalized peak area obtained by LC-MS. Linear regression curve is fitted to the data points.

The obtained peak areas from these injections were used to construct a calibration curve, which we used to convert the peak areas obtained from cellular extracts into absolute molar amounts. We estimated the intracellular volume to be $148.5 \mu\text{m}^3$ in case of vegetative cells [152], and 1/3 or 2/3 of the vegetative cell volume, in case of nitrogen-starved or glucose-starved cells, respectively. Using the obtained molar amounts and estimated intracellular volumes, we calculated the intracellular ergothioneine concentrations in each condition (Table 4.3).

Table 4.3. Absolute intracellular concentrations (μM) of ergothioneine in *S. pombe* cells in vegetative, nitrogen-starved, glucose-starved, and *egt1*⁺-overexpressing conditions.

Cell condition	Culture medium	Intracellular ergothioneine (μM)
WT vegetative	EMM2	0.3
WT nitrogen starvation	EMM2-N (24 h)	157.4
WT glucose starvation	EMM2-LG (24 h)	41.6
<i>P81nmt1-egt1</i> ⁺	EMM2	32.4
<i>P41nmt1-egt1</i> ⁺	EMM2	181.2
<i>P3nmt1-egt1</i> ⁺	EMM2	1,606.3

4.5 Role of *egt1*⁺ in protection from peroxide

Ergothioneine is widely regarded as a physiological antioxidant (see Introduction). In *N. crassa*, the ergothioneine-deficient $\Delta NcEgt-1$ mutant showed sensitivity to *tert*-butyl hydroperoxide in conidia [116]. We thus prepared EMM2 agar plates with various concentrations of two different oxidants, hydrogen peroxide (H_2O_2) and *tert*-butyl hydroperoxide (*t*-BOOH). We prepared cell cultures of the deletion and overexpression strains constructed in this study and conducted spot test experiments. The stress-sensitive MAP-kinase deletion strain $\Delta sty1$ was used as a positive control. However, neither sensitivity nor resistance to the tested oxidants was observed in any of the constructed strains (Fig. 4.9 and 4.10). We thus concluded that ergothioneine might not be among the primary mechanisms that protect *S. pombe* cells from exogenous peroxide.

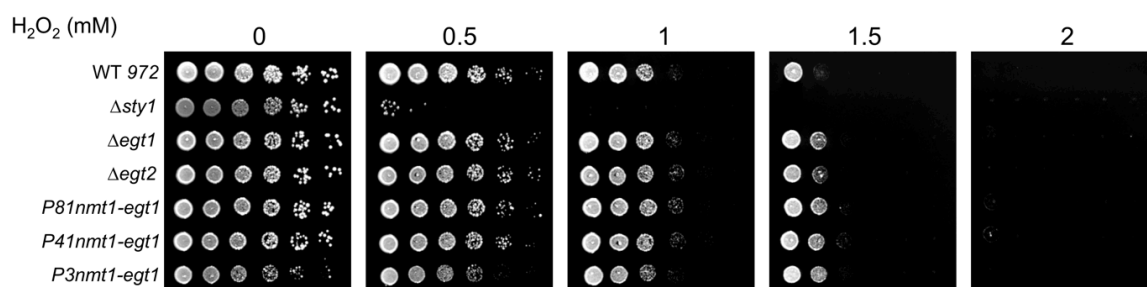


Fig. 4.9. Spot test experiments on EMM2 plates with addition of H_2O_2 . The leftmost spots originated from plating approximately 25,000 cells, with serial dilutions 5-fold in each consecutive step (rightmost spots thus originated from approximately 8 individual cells).

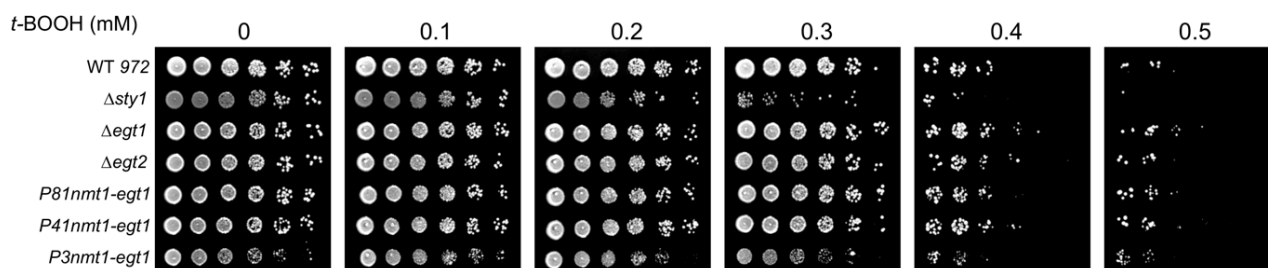


Fig. 4.10. Spot test experiments on EMM2 plates with addition of *tert*-butyl hydroperoxide. The leftmost spots originated from plating approximately 25,000 cells, with serial dilutions 5-fold in each step (rightmost spots thus originated from approximately 8 individual cells).

4.6 Biosynthesis of selenoneine

Selenoneine (Fig. 4.11) is a derivative of ergothioneine, in which the sulfur atom is replaced with a selenium atom. It was first isolated from tuna, with indications that it might have a role in methylmercury detoxification [153,154]. In predominantly fish-eating human populations, selenoneine represents the major form of selenium in blood [155]. Furthermore, it was suggested that the radical-scavenging activity of selenoneine might be higher compared to that of ergothioneine [154]. In our previous metabolome experiments, we did not find any selenoneine, presumably because the standard EMM2 medium does not contain any source of selenium.

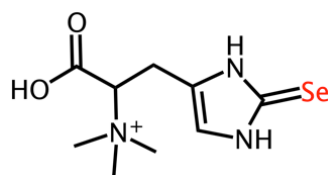


Fig. 4.11. Chemical structure of selenoneine. The selenium atom is highlighted.

To test whether *S. pombe* can produce selenoneine, we supplemented the EMM2 medium with 10 μM Na_2SeO_4 (denoted EMM2+Se, or EMM2-N+Se for medium lacking NH_4Cl). Cell cultures were cultivated in the selenium-supplemented media for 24 h, and metabolome analysis was conducted using WT and *P3nmt1-egt1*⁺ overexpression mutant cells (Fig. 4.12). The selenoneine ion was identified by its predicted mass value (278.040 m/z, calculated from formula $\text{C}_9\text{H}_{16}\text{N}_3\text{O}_2\text{Se}^+$). In WT nitrogen-starved cells, only trace amount of selenoneine was found (less than 1% of the ergothioneine peak area). However, in the *P3nmt1-egt1*⁺ strain, selenoneine was abundant, suggesting that the Egt1 enzyme was responsible for its biosynthesis.

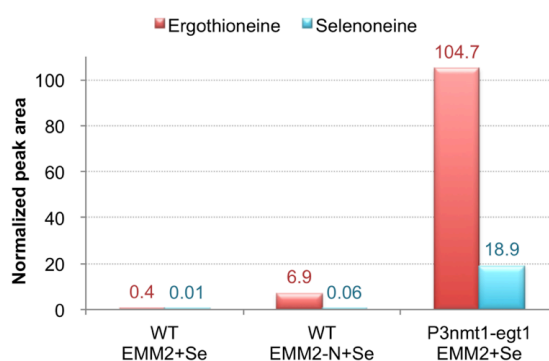


Fig. 4.12. Normalized peak areas of ergothioneine and selenoneine peaks in WT and *P3nmt1-egt1*⁺ cells cultivated for 24 h in EMM2+Se and EMM2-N+Se (nitrogen starvation) media.

The signals of ergothioneine and selenoneine were both diminished in the Δegt1 mutant, thus providing additional evidence that Egt1 is indeed the key enzyme that produces this compound (Fig. 4.13).

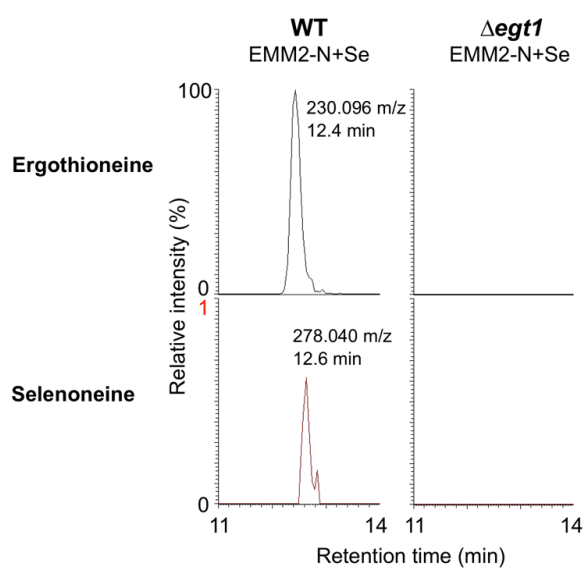


Fig. 4.13. Raw LC-MS metabolome data (extracted ion chromatograms) of ergothioneine and selenoneine from nitrogen-starved cells (24 h in EMM2-N+Se medium). The scale of the selenoneine chromatogram is 1% relative to that of the ergothioneine chromatogram.

Even with this evidence, however, it was still possible that the detected selenoneine had been produced by direct conversion from ergothioneine, without requiring any Egt1 activity *per se* for this conversion. To rule out this possibility, we cultivated the $\Delta egt1$ mutant cells in the presence of 1 mM ergothioneine. The extracellular ergothioneine was transported into the cells and produced a strong signal of ergothioneine mass (230.096 m/z) in the LC-MS data (Fig. 4.14). However, no selenoneine signal was detected. In addition, the small selenoneine peak found in WT cells was not increased by the addition of the large amount of ergothioneine. We thus conclude that the observed selenoneine was not produced by direct conversion from ergothioneine, and that the Egt1 enzyme was required for its biosynthesis.

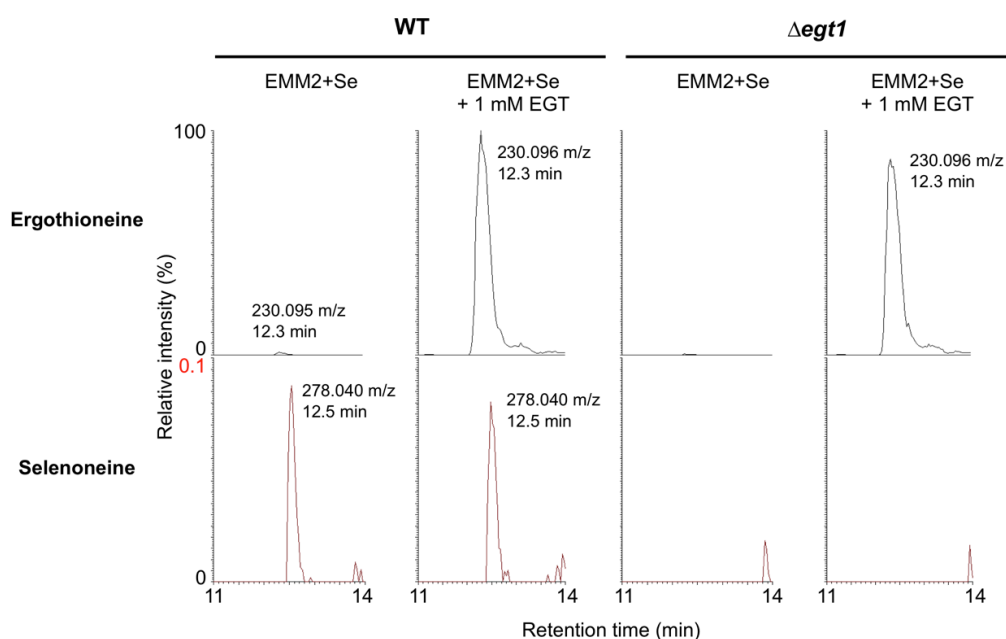


Fig. 4.14. Raw LC-MS metabolome data of ergothioneine and selenoneine from cells cultivated in EMM2 medium supplemented with 1 mM ergothioneine, as indicated. The intensity scale of the selenoneine chromatogram is 0.1% relative to that of the ergothioneine chromatogram.

The remaining questions are whether selenoneine was produced from the expected precursor metabolite, hercynylselenocysteine selenoxide (in analogy to the ergothioneine precursor, hercynylcysteine sulfoxide), and whether this reaction was also mediated by Egt2. Since we did not observe any signal of the predicted mass of hercynylselenocysteine selenoxide (381.067 m/z, calculated from formula $C_{12}H_{21}N_4O_5Se^+$) in previous experiments, we constructed a double mutant of $P3nmt1-egt1^+$ and $\Delta egt2$. If Egt2 is involved in selenoneine biosynthesis, this strain should accumulate the highest amount of its direct precursor. Indeed, we found a strong peak of hercynylselenocysteine precursor. This compound, however, did not appear in the expected selenoxide form, but rather as a plain conjugate of hercynine and selenocysteine with m/z value of 365.072 m/z (Fig 4.15). This difference in the precursors of ergothioneine and selenoneine can be explained by the known instability of most selenoxides, in contrast with sulfoxides [156]. It is possible that hercynylselenocysteine selenoxide is transiently formed

during the synthesis, but due to its instability, the oxygen quickly dissociates and only hercynylselenocysteine remains detectable. The peak of hercynylselenocysteine was large in the double mutant, but much smaller in the *P3nmt1-egt1*⁺ single mutant, thus confirming that Egt2 catalyzes the conversion from hercynylselenocysteine to selenoneine.

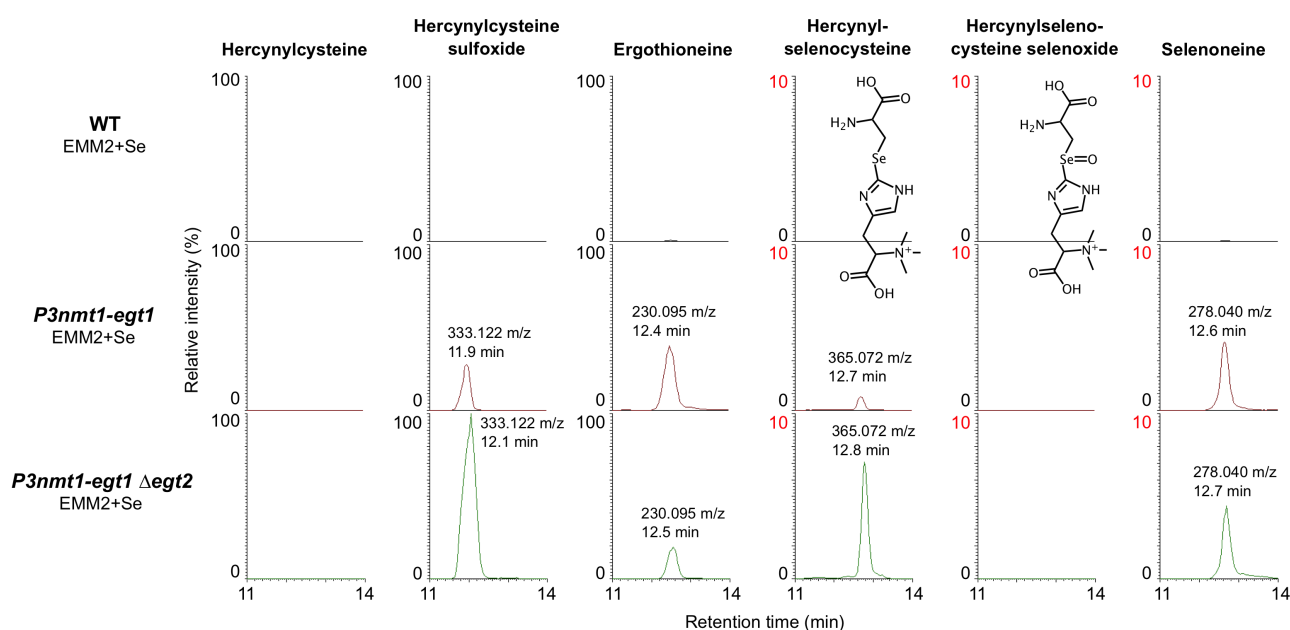


Fig. 4.15. Raw LC-MS data showing extracted ion chromatograms of predicted masses corresponding to six different compounds, as indicated (hercynylcysteine = 317.128 m/z; hercynylselenocysteine selenoxide = 381.067 m/z). The intensity scale of the chromatograms in the right half of the figure is adjusted to 10% relative to the chromatograms in the left half of the figure. The chemical structures of hercynylselenocysteine and hercynylselenocysteine selenoxide are shown in the figure, for clarity.

Since selenium occurs in nature in a very characteristic set of isotopes, we confirmed the identity of hercynylselenocysteine peak by its isotope distribution pattern (Fig 4.16; see also section 2.3.2, which describes the use of isotope patterns for compound identification).

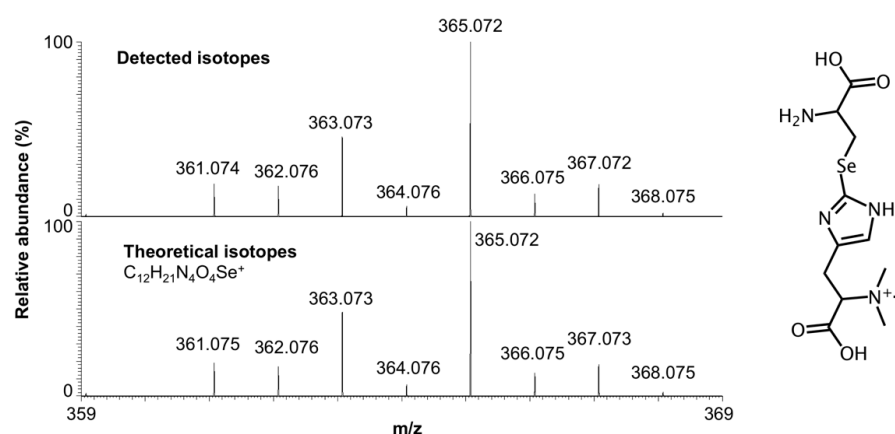


Fig. 4.16. Comparison of detected vs. calculated isotope distribution of hercynylselenocysteine (chemical structure shown on the right).

Finally, as selenium is fairly toxic to *S. pombe* [157], we checked whether the Egt1/Egt2 pathway could be involved in selenium detoxification in *S. pombe*. We prepared EMM2 agar plates with various concentrations of sodium selenate (Na_2SeO_4) and performed a spot test experiment using the constructed mutant strains. Similarly to previous experiments, the stress-sensitive MAP-kinase deletion strain Δsty1 was used as a positive control. However, no significant change in sensitivity to selenium was observed in any of the constructed strains (Fig. 4.17).

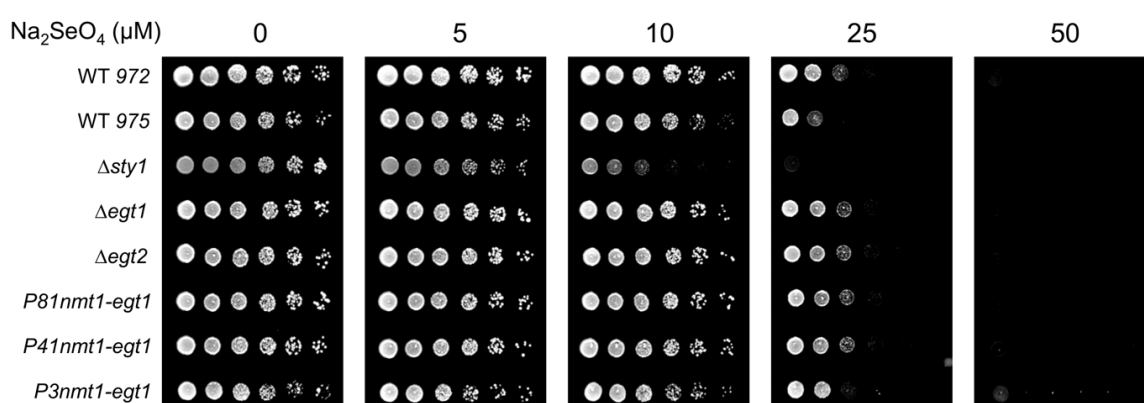


Fig. 4.17. Spot test experiments on EMM2 plates with addition of Na_2SeO_4 . The leftmost spots originated from plating approximately 25,000 cells, with serial dilutions 5-fold in each consecutive step (rightmost spots thus originated from approximately 8 individual cells).

4.7 Summary

In this study we applied genetic and metabolomic analyses to identify the *egt1*⁺ and *egt2*⁺ genes that constitute the ergothioneine and selenoneine biosynthesis pathway in *S. pombe* (Figure 4.18). Our results manifest the power of combining these two experimental approaches. Based on previously published transcriptomic analyses, the *egt1*⁺ gene is transcriptionally activated by H₂O₂ or cadmium [158], and strongly up-regulated under meiosis [60]. Furthermore, *egt1*⁺ was reported as a regulatory target of meiotic transcription factors *stell1*⁺ and *mei4*⁺ [159,160], and stress-responsive basic leucine zipper (bZIP) transcription factors *atf21*⁺ and *atf31*⁺ [160]. An analysis of multiple genome-wide microarray datasets [161] suggested that *egt1*⁺ might also be a target of transcription factors *ams2*⁺ [162], *php5*⁺ [163], and *pcr1*⁺ [164,165]. On the other hand, transcription of *egt2*⁺ does not seem to be activated by environmental stress [158], and is only mildly (~2-fold) up-regulated under meiosis [60]. We thus propose that *egt1*⁺ might act as the principal regulatory target of this pathway.

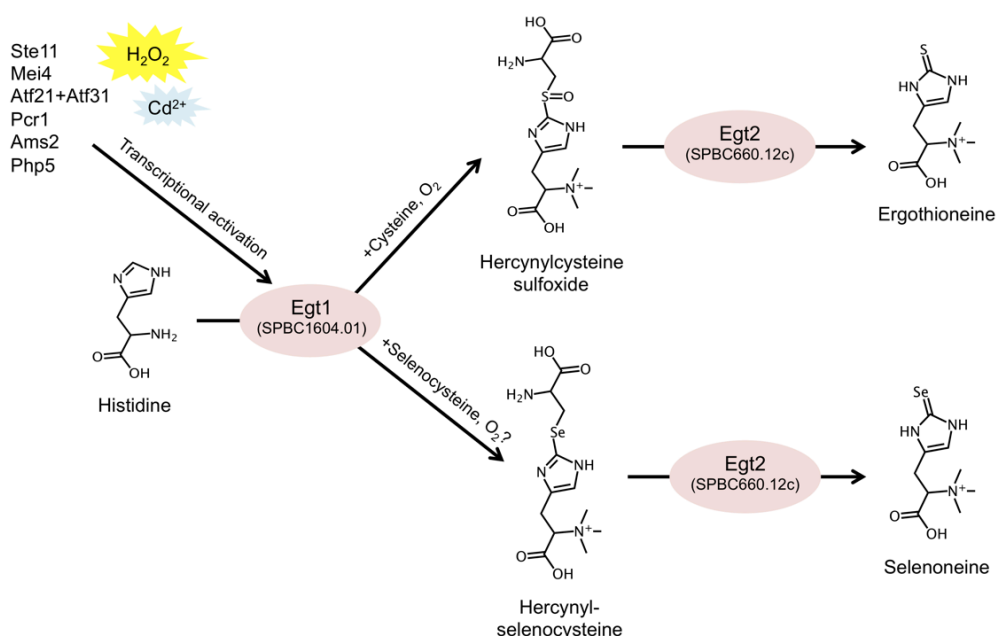


Fig. 4.18. A schema of the described Egt1/Egt2 pathway for biosynthesis of ergothioneine and selenoneine. Known transcriptional activators of Egt1 are shown in the upper left corner.

The *egt1*⁺ overexpression strain *P3nmt1-egt1* has proven to be extremely useful to elucidate the complete pathway, including the newly identified intermediate in selenoneine biosynthesis, mercynylselenocysteine. We propose this strain could thus be employed as a biofactory to produce ergothioneine, mercynylcysteine sulfoxide, selenoneine, or mercynylselenocysteine (among these four compounds, only ergothioneine is commercially available, to our knowledge).

The *egt1*⁺ and *egt2*⁺ genes have no homologs in the budding yeast *S. cerevisiae*, consistently with the observation that budding yeast does not produce ergothioneine [166]. This divergence between the two yeast species might reflect differences in their ecology. In the future, comparison between budding and fission yeasts might thus provide valuable clues regarding the physiological function of ergothioneine or selenoneine. For ergothioneine, numerous mechanisms were proposed in the past [115,167,168]. However, limited evidence from *in vivo* experiments suggests that the truly beneficial role of this compound is still elusive. Selenoneine was only recently discovered, and research data regarding its function are still scarce. In our metabolome datasets, ergothioneine was much more abundant than selenoneine. This could partly be explained by the constitution of the EMM2+Se medium, which contained only 10 μ M selenate, but almost 0.3 mM sulfate (see Table 2.1). Nevertheless, it is unclear whether selenoneine has any physiological function in *S. pombe*, or whether it is simply a byproduct of ergothioneine biosynthesis. This question might be answered in the future by supplementing the Δ *egt1* mutant with pure ergothioneine or selenoneine, and comparing the resulting phenotypes. Importantly, we showed that selenoneine does not seem to be implicated in selenium detoxification in *S. pombe*. In conclusion, we propose that the methods and strains introduced in this study might greatly assist in studying the function of these two enigmatic metabolites.

Chapter 5. Conclusions

5.1 Achievements of this thesis

Metabolomics is a frontier research technique that still suffers from poor standardization and immature tools; however, technology is improving rapidly and many exciting research projects are on the way. In this thesis we introduced the methodology for metabolomic analysis in the fission yeast, *S. pombe*. Our protocols were optimized mainly for extraction and detection of polar metabolites. Besides the initial proof-of-concept study, we demonstrated two applications of this technique: characterization of the effects of glucose starvation, and dissection of the complete biosynthetic pathway of ergothioneine and selenoneine. While the experiments on glucose starvation were performed using WT *S. pombe* strain, the experiments on ergothioneine biosynthesis involved genetic manipulation. We thus confirmed that metabolome analysis could be successfully applied for both environmental and genetic studies.

Besides the articles included in this thesis, the same method was applied in several other studies published by our group, mostly related to nutrition and regulation of quiescence (see Thesis Supplements). In Takeda et al. [169], we described the accumulation of glutathione and ergothioneine in the proteasome regulatory subunit mutant strain *mts3-1* under nitrogen starvation. In Nakamura et al. [170], we measured the intermediates of coenzyme A biosynthetic pathway, and described the accumulation of 4'-phosphopantothenate in the phosphopantothenoylcysteine synthetase mutant strain *ppc1-537*. In Shimanuki et al. [143], we reported accumulations of *N*-acetyl-D-glucosamine, ergothioneine, and *S*-adenosyl methionine,

in the deletion mutant of C₂H₂ zinc finger transcription factor $\Delta klf1$ following long-term quiescence. In Sajiki et al. [141], we characterized rapid transformation of the metabolome during the first hour of nitrogen starvation, represented mainly by the diminishing of purine metabolism, decrease in free amino acids and increase in 2-oxoglutarate, trehalose, succinate, and mercynylcysteine sulfoxide. In addition, the author of this thesis has contributed to the metabolomics field by the development of MZmine 2, a software framework for mass spectrometry data analysis [99], and a set of algorithms for automatic chemical formula prediction from MS data [88]. These tools and LC-MS methods were also recently applied to the analysis of human blood cells and plasma [171,172].

5.2 Limitations and challenges of metabolomics

Although the estimated scale of metabolome is smaller than that of genome, transcriptome, or proteome (~5 thousand protein-coding genes in fission yeast, compared to ~2-3 thousand expected metabolites), measurement of the whole metabolome remains a technological challenge, due to immense chemical diversity among metabolites. Furthermore, identification of unknown compounds is a major bottleneck of contemporary metabolomics. After all, the constituents of genome, transcriptome, or proteome (DNA, RNA, and proteins) are composed of repeating units that belong to the same chemical category (nucleotides and amino acids). Metabolites, on the contrary, vary greatly in their chemical properties, such as molecular weight, polarity, and solubility. Their identification is further complicated by the presence of structural isomers. Range of native intracellular concentrations is another factor to be considered. While the most abundant metabolites in *S. pombe*, such as ATP or glutathione, are present in mM-level concentrations [173,174], the least abundant metabolites might be below 0.1 nM (assuming several individual molecules per cell having an intracellular volume of ~150 fL).

That results in a dynamic range of 7 orders of magnitude, presenting a challenge even for the most sensitive detection methods. Furthermore, some metabolites might be synthesized only in specific cellular conditions. Altogether, it is not surprising that despite thousands of different metabolites being presumably present in the cell, metabolomic studies rarely report more than ~150 different compounds.

5.3 Future developments

Common applications of metabolomics might overlap with the study of natural products, which are often derived from secondary metabolites. Natural products research has a long history, particularly in medical sciences. However, we mainly focused on the measurement of primary cellular metabolites, as our goal is to improve the understanding of the fission yeast as a model organism for cell biology. In fact, little is known about secondary metabolites produced by *S. pombe*. Identification of secondary metabolites is thus an interesting area for possible future expansion of this technique.

In budding yeast field, the scope of metabolomics is presently expanding in several directions. One such direction is the analysis of metabolic fluxes, or fluxomics [175,176]. Going towards miniaturization, first publications have appeared that describe metabolomic measurements on a single-cell scale [177,178]. Methods for high-throughput metabolomics screenings of low-volume cell cultures in 96-well format have also been developed [179]. We anticipate such methods will also be applied in fission yeast metabolomics in a foreseeable future.

One aspect of metabolomic research that has not been deeply covered in microorganisms [180] and remains virtually untouched in fission yeast is that of extracellular metabolome (exometabolome). It is known that fission yeast cells can secrete various enzymes,

but the composition and amount of secreted metabolites are mostly unknown. While this aspect might be most attractive for industrial applications, the composition and dynamics of metabolites secreted outside of the cells might potentially reveal exciting new aspects of microbial metabolism and adaptation to different environments.

References

- [1] Nielsen J, Jewett MC (2007) *Metabolomics: A Powerful Tool in Systems Biology*. Springer.
- [2] Villas-Boas SG, Nielsen J, Smedsgaard J, Hansen MAE, Roessner-Tunali U (2007) *Metabolome Analysis: An Introduction*. Wiley.
- [3] Nikolau BJ, Wurtele ES (2007) *Concepts in Plant Metabolomics*. Springer.
- [4] Wishart DS (2007) Current progress in computational metabolomics. *Brief Bioinform* **8**: 279-293.
- [5] Di Lena M, Travaglio E, Altomare DF (2014) Metabolomics: a potential powerful ally in the fight against cancer. *Colorectal Dis* **16**: 235-238.
- [6] delCardayre SB, Stock KP, Newton GL, Fahey RC, Davies JE (1998) Coenzyme A disulfide reductase, the primary low molecular weight disulfide reductase from *Staphylococcus aureus*. Purification and characterization of the native enzyme. *J Biol Chem* **273**: 5744-5751.
- [7] Yokoyama A, Murata M, Oshima Y, Iwashita T, Yasumoto T (1988) Some chemical properties of maitotoxin, a putative calcium channel agonist isolated from a marine dinoflagellate. *J Biochem* **104**: 184-187.
- [8] Wink M (2010) Introduction: biochemistry, physiology and ecological functions of secondary metabolites. *Annual Plant Reviews Volume 40: Biochemistry of Plant Secondary Metabolism*. Wiley-Blackwell.
- [9] Demain AL, Fang A (2000) The natural functions of secondary metabolites. *Adv Biochem Eng Biotechnol* **69**: 1-39.
- [10] Hartmann T (2007) From waste products to ecochemicals: fifty years research of plant secondary metabolism. *Phytochemistry* **68**: 2831-2846.
- [11] Sandermann H, Jr. (1992) Plant metabolism of xenobiotics. *Trends Biochem Sci* **17**: 82-84.
- [12] Oliver SG, Winson MK, Kell DB, Baganz F (1998) Systematic functional analysis of the yeast genome. *Trends Biotechnol* **16**: 373-378.
- [13] Kanehisa M, Goto S, Sato Y, Kawashima M, Furumichi M, et al. (2014) Data, information, knowledge and principle: back to metabolism in KEGG. *Nucleic Acids Res* **42**: D199-205.
- [14] Caspi R, Altman T, Billington R, Dreher K, Foerster H, et al. (2014) The MetaCyc database of metabolic pathways and enzymes and the BioCyc collection of Pathway/Genome

References

- Databases. *Nucleic Acids Res* **42**: D459-471.
- [15] Zhu ZJ, Schultz AW, Wang J, Johnson CH, Yannone SM, et al. (2013) Liquid chromatography quadrupole time-of-flight mass spectrometry characterization of metabolites guided by the METLIN database. *Nat Protoc* **8**: 451-460.
- [16] Wishart DS, Jewison T, Guo AC, Wilson M, Knox C, et al. (2013) HMDB 3.0--The Human Metabolome Database in 2013. *Nucleic Acids Res* **41**: D801-807.
- [17] Jewison T, Knox C, Neveu V, Djoumbou Y, Guo AC, et al. (2012) YMDB: the Yeast Metabolome Database. *Nucleic Acids Res* **40**: D815-820.
- [18] Guo AC, Jewison T, Wilson M, Liu Y, Knox C, et al. (2013) ECMDB: the *E. coli* Metabolome Database. *Nucleic Acids Res* **41**: D625-630.
- [19] Lucas X, Senger C, Erxleben A, Gruning BA, Doring K, et al. (2013) StreptomeDB: a resource for natural compounds isolated from *Streptomyces* species. *Nucleic Acids Res* **41**: D1130-1136.
- [20] Jewison T, Su Y, Disfany FM, Liang Y, Knox C, et al. (2014) SMPDB 2.0: big improvements to the Small Molecule Pathway Database. *Nucleic Acids Res* **42**: D478-484.
- [21] Afendi FM, Okada T, Yamazaki M, Hirai-Morita A, Nakamura Y, et al. (2012) KNApSAcK family databases: integrated metabolite-plant species databases for multifaceted plant research. *Plant Cell Physiol* **53**: e1.
- [22] Brown M, Dunn WB, Dobson P, Patel Y, Winder CL, et al. (2009) Mass spectrometry tools and metabolite-specific databases for molecular identification in metabolomics. *Analyst* **134**: 1322-1332.
- [23] Fahy E, Subramaniam S, Murphy RC, Nishijima M, Raetz CR, et al. (2009) Update of the LIPID MAPS comprehensive classification system for lipids. *J Lipid Res* **50**: S9-14.
- [24] Fiehn O (2001) Combining genomics, metabolome analysis, and biochemical modelling to understand metabolic networks. *Comp Funct Genomics* **2**: 155-168.
- [25] Goodacre R (2005) Metabolomics--the way forward. *Metabolomics* **1**: 1-2.
- [26] Crick FH (1958) On protein synthesis. *Symp Soc Exp Biol* **12**: 138-163.
- [27] Harrigan GG, Goodacre R (2003) Metabolic profiling: its role in biomarker discovery and gene function analysis. *Springer*.
- [28] Patti GJ, Yanes O, Siuzdak G (2012) Innovation: Metabolomics: the apogee of the omics trilogy. *Nat Rev Mol Cell Biol* **13**: 263-269.
- [29] Ellis DI, Dunn WB, Griffin JL, Allwood JW, Goodacre R (2007) Metabolic fingerprinting

- as a diagnostic tool. *Pharmacogenomics* **8**: 1243-1266.
- [30] Kell DB, Brown M, Davey HM, Dunn WB, Spasic I, et al. (2005) Metabolic footprinting and systems biology: the medium is the message. *Nat Rev Microbiol* **3**: 557-565.
- [31] Nicholson JK, Lindon JC (2008) Systems biology: Metabonomics. *Nature* **455**: 1054-1056.
- [32] Fiehn O (2002) Metabolomics--the link between genotypes and phenotypes. *Plant Mol Biol* **48**: 155-171.
- [33] Dunn WB, Ellis DI (2005) Metabolomics: Current analytical platforms and methodologies. *Trends in Analytical Chemistry* **24**: 285-294.
- [34] Lindon JC, Nicholson JK (2008) Spectroscopic and statistical techniques for information recovery in metabonomics and metabolomics. *Annu Rev Anal Chem (Palo Alto Calif)* **1**: 45-69.
- [35] Coen M, Holmes E, Lindon JC, Nicholson JK (2008) NMR-based metabolic profiling and metabonomic approaches to problems in molecular toxicology. *Chem Res Toxicol* **21**: 9-27.
- [36] Powers R (2009) NMR metabolomics and drug discovery. *Magn Reson Chem* **47**: S2-11.
- [37] Weljie AM, Newton J, Mercier P, Carlson E, Slupsky CM (2006) Targeted profiling: quantitative analysis of ¹H NMR metabolomics data. *Anal Chem* **78**: 4430-4442.
- [38] Huang X, Powers R, Tymiak A, Espina R, Roongta V (2007) Introduction to NMR and its application in metabolite structure determination. Drug metabolism in drug design and development. *John Wiley & Sons, Inc.* pp. 369-409.
- [39] Dass C (2007) Fundamentals of contemporary mass spectrometry. *John Wiley & Sons*.
- [40] Knolhoff AM, Callahan JH, Croley TR (2014) Mass accuracy and isotopic abundance measurements for HR-MS instrumentation: capabilities for non-targeted analyses. *J Am Soc Mass Spectrom*, doi:10.1007/s13361-014-0880-5.
- [41] Al-Dirbashi OY, Nakashima K (2000) Hyphenated chromatographic methods for biomaterials. *Biomed Chromatogr* **14**: 406-421.
- [42] Cody RB, Laramée JA, Durst HD (2005) Versatile new ion source for the analysis of materials in open air under ambient conditions. *Anal Chem* **77**: 2297-2302.
- [43] Takats Z, Wiseman JM, Gologan B, Cooks RG (2004) Mass spectrometry sampling under ambient conditions with desorption electrospray ionization. *Science* **306**: 471-473.
- [44] Milne SB, Mathews TP, Myers DS, Ivanova PT, Brown HA (2013) Sum of the parts: mass spectrometry-based metabolomics. *Biochemistry* **52**: 3829-3840.
- [45] Wood V, Gwilliam R, Rajandream MA, Lyne M, Lyne R, et al. (2002) The genome

- sequence of *Schizosaccharomyces pombe*. *Nature* **415**: 871-880.
- [46] Wood V, Harris MA, McDowall MD, Rutherford K, Vaughan BW, et al. (2012) PomBase: a comprehensive online resource for fission yeast. *Nucleic Acids Res* **40**: D695-699.
- [47] Forsburg SL, Rhind N (2006) Basic methods for fission yeast. *Yeast* **23**: 173-183.
- [48] Egel R (2004) The molecular biology of *Schizosaccharomyces pombe*: genetics, genomics and beyond. *Springer*.
- [49] Kim DU, Hayles J, Kim D, Wood V, Park HO, et al. (2010) Analysis of a genome-wide set of gene deletions in the fission yeast *Schizosaccharomyces pombe*. *Nat Biotechnol* **28**: 617-623.
- [50] Su SS, Tanaka Y, Samejima I, Tanaka K, Yanagida M (1996) A nitrogen starvation-induced dormant G0 state in fission yeast: the establishment from uncommitted G1 state and its delay for return to proliferation. *J Cell Sci* **109 (Pt 6)**: 1347-1357.
- [51] Nurse P (1975) Genetic control of cell size at cell division in yeast. *Nature* **256**: 547-551.
- [52] Yanagida M (2005) Basic mechanism of eukaryotic chromosome segregation. *Philos Trans R Soc Lond B Biol Sci* **360**: 609-621.
- [53] Yamamoto M (1996) Regulation of meiosis in fission yeast. *Cell Struct Funct* **21**: 431-436.
- [54] Hagan IM (1998) The fission yeast microtubule cytoskeleton. *J Cell Sci* **111 (Pt 12)**: 1603-1612.
- [55] Rowley R, Hudson J, Young PG (1992) The *wee1* protein kinase is required for radiation-induced mitotic delay. *Nature* **356**: 353-355.
- [56] Kelly TJ, Martin GS, Forsburg SL, Stephen RJ, Russo A, et al. (1993) The fission yeast *cdc18⁺* gene product couples S phase to START and mitosis. *Cell* **74**: 371-382.
- [57] Grewal SI (2000) Transcriptional silencing in fission yeast. *J Cell Physiol* **184**: 311-318.
- [58] Volpe TA, Kidner C, Hall IM, Teng G, Grewal SI, et al. (2002) Regulation of heterochromatic silencing and histone H3 lysine-9 methylation by RNAi. *Science* **297**: 1833-1837.
- [59] Shimanuki M, Chung SY, Chikashige Y, Kawasaki Y, Uehara L, et al. (2007) Two-step, extensive alterations in the transcriptome from G0 arrest to cell division in *Schizosaccharomyces pombe*. *Genes Cells* **12**: 677-692.
- [60] Mata J, Lyne R, Burns G, Bahler J (2002) The transcriptional program of meiosis and sporulation in fission yeast. *Nat Genet* **32**: 143-147.
- [61] Rustici G, van Bakel H, Lackner DH, Holstege FC, Wijmenga C, et al. (2007) Global

- transcriptional responses of fission and budding yeast to changes in copper and iron levels: a comparative study. *Genome Biol* **8**: R73.
- [62] Marguerat S, Schmidt A, Codlin S, Chen W, Aebersold R, et al. (2012) Quantitative analysis of fission yeast transcriptomes and proteomes in proliferating and quiescent cells. *Cell* **151**: 671-683.
- [63] Schmidt MW, Houseman A, Ivanov AR, Wolf DA (2007) Comparative proteomic and transcriptomic profiling of the fission yeast *Schizosaccharomyces pombe*. *Mol Syst Biol* **3**: 79.
- [64] Gunaratne J, Schmidt A, Quandt A, Neo SP, Sarac OS, et al. (2013) Extensive mass spectrometry-based analysis of the fission yeast proteome: the *Schizosaccharomyces pombe* PeptideAtlas. *Mol Cell Proteomics* **12**: 1741-1751.
- [65] Sajiki K, Hatanaka M, Nakamura T, Takeda K, Shimanuki M, et al. (2009) Genetic control of cellular quiescence in *S. pombe*. *J Cell Sci* **122**: 1418-1429.
- [66] Yanagida M (2009) Cellular quiescence: are controlling genes conserved? *Trends Cell Biol* **19**: 705-715.
- [67] Pluskal T, Nakamura T, Villar-Briones A, Yanagida M (2010) Metabolic profiling of the fission yeast *S. pombe*: quantification of compounds under different temperatures and genetic perturbation. *Molecular BioSystems* **6**: 172.
- [68] Raamsdonk LM, Teusink B, Broadhurst D, Zhang N, Hayes A, et al. (2001) A functional genomics strategy that uses metabolome data to reveal the phenotype of silent mutations. *Nat Biotechnol* **19**: 45-50.
- [69] Clasquin MF, Melamud E, Singer A, Gooding JR, Xu X, et al. (2011) Riboneogenesis in yeast. *Cell* **145**: 969-980.
- [70] Boer VM, Crutchfield CA, Bradley PH, Botstein D, Rabinowitz JD (2010) Growth-limiting intracellular metabolites in yeast growing under diverse nutrient limitations. *Mol Biol Cell* **21**: 198-211.
- [71] Hasunuma T, Sanda T, Yamada R, Yoshimura K, Ishii J, et al. (2011) Metabolic pathway engineering based on metabolomics confers acetic and formic acid tolerance to a recombinant xylose-fermenting strain of *Saccharomyces cerevisiae*. *Microb Cell Fact* **10**: 2.
- [72] Walther T, Novo M, Rossger K, Letisse F, Loret MO, et al. (2010) Control of ATP homeostasis during the respiro-fermentative transition in yeast. *Mol Syst Biol* **6**: 344.
- [73] Weeks ME, Sinclair J, Butt A, Chung YL, Worthington JL, et al. (2006) A parallel

- proteomic and metabolomic analysis of the hydrogen peroxide- and Sty1p-dependent stress response in *Schizosaccharomyces pombe*. *Proteomics* **6**: 2772-2796.
- [74] Bolten CJ, Wittmann C (2008) Appropriate sampling for intracellular amino acid analysis in five phylogenetically different yeasts. *Biotechnol Lett* **30**: 1993-2000.
- [75] Hucka M, Finney A, Sauro HM, Bolouri H, Doyle JC, et al. (2003) The systems biology markup language (SBML): a medium for representation and exchange of biochemical network models. *Bioinformatics* **19**: 524-531.
- [76] Osterlund T, Nookaew I, Nielsen J (2012) Fifteen years of large scale metabolic modeling of yeast: developments and impacts. *Biotechnol Adv* **30**: 979-988.
- [77] Herrgard MJ, Swainston N, Dobson P, Dunn WB, Arga KY, et al. (2008) A consensus yeast metabolic network reconstruction obtained from a community approach to systems biology. *Nat Biotechnol* **26**: 1155-1160.
- [78] Sohn SB, Kim TY, Lee JH, Lee SY (2012) Genome-scale metabolic model of the fission yeast *Schizosaccharomyces pombe* and the reconciliation of in silico/in vivo mutant growth. *BMC Syst Biol* **6**: 49.
- [79] Baidoo EE, Benke PI, Keasling JD (2012) Mass spectrometry-based microbial metabolomics. *Methods Mol Biol* **881**: 215-278.
- [80] Nguyen HP, Schug KA (2008) The advantages of ESI-MS detection in conjunction with HILIC mode separations: Fundamentals and applications. *J Sep Sci* **31**: 1465-1480.
- [81] Makarov A, Denisov E, Kholomeev A, Balschun W, Lange O, et al. (2006) Performance evaluation of a hybrid linear ion trap/orbitrap mass spectrometer. *Anal Chem* **78**: 2113-2120.
- [82] Horai H, Arita M, Kanaya S, Nihei Y, Ikeda T, et al. (2010) MassBank: a public repository for sharing mass spectral data for life sciences. *J Mass Spectrom* **45**: 703-714.
- [83] Rojas-Cherto M, van Vliet M, Peironcely JE, van Doorn R, Kooyman M, et al. (2012) MetiTree: a web application to organize and process high-resolution multi-stage mass spectrometry metabolomics data. *Bioinformatics* **28**: 2707-2709.
- [84] Wolf S, Schmidt S, Muller-Hannemann M, Neumann S (2010) In silico fragmentation for computer assisted identification of metabolite mass spectra. *BMC Bioinformatics* **11**: 148.
- [85] Zhou J, Weber RJ, Allwood JW, Mistrik R, Zhu Z, et al. (2014) HAMMER: automated operation of mass frontier to construct in silico mass spectral fragmentation libraries. *Bioinformatics* **30**: 581-583.

- [86] Gerlich M, Neumann S (2013) MetFusion: integration of compound identification strategies. *J Mass Spectrom* **48**: 291-298.
- [87] Berglund M, Wieser ME (2011) Isotopic compositions of the elements 2009 (IUPAC Technical Report). *Pure and Applied Chemistry* **83**: 397-410.
- [88] Pluskal T, Uehara T, Yanagida M (2012) Highly accurate chemical formula prediction tool utilizing high-resolution mass spectra, MS/MS fragmentation, heuristic rules, and isotope pattern matching. *Anal Chem* **84**: 4396-4403.
- [89] Schrettl M, Winkelmann G, Haas H (2004) Ferrichrome in *Schizosaccharomyces pombe*--an iron transport and iron storage compound. *Biometals* **17**: 647-654.
- [90] de Koning W, van Dam K (1992) A method for the determination of changes of glycolytic metabolites in yeast on a subsecond time scale using extraction at neutral pH. *Anal Biochem* **204**: 118-123.
- [91] Canelas AB, Ras C, ten Pierick A, van Dam JC, Heijnen JJ, et al. (2008) Leakage-free rapid quenching technique for yeast metabolomics. *Metabolomics* **4**: 226-239.
- [92] Dunn WB, Winder CL (2011) Sample preparation related to the intracellular metabolome of yeast methods for quenching, extraction, and metabolite quantitation. *Methods Enzymol* **500**: 277-297.
- [93] Villas-Bôas SG, Højer-Pedersen J, Akesson M, Smedsgaard J, Nielsen J (2005) Global metabolite analysis of yeast: evaluation of sample preparation methods. *Yeast* **22**: 1155-1169.
- [94] Canelas AB, ten Pierick A, Ras C, Seifar RM, van Dam JC, et al. (2009) Quantitative evaluation of intracellular metabolite extraction techniques for yeast metabolomics. *Anal Chem* **81**: 7379-7389.
- [95] Sporty JL, Kabir MM, Turteltaub KW, Ognibene T, Lin SJ, et al. (2008) Single sample extraction protocol for the quantification of NAD and NADH redox states in *Saccharomyces cerevisiae*. *J Sep Sci* **31**: 3202-3211.
- [96] Kim S, Lee do Y, Wohlgemuth G, Park HS, Fiehn O, et al. (2013) Evaluation and optimization of metabolome sample preparation methods for *Saccharomyces cerevisiae*. *Anal Chem* **85**: 2169-2176.
- [97] Castillo S, Gopalacharyulu P, Yetukuri L, Orešič M (2011) Algorithms and tools for the preprocessing of LC-MS metabolomics data. *Chemometrics and Intelligent Laboratory Systems* **108**: 23-32.

- [98] Sugimoto M, Kawakami M, Robert M, Soga T, Tomita M (2012) Bioinformatics tools for mass spectroscopy-based metabolomic data processing and analysis. *Curr Bioinform* **7**: 96-108.
- [99] Pluskal T, Castillo S, Villar-Briones A, Orešič M (2010) MZmine 2: modular framework for processing, visualizing, and analyzing mass spectrometry-based molecular profile data. *BMC Bioinformatics* **11**: 395.
- [100] Neilands JB (1952) A Crystalline Organo-iron Pigment from a Rust Fungus (*Ustilago sphaerogena*). *Journal of the American Chemical Society* **74**: 4846-4847.
- [101] Katayama S, Adachi N, Takao K, Nakagawa T, Matsuda H, et al. (1995) Molecular cloning and sequencing of the *hcs* gene, which encodes 3-hydroxy-3-methylglutaryl coenzyme A synthase of *Schizosaccharomyces pombe*. *Yeast* **11**: 1533-1537.
- [102] Hayashi T, Fujita Y, Iwasaki O, Adachi Y, Takahashi K, et al. (2004) Mis16 and Mis18 are required for CENP-A loading and histone deacetylation at centromeres. *Cell* **118**: 715-729.
- [103] Elbein AD, Pan YT, Pastuszak I, Carroll D (2003) New insights on trehalose: a multifunctional molecule. *Glycobiology* **13**: 17R-27R.
- [104] Cansado J, Vicente-Soler J, Soto T, Fernandez J, Gacto M (1998) Trehalose-6P synthase is essential for trehalase activation triggered by glucose, nitrogen source or heat shock, but not by osmotic stress, in *Schizosaccharomyces pombe*. *Biochim Biophys Acta* **1381**: 271-278.
- [105] Pluskal T, Hayashi T, Saitoh S, Fujisawa A, Yanagida M (2011) Specific biomarkers for stochastic division patterns and starvation-induced quiescence under limited glucose levels in fission yeast. *FEBS J* **278**: 1299-1315.
- [106] Le T, Bhushan V, Vasan N (2010) First Aid for the USMLE Step 1. *McGraw-Hill Medical*.
- [107] American Diabetes Association (2014) Diagnosis and classification of diabetes mellitus. *Diabetes Care* **37**: S81-S90.
- [108] Vander Heiden MG, Cantley LC, Thompson CB (2009) Understanding the Warburg effect: the metabolic requirements of cell proliferation. *Science* **324**: 1029-1033.
- [109] Roux AE, Leroux A, Alaamery MA, Hoffman CS, Chartrand P, et al. (2009) Pro-aging effects of glucose signaling through a G protein-coupled glucose receptor in fission yeast. *PLoS Genet* **5**: e1000408.
- [110] Roux AE, Chartrand P, Ferbeyre G, Rokeach LA (2010) Fission yeast and other yeasts as

- emergent models to unravel cellular aging in eukaryotes. *J Gerontol A Biol Sci Med Sci* **65**: 1-8.
- [111] Hanyu Y, Imai KK, Kawasaki Y, Nakamura T, Nakaseko Y, et al. (2009) *Schizosaccharomyces pombe* cell division cycle under limited glucose requires Ssp1 kinase, the putative CaMKK, and Sds23, a PP2A-related phosphatase inhibitor. *Genes Cells* **14**: 539-554.
- [112] Gutz H, Heslot H, Leupold U, Loprieno N (1974) *Schizosaccharomyces pombe*. *Handb Genet* **1**: 395-446.
- [113] Marchetti MA, Weinberger M, Murakami Y, Burhans WC, Huberman JA (2006) Production of reactive oxygen species in response to replication stress and inappropriate mitosis in fission yeast. *J Cell Sci* **119**: 124-131.
- [114] Lee J, Dawes IW, Roe JH (1995) Adaptive response of *Schizosaccharomyces pombe* to hydrogen peroxide and menadione. *Microbiology* **141 (Pt 12)**: 3127-3132.
- [115] Cheah IK, Halliwell B (2012) Ergothioneine; antioxidant potential, physiological function and role in disease. *Biochimica et Biophysica Acta (BBA) - Molecular Basis of Disease* **1822**: 784-793.
- [116] Bello MH, Barrera-Perez V, Morin D, Epstein L (2012) The *Neurospora crassa* mutant *NcΔEgt-1* identifies an ergothioneine biosynthetic gene and demonstrates that ergothioneine enhances conidial survival and protects against peroxide toxicity during conidial germination. *Fungal genetics and biology* **49**: 160-172.
- [117] Pluskal T, Ueno M, Yanagida M (2014) Genetic and metabolomic dissection of the ergothioneine and selenoneine biosynthetic pathway in the fission yeast, *S. pombe*, and construction of an overproduction system. *PLoS One* **9**: e97774.
- [118] Yancey PH (2001) Water stress, osmolytes and proteins. *American Zoologist* **41**: 699-709.
- [119] Rademacher TW, Parekh RB, Dwek RA (1988) Glycobiology. *Annu Rev Biochem* **57**: 785-838.
- [120] Blazquez MA, Stucka R, Feldmann H, Gancedo C (1994) Trehalose-6-P synthase is dispensable for growth on glucose but not for spore germination in *Schizosaccharomyces pombe*. *J Bacteriol* **176**: 3895-3902.
- [121] Franco A, Soto T, Vicente-Soler J, Guillen PV, Cansado J, et al. (2000) Characterization of *tpp1*⁺ as encoding a main trehalose-6P phosphatase in the fission yeast *Schizosaccharomyces pombe*. *J Bacteriol* **182**: 5880-5884.

- [122] Levi S, Rovida E (2009) The role of iron in mitochondrial function. *Biochim Biophys Acta* **1790**: 629-636.
- [123] Zuin A, Carmona M, Morales-Ivorra I, Gabrielli N, Vivancos AP, et al. (2010) Lifespan extension by calorie restriction relies on the Sty1 MAP kinase stress pathway. *EMBO J* **29**: 981-991.
- [124] Schlake T, Gutz H (1993) Mating configurations in *Schizosaccharomyces pombe* strains of different geographical origins. *Curr Genet* **23**: 108-114.
- [125] Patch AM, Aves SJ (2007) Fingerprinting fission yeast: polymorphic markers for molecular genetic analysis of *Schizosaccharomyces pombe* strains. *Microbiology* **153**: 887-897.
- [126] Tanret C (1909) Sur une base nouvelle retirée du seigle ergote, l'ergothioneine. *Compt Rendes* **149**: 222-224.
- [127] Melville DB, Otken CC, Kovalenko V (1955) On the origin of animal ergothioneine. *J Biol Chem* **216**: 325-331.
- [128] Shires TK, Brummel MC, Pulido JS, Stegink LD (1997) Ergothioneine distribution in bovine and porcine ocular tissues. *Comp Biochem Physiol C Pharmacol Toxicol Endocrinol* **117**: 117-120.
- [129] Ey J, Schömig E, Taubert D (2007) Dietary sources and antioxidant effects of ergothioneine. *Journal of agricultural and food chemistry* **55**: 6466-6474.
- [130] Melville DB, Horner WH, Lubschez R (1954) Tissue ergothioneine. *J Biol Chem* **206**: 221-228.
- [131] Leone E, Mann T (1951) Ergothioneine in the seminal vesicle secretion. *Nature* **168**: 205-206.
- [132] Gründemann D, Harlfinger S, Golz S, Geerts A, Lazar A, et al. (2005) Discovery of the ergothioneine transporter. *Proceedings of the National Academy of Sciences of the United States of America* **102**: 5256-5261.
- [133] Kawano H, Otani M, Takeyama K, Kawai Y, Mayumi T, et al. (1982) Studies on ergothioneine. VI. Distribution and fluctuations of ergothioneine in rats. *Chem Pharm Bull (Tokyo)* **30**: 1760-1765.
- [134] Kato Y, Kubo Y, Iwata D, Kato S, Sudo T, et al. (2010) Gene knockout and metabolome analysis of carnitine/organic cation transporter OCTN1. *Pharm Res* **27**: 832-840.
- [135] Paul BD, Snyder SH (2009) The unusual amino acid L-ergothioneine is a physiologic

- cytoprotectant. *Cell death and differentiation* **17**: 1134-1140.
- [136] Hartman PE (1990) Ergothioneine as antioxidant. *Methods in enzymology* **186**: 310-318.
- [137] Markova NG, Karaman-Jurukovska N, Dong KK, Damaghi N, Smiles KA, et al. (2009) Skin cells and tissue are capable of using L-ergothioneine as an integral component of their antioxidant defense system. *Free Radic Biol Med* **46**: 1168-1176.
- [138] Akanmu D, Cecchini R, Aruoma OI, Halliwell B (1991) The antioxidant action of ergothioneine. *Archives of biochemistry and biophysics* **288**: 10-16.
- [139] Zhu B-Z, Mao L, Fan R-M, Zhu J-G, Zhang Y-N, et al. (2011) Ergothioneine prevents copper-induced oxidative damage to DNA and protein by forming a redox-inactive ergothioneine–copper complex. *Chemical Research in Toxicology* **24**: 30-34.
- [140] Seebeck FP (2010) In vitro reconstitution of mycobacterial ergothioneine biosynthesis. *J Am Chem Soc* **132**: 6632-6633.
- [141] Sajiki K, Pluskal T, Shimanuki M, Yanagida M (2013) Metabolomic analysis of fission yeast at the onset of nitrogen starvation. *Metabolites* **3**: 1118-1129.
- [142] Takeda K, Yoshida T, Kikuchi S, Nagao K, Kokubu A, et al. (2010) Synergistic roles of the proteasome and autophagy for mitochondrial maintenance and chronological lifespan in fission yeast. *Proceedings of the National Academy of Sciences of the United States of America* **107**: 3540-3545.
- [143] Shimanuki M, Uehara L, Pluskal T, Yoshida T, Kokubu A, et al. (2013) Klf1, a C2H2 zinc finger-transcription factor, is required for cell wall maintenance during long-term quiescence in differentiated G0 phase. *PLOS ONE* **8**: e78545.
- [144] Leupold U (1950) Die Vererbung von Homothallie und Heterothallie bei *Schizosaccharomyces pombe*. *C R Lab Carsberg Sér Physiol* **24**: 381–480.
- [145] Shiozaki K, Russell P (1995) Cell-cycle control linked to extracellular environment by MAP kinase pathway in fission yeast. *Nature* **378**: 739-743.
- [146] Hentges P, Van Driessche B, Tafforeau L, Vandenhoute J, Carr AM (2005) Three novel antibiotic marker cassettes for gene disruption and marker switching in *Schizosaccharomyces pombe*. *Yeast* **22**: 1013-1019.
- [147] Goldstein AL, McCusker JH (1999) Three new dominant drug resistance cassettes for gene disruption in *Saccharomyces cerevisiae*. *Yeast* **15**: 1541-1553.
- [148] Bähler J, Wu JQ, Longtine MS, Shah NG, McKenzie A, et al. (1998) Heterologous modules for efficient and versatile PCR-based gene targeting in *Schizosaccharomyces*

- pombe*. *Yeast* **14**: 943-951.
- [149] Marchler-Bauer A, Zheng C, Chitsaz F, Derbyshire MK, Geer LY, et al. (2013) CDD: conserved domains and protein three-dimensional structure. *Nucleic Acids Res* **41**: D348-352.
- [150] McGinnis S, Madden TL (2004) BLAST: at the core of a powerful and diverse set of sequence analysis tools. *Nucleic Acids Res* **32**: W20-25.
- [151] Maundrell K (1990) *nmt1* of fission yeast. A highly transcribed gene completely repressed by thiamine. *J Biol Chem* **265**: 10857-10864.
- [152] Mitchison JM (1957) The growth of single cells. I. *Schizosaccharomyces pombe*. *Exp Cell Res* **13**: 244-262.
- [153] Yamashita Y, Yabu T, Yamashita M (2010) Discovery of the strong antioxidant selenoneine in tuna and selenium redox metabolism. *World J Biol Chem* **1**: 144-150.
- [154] Yamashita Y, Yamashita M (2010) Identification of a novel selenium-containing compound, selenoneine, as the predominant chemical form of organic selenium in the blood of bluefin tuna. *J Biol Chem* **285**: 18134-18138.
- [155] Yamashita M, Yamashita Y, Ando T, Wakamiya J, Akiba S (2013) Identification and determination of selenoneine, 2-selenyl-*Nα,Nα,Nα*-trimethyl-L-histidine, as the major organic selenium in blood cells in a fish-eating population on remote Japanese islands. *Biol Trace Elem Res* **156**: 36-44.
- [156] Davis FA, Billmers JM, Stringer OD (1983) First synthesis of simple optically active selenoxides. *Tetrahedron Letters* **24**: 3191-3194.
- [157] Banzky L, Simonics T, Maraz A (2003) Sulphate metabolism of selenate-resistant *Schizosaccharomyces pombe* mutants. *J Gen Appl Microbiol* **49**: 271-278.
- [158] Chen D, Toone WM, Mata J, Lyne R, Burns G, et al. (2003) Global transcriptional responses of fission yeast to environmental stress. *Mol Biol Cell* **14**: 214-229.
- [159] Mata J, Bähler J (2006) Global roles of Ste11p, cell type, and pheromone in the control of gene expression during early sexual differentiation in fission yeast. *Proceedings of the National Academy of Sciences of the United States of America* **103**: 15517-15522.
- [160] Mata J, Wilbrey A, Bahler J (2007) Transcriptional regulatory network for sexual differentiation in fission yeast. *Genome Biol* **8**: R217.
- [161] Bushel PR, Heard NA, Gutman R, Liu L, Peddada SD, et al. (2009) Dissecting the fission yeast regulatory network reveals phase-specific control elements of its cell cycle. *BMC Syst*

- Biol* **3**: 93.
- [162] Chen ES, Saitoh S, Yanagida M, Takahashi K (2003) A cell cycle-regulated GATA factor promotes centromeric localization of CENP-A in fission yeast. *Mol Cell* **11**: 175-187.
- [163] Mercier A, Pelletier B, Labbe S (2006) A transcription factor cascade involving Fep1 and the CCAAT-binding factor Php4 regulates gene expression in response to iron deficiency in the fission yeast *Schizosaccharomyces pombe*. *Eukaryot Cell* **5**: 1866-1881.
- [164] Sanso M, Gogol M, Ayte J, Seidel C, Hidalgo E (2008) Transcription factors Pcr1 and Atf1 have distinct roles in stress- and Styl1-dependent gene regulation. *Eukaryot Cell* **7**: 826-835.
- [165] Watanabe Y, Yamamoto M (1996) *Schizosaccharomyces pombe pcr1*⁺ encodes a CREB/ATF protein involved in regulation of gene expression for sexual development. *Mol Cell Biol* **16**: 704-711.
- [166] Genghof DS (1970) Biosynthesis of ergothioneine and hercynine by fungi and Actinomycetales. *J Bacteriol* **103**: 475-478.
- [167] Brummel MC (1989) In search of a physiological function for L-ergothioneine--II. *Med Hypotheses* **30**: 39-48.
- [168] Brummel MC (1985) In search of a physiological function for L-ergothioneine. *Med Hypotheses* **18**: 351-370.
- [169] Takeda K, Yoshida T, Kikuchi S, Nagao K, Kokubu A, et al. (2010) Synergistic roles of the proteasome and autophagy for mitochondrial maintenance and chronological lifespan in fission yeast. *Proc Natl Acad Sci U S A* **107**: 3540-3545.
- [170] Nakamura T, Pluskal T, Nakaseko Y, Yanagida M (2012) Impaired coenzyme A synthesis in fission yeast causes defective mitosis, quiescence-exit failure, histone hypoacetylation and fragile DNA. *Open Biol* **2**: 120117.
- [171] Chaleckis R, Ebe M, Pluskal T, Murakami I, Kondoh H, et al. (2014) Unexpected similarities between the *Schizosaccharomyces* and human blood metabolomes, and novel human metabolites. *Molecular BioSystems*, doi:10.1039/C4MB00346B.
- [172] Chaleckis R, Pluskal T, Hayashi T, Kondoh H, Yanagida M (2013) [Metabolomic analysis of human blood, plasma and red blood cells in comparison with eukaryotic microbe]. *The Japanese Journal of Clinical Hematology* **54**: 1603-1614.
- [173] Ingram SW, Barnes LD (2000) Disruption and overexpression of the *Schizosaccharomyces pombe aph1* gene and the effects on intracellular diadenosine

References

- 5',5'''-P₁, P₄-tetrphosphate (Ap₄A), ATP and ADP concentrations. *Biochem J* **350 Pt 3**: 663-669.
- [174] Song SH, Lim CJ (2008) Nitrogen depletion causes up-regulation of glutathione content and gamma-glutamyltranspeptidase in *Schizosaccharomyces pombe*. *J Microbiol* **46**: 70-74.
- [175] Mo ML, Palsson BO, Herrgard MJ (2009) Connecting extracellular metabolomic measurements to intracellular flux states in yeast. *BMC Syst Biol* **3**: 37.
- [176] Celton M, Sanchez I, Goelzer A, Fromion V, Camarasa C, et al. (2012) A comparative transcriptomic, fluxomic and metabolomic analysis of the response of *Saccharomyces cerevisiae* to increases in NADPH oxidation. *BMC Genomics* **13**: 317.
- [177] Ibanez AJ, Fagerer SR, Schmidt AM, Urban PL, Jefimovs K, et al. (2013) Mass spectrometry-based metabolomics of single yeast cells. *Proc Natl Acad Sci U S A* **110**: 8790-8794.
- [178] Zenobi R (2013) Single-cell metabolomics: analytical and biological perspectives. *Science* **342**: 1243259.
- [179] Ewald JC, Heux S, Zamboni N (2009) High-throughput quantitative metabolomics: workflow for cultivation, quenching, and analysis of yeast in a multiwell format. *Anal Chem* **81**: 3623-3629.
- [180] Paczia N, Nilgen A, Lehmann T, Gatgens J, Wiechert W, et al. (2012) Extensive exometabolome analysis reveals extended overflow metabolism in various microorganisms. *Microb Cell Fact* **11**: 122.

Acknowledgements

Above all, I would like to express my deepest gratitude to my two direct supervisors. My first supervisor, Professor Mitsuhiro Yanagida, showed a great deal of faith in my ability and offered me a position in his laboratory despite the fact I had had no prior experience in the field. Thanks to him, I had the opportunity to develop the taste and feeling for good science. My second advisor, Associate Professor Masaru Ueno, was kind enough to accept me as an external student in his laboratory at Hiroshima University; he provided a wealth of invaluable advice and guidance. Further, I would like to thank Ms. Junko Kimata for explaining the fundamental principles of mass spectrometry, Dr. Koji Nagao and Dr. Yoshiya Oda for their assistance with the initial LC-MS method development, and Ms. Eulalia Lopez for her excellent technical assistance. I truly appreciate the support of all present and past members of the G0 Cell Unit at OIST, and the generous funding provided by OIST to pursue our research goals. I would like to acknowledge the contributions of all co-authors of the MZmine 2 software framework, a tool that is now used daily in our laboratory as well as in many others. On the personal side, I am greatly indebted to my karate sensei, Mr. Kiyohide Shinjō, for teaching me that strength comes through pain. Without him, I doubt this thesis would ever come into existence. Last, but not least, I would like to thank my family for their everlasting support, and to my amazing wife for her loving kindness, tolerance, and understanding.